IRON AND REACTIVE OXYGEN IN WHEAT-PATHOGEN INTERACTIONS

A Thesis Submitted to the College of

Graduate Studies and Research

In Partial Fulfillment of the Requirements

For the Degree of Doctor of Philosophy

In the Department of Biology

University of Saskatchewan

Saskatoon

By

DAVID L. GREENSHIELDS

PERMISSION TO USE

In presenting this thesis in partial fulfilment of the requirements for a Postgraduate degree from the University of Saskatchewan, I agree that the Libraries of this University may make it freely available for inspection. I further agree that permission for copying of this thesis in any manner, in whole or in part, for scholarly purposes may be granted by the professor or professors who supervised my thesis work or, in their absence, by the Head of the Department or the Dean of the College in which my thesis work was done. It is understood that any copying or publication or use of this thesis or parts thereof for financial gain shall not be allowed without my written permission. It is also understood that due recognition shall be given to me and to the University of Saskatchewan in any scholarly use which may be made of any material in my thesis.

Requests for permission to copy or to make other use of material in this thesis in whole or part should be addressed to:

Head of the Department of Biology

University of Saskatchewan

112 Science Place

Saskatoon, Saskatchewan S7N 5E2

ABSTRACT

Iron is an essential component of various proteins and pigments for both plants and pathogenic fungi. However, redox cycling between the ferric and ferrous forms of iron can also catalyse the production of dangerous free radicals and iron homeostasis is therefore tightly regulated. During pathogen attack, plants quickly produce large amounts of reactive oxygen species at the site of attempted pathogen ingress. This so-called oxidative burst has received considerable attention, but no single enzyme has been shown to account for the phenomenon. Using inductively coupled plasma mass spectrometry and histochemistry, I show that iron is secreted to the apoplast of the diploid wheat *Triticum monococcum* during attack by the powdery mildew fungus *Blumeria graminis* f.sp. *tritici*. This iron accumulates at cell wall appositions synthesised *de novo* beneath sites of pathogen attack. I further show, using histochemistry and pharmaceutical inhibitors, that this apoplastic iron accumulation is required for production of H_2O_2 in the oxidative burst. To understand the impact of this massive change in iron homeostasis on gene transcription, I employ a 187 gene targeted macroarray platform and establish that iron overload induces the expression of iron homeostasis-related genes and defence-related genes through iron itself and iron-mediated H_2O_2 production, respectively. To illustrate how the plant is able to withstand the negative effects of its own oxidative defences, I characterise a novel quinone redox cycle, and show that simultaneous induction of a protective quinone reductase isoform and downregulation of reactive oxygen-producing quinone reductase isoform prevents the spread of reactive oxygen during pathogen attack. Finally, in an effort to understand the impact of iron on fungal pathogenicity, I investigate iron uptake in the head blight pathogen, *Fusarium graminearum*. Fungi use at least two separate systems to take up iron, one based on enzymatic iron reduction and the other based on the synthesis and secretion of small iron chelators termed siderophores. Using mutants disrupted in either of two modes of iron uptake, I establish that siderophore production is essential for full *F. graminearum* virulence on wheat. This thesis exposes iron as an important component of both plant defence and fungal virulence.

ACKNOWLEDGEMENTS

First, I thank my supervisors, Drs. Gopalan Selvaraj and Yangdou Wei. Together, they offered a unique blend of mentorship and friendship, and showed continued support through the ebbs and flows of my productivity and focus; I owe them a great deal.

I thank my advisory committee, Drs. Art Davis, Gord Gray, Ken Wilson and Doug Chivers for their guidance and advice. I also thank Dr. Zamir Punja, who acted as the external examiner for this thesis. Thanks to Drs. Ken Shirasu and Kazuya Ichimura for graciously hosting me at RIKEN, Yokohama during the summer of 2006.

This work was supported by operating grants from the Natural Sciences and Engineering Research Council (NSERC) and National Research Council to Drs. Wei and Selvaraj, respectively. I was supported by graduate fellowships from NSERC, the Canadian Wheat Board and the Japan Society for the Promotion of Science, and by awards from the Vanterpool family, Pacific Regenerations Technology and CellFor Inc., and Genome Canada.

I thank friends and colleagues who helped me along the way: Andrea Bena, Tarik Dessouki, Jerry Feng, Lily Forseille, Rozina Hirji, Dr. Susan Kaminskyj, Regan Kennedy, Eugen Kurylo, Dr. Guosheng Liu, Dr. Shelly Payne, Dr. Ramaswami Sammynaiken, Matt Todd, Feng Wang, Dr. Bob Watson, and Dr. Jin-Rong Xu.

I thank my Mom and Dad and brothers and sister for their love and support. Finally and most importantly, I thank my wife Tara, whose love, support and patience made this possible.

TABLE OF CONTENTS

LIST OF FIGURES

LIST OF TABLES

LIST OF ABBREVIATIONS

a.u.: arbitrary unit
ABC: ATP-binding cassette
Avr: avirulence
Bgt: *Blumeria graminis* f.sp. *tritici*
BPS: Bathophenanthrolinedisulfonic acid
CK: check
CWA: cell wall appostion
CytA: cytochalasin A
DFO: deferoxamine
DON: deoxynivalenol
dpi: days post-inoculation
EPR: electron paramagnetic spectroscopy
DAB: 3,3'-diaminobenzidine
EST: expressed sequence tag
FHB: Fusarium Head Blight
GSH: reduced glutathione
GSSG: glutathione disulfide
HR: hypersensitive response
ICPMS: inductively coupled plasma mass spectrometry
MAPK: mitogen-associated protein kinase
MDA: monodehydroascorbate
MM: minimal medium
MnTBAP: manganese (III) tetrakis (4-benzoic acid) porphyrin
NA: nicotianamine
NBT: nitro blue tetrazolium
NES: nuclear export signal
NPS: nonribosomal peptide synthase
NRAMP: natural resistance-associated macrophage protein
PAMP: pathogen-associated molecular pattern
PCR: polymerase chain reaction
PR: pathogenesis-related
QR: quinone reductase
QR1: ζ crystallin-like QR
QR2: DT-diaphorase-like QR
R: resistance
RBOH: respiratory burst oxidase homologue
Redox: reduction-oxidation
ROS: reactive oxygen species
SAR: systemic acquired resistance
SOD: superoxide dismutase
UTR: untranslated region
WT: wild type

LICENCING

This thesis contains material from previously published articles, as noted at the beginning of each chapter. Chapter 4 is reprinted with permission from Springer under licence number 1704281114995, which was issued May 8th, 2007. Chapters 2, 3 and 5 are reprinted from journals that allow reprinting in theses.

CHAPTER 1

GENERAL INTRODUCTION

1.1 Introduction to Plant-Pathogen Interactions

1.1.1 Types of interactions

Plants are photosynthetic machines that fix carbon for entry into the food chain. Plants are therefore in constant contact with other organisms that seek to reap the plant's metabolic effort for their own benefit. Interactions with microbes range from beneficial to lethal to the plant, and various microbial groups have carved out specific niches for themselves through their ability to capture plant nutrients. Table 1.1 illustrates the spectrum of plant-microbe interactions; interactions between plants and pathogenic fungi, which are the focus of this thesis, are discussed in more detail below.

Table 1.1 Degrees of synchronization between host plants and microbes.

Synchronization →	**Interaction type**	**Examples**			
		Fungi/Oomycetes	**Bacteria**	**Viruses**	**Phytoplasmas**
	Symbiotic	Mycorrhizae Lichens	Rhizobium spp.	n/a[a]	n/a
	Biotrophic	Powdery mildews Downy mildews Rusts	n/a	Viruses Viroids	Phytoplasmas
	Hemibiotrophic	*Phytophthora* spp. *Colletotrichum* spp.	*Agrobacterium* spp.	n/a	n/a
	Necrotrophic	*Fusarium* spp. *Pythium* spp. *Rhizoctonia* spp.	*Pseudomonas* spp. *Xanthomonas* spp. *Erwinia* spp.	n/a	n/a
	Saprotrophic	Various	various	n/a	n/a

[a]n/a: not applicable

1.1.1.1 *Hosts and nonhosts*

Although plant pathogens are estimated to destroy 10% of world crop production annually (Strange and Scott, 2005), only a small fraction of potential pathogens are able to cause disease on a given plant. Plant species which are able to support members of a

given pathogen species are referred to as hosts. However, certain host plants may be resistant to members of an otherwise infective pathogen group: this is termed host resistance. Host resistance is governed by specific *Resistance* (*R*) genes, which encode products that can recognize the products of specific pathogen *Avirulence* (*Avr*) genes (Flor, 1955; Heath, 1991; Ellis et al., 2000). This type of resistance is particularly effective in plant breeding programs because of the ease with which a single resistance locus can be incorporated into a breeding line. *R* gene-mediated resistance often lacks durability because of shifts in pathogen population structure towards races lacking a recognizable *Avr* gene; this phenomenon is governed by the so-called Red Queen Hypothesis where "it takes all the running you can do to keep in the same place" (Clay and Kover, 1996). One common type of host resistance manifests itself as localized programmed cell death surrounding host-pathogen interaction sites and is termed the hypersensitive response (HR). The HR has been the subject of research for over 90 years (Stakman, 1915), and has been expertly reviewed many times (Mittler et al., 1997; Morel and Dangl, 1997; Gilchrist, 1998; Heath, 1999; Greenberg and Yao, 2004). Several phenomena are associated with the HR including direct or indirect interaction between *Avr* and *R* gene products (Dodds et al., 2006), ion fluxes (Atkinson et al., 1996) and reactive oxygen species (ROS) production (Alvarez et al., 1998), mitochondrial leakage (Lam et al., 2001) and chloroplast morphological changes (Chen and Dickman, 2004), DNA fragmentation (Mittler and Lam, 1997), and eventual cell death.

While host resistance remains the favoured tool of plant breeders, increasing effort is now focused on how an entire plant species can be resistant to all pathogens of a given species. This type of resistance is termed nonhost resistance. Because both host and nonhost pathogens likely trip the same plant surveillance mechanisms (bacterial flagellin (Asai et al., 2002) or fungal chitin (Kaku et al., 2006), for instance), the processes leading to host and nonhost resistance share at least some commonalities (Thordal-Christensen, 2003; Nürnberger and Lipka, 2005; Ellis, 2006). Nonhost resistance can be separated into penetration resistance and postpenetration resistance (Lipka et al., 2005). Penetration resistance overlaps with basal resistance, the resistance that all plants (including susceptible hosts) show to all pathogens, which is discussed below in section 1.1.2. *Arabidopsis* mutant screens have uncovered three loci, *pen1*,

pen2 and *pen3*, that are required for full nonhost resistance against *Blumeria graminis* (Collins et al., 2003; Assaad et al., 2004; Lipka et al., 2005; Kobae et al., 2006; Stein et al., 2006; Ellis, 2006). PEN1 is a plasma membrane syntaxin that is localized to the cup-shaped plasma membrane domain surrounding the cell wall appositions (CWAs) formed beneath penetration attempts of nonhost *B. graminis* f.sp. *hordei* on *Arabidopsis* (Collins et al., 2003; Assaad et al., 2004). Syntaxins mediate vesicle fusion events during endocytosis and exocytosis (Teng et al., 2001). *Arabidopsis pen1* mutants show normal CWAs, but their formation is delayed by ca. 2 h compared to wild type plants, and PEN1 is therefore thought to aid in CWA-destined vesicle recruitment (the process leading to CWA formation is discussed further in section 1.1.2). PEN2 is a glycosyl hydrolase that is localized to peroxisomes surrounding penetration attempts (Lipka et al., 2005). Although no function has been assigned to PEN2, *pen1pen2* double mutants show enhanced susceptibility compared to either single mutant and the respective proteins are therefore thought to work through separate pathways of penetration resistance. PEN3 is a plasma membrane-resident ATP-binding cassette (ABC) transporter with sequence homology to yeast PLEIOTROPIC DRUG RESISTANCE8 (Stein et al., 2006). Interestingly, *pen3* mutants are more susceptible to nonhost *B. graminis* f. sp. *hordei* and *Phytophthora infestans*, but show greater resistance to the host pathogen *Pseudomonas syringae* DC3000 (Kobae et al., 2006; Stein et al., 2006), suggesting that while host and nonhost resistances can overlap, this is not always the case. Figure 1.1 shows the layers of resistance that pathogens encounter when interacting with plants.

Despite the discovery of the *pen* mutants, events at the apex of the network of pathways leading to eventual disease or resistance in a plant-pathogen interaction are governed in many cases by the pathogen. The ability to germinate on a given surface, for example, is often based on recognition of compounds that inform the pathogen about its would-be host. The association between the obligate biotroph *B. graminis* and its cereal host begins with the fungal conidium releasing a proteinaceous matrix which contains enzymes that break apart the host epicuticular wax (Nielsen et al., 2000; Feng et al., unpublished). Components of this hydrolyzed wax are then reabsorbed by the conidium and, given the appropriate wax constituents, the condium germinates (Nielsen et al., 2000). Similarly, in the bean rust, *Uromyces appendiculatus*, germ tubes sense the ridges

surrounding stomata on the leaf surface and use this thigmotropism to trigger appressorial formation (Wynn, 1976). Thus, in plant-pathogen interactions, it is neither the host nor the pathogen, but a complex series of contributions from both, that decides the eventual disease or resistance outcome of a given interaction.

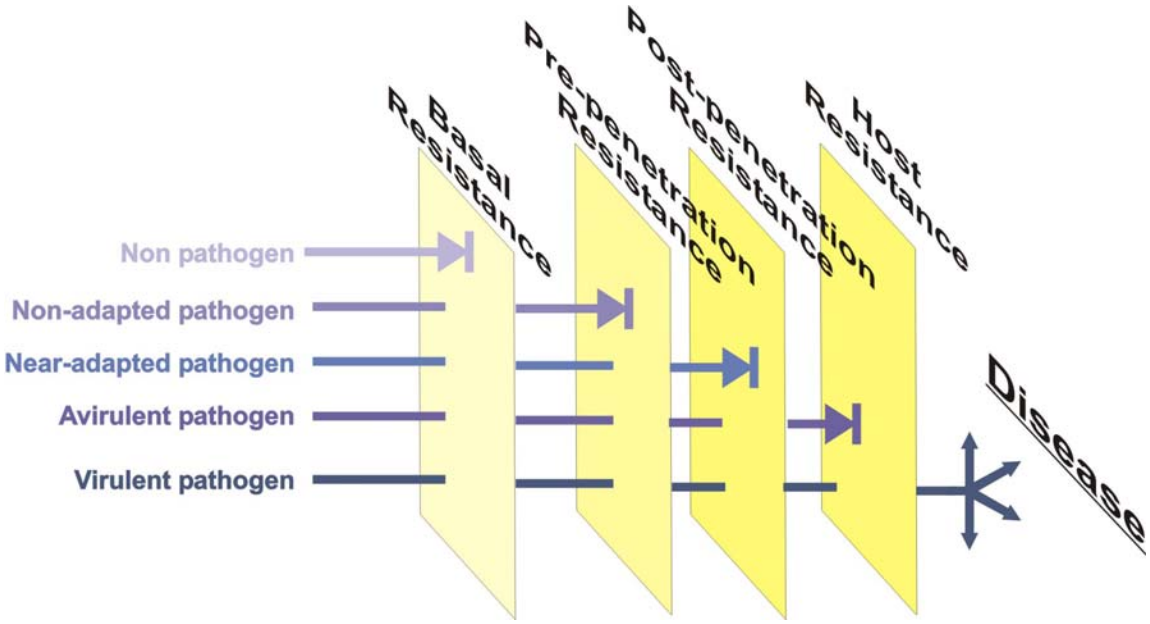

Figure 1.1 Layers of plant resistance. All microbes that germinate on a plant surface meet at least one of these successive layers. Growth of non pathogens (saprotrophs) is easily halted by basal resistance, which is active but ineffective against pathogens. Nonhost pathogens are described here as either non-adapted or near-adapted and are stopped by pre- or post-penetration resistance, respectively. This duality in nonhost resistance is the subject of Lipka et al. (2005). Avirulent pathogens also encounter nonhost resistance, but are able to withstand its effects, and are defeated instead by host resistance. Virulent pathogens are able to endure all of the layers of plant resistance, thereby infecting the plant host and causing disease. Further details of each of these types of resistance are discussed in the text.

1.1.1.2 *Biotrophy*

Biotrophic plant pathogenic fungi require a living host in order to complete their life cycles. The goal of biotrophs is therefore to keep the host plant alive for as long as possible. Mendgen and Hahn (2002) identified five hallmarks common to biotrophic fungal pathogens: "(1) highly developed infection structures; (2) limited secretory

activity, especially of lytic enzymes; (3) carbohydrate-rich and protein-containing interfacial layers that separate fungal and plant plasma membranes; (4) long-term suppression of host defence; (5) haustoria, which are specialized hyphae for nutrient absorption and metabolism." All of these five characteristics are aimed at bypassing the host's surveillance systems.

In the case of *B. graminis*, which is the focus of a large part of this thesis, Mendgen and Hahn's (2002) first and second hallmarks of biotrophic fungal pathogens are tightly linked. In an effort to avoid host perception, *B. graminis* does not secrete many cell wall degrading enzymes, likely because the break down products of the cell wall are themselves potent plant defence inducers (Davis and Hahlbrock, 1987; Zhang et al., 1998). Because of this lack of cell wall hydrolytic activity, the fungus must elaborate a complex germ tube derivative called an appressorium with which to enter the host. The appressorium is a swollen cushion-like structure that builds up turgor pressure, possibly using glycerol as a solute (Thomas et al., 2001), to drive a tiny penetration peg through the host cell wall.

Perhaps the most unusual and interesting hallmark of biotrophy is the development of a specialized feeding hypha termed a haustorium. Haustoria form within the host cell wall and are thought to be the major avenue through which nutrients are absorbed. Haustoria are surrounded by, from the inside out, a haustorial membrane, a gel-like intermembrane matrix, an extrahaustorial membrane (the invaginated plant plasma membrane), and the host cytoplasm (reviewed by Green et al., 2002). These layers prevent contact between the host and fungus, likely to hinder host recognition of the invader as suggested by Mendgen and Hahn's (2002) third hallmark of biotrophy. Although the structural features of this interface are well characterized, little is known about the molecular aspects of nutrient transport across it. While sucrose is the major translocation form of carbon in most plants, many studies have focused on glucose as the major import source of carbon taken up by the fungal pathogens. Mendgen and Nass (1988) showed that glucose was taken up more readily than fructose or sucrose by intact haustoria in wheat infected with powdery mildew, as indicated by potentiometric cyanine dye. Using asymmetrically radiolabelled sucrose, Sutton et al. (1999) showed that [^{14}C]glucose was the major sugar present in the mycelium of powdery mildew on

wheat. Fotopoulos et al. (2003) showed that glucose uptake by fungi causing powdery mildew on *Arabidopsis* coincides with the induction of genes encoding a monosaccharide transporter and a cell wall bound invertase. Unlike *Arabidopsis*, in wheat, soluble extracellular invertase (rather than cell wall bound invertase) transcript accumulation and activity are correlated to infection by powdery mildew (Greenshields et al., 2004b).

1.1.1.3 *Necrotrophy*

Necrotrophic plant pathogens feed on the dead cells of infected plants (Agrios, 1999). Necrotrophs kill the cells before taking up the cellular contents and therefore often secrete a range of lytic enzymes and toxins that degrade cells ahead of the fungal growth front (Wolpert et al., 2002; Hegedus and Rimmer, 2005). *Fusarium graminearum*, which is the subject of Chapter 5, is a necrotrophic cereal pathogen that causes Fusarium Head Blight (FHB), a disease that is becoming a serious constraint to Western Canadian wheat and barley production (Dexter et al., 1996). Like many other necrotrophs (Wolpert et al., 2002; Quayyum et al., 2003; Oliver and Ipcho, 2004), *F. graminearum* produces mycotoxins, most notably the trichothecene deoxynivalenol (DON, vomitoxin), that kill host tissues prior to fungal entry (Proctor et al., 1997; Lemmens et al., 2005). Toxin accumulation is needed for efficient killing of wheat cells, and resistance to FHB can be correlated with DON detoxification (Lemmens et al., 2005). As the common name vomitoxin suggests, DON is not only toxic to the cereal host, but can also cause nausea, haemorrhaging, circulatory shock and, eventually, death in animals (Pestka and Smolinski, 2005). Thus, DON is a concern for both grain producers and consumers alike, and this has prompted regulations on the allowable levels of FHB-damaged wheat kernels (currently 0.25-5.0%, depending on grade and end use; Canadian Grain Commission, 2006).

Because necrotrophs need only dead cells to survive, they are often characterized by a wide host range. Indeed, necrotrophic plant pathogens of the genus *Alternaria* can associate with over 4000 different host species (Farr et al., 1989). The requirement for dead host cells renders apoptosis-dependent defences useless in combating necrotrophs. *Botrytis cinerea*, a necrotroph with over 200 hosts, uses the HR to aid infection (Govrin

and Levine, 2000); when the plant kills itself, it reduces the necrotroph's workload. The recruitment of plant defences to aid infection has also been noted for the oxidative burst in the necrotrophic interactions of *Rhynchosporium secalis* and *Pyrenophora teres* with barley, where a greater accumulation of ROS was seen in susceptible rather than resistant associations (Able, 2003). Similarly, treatment of bean leaves with the ROS scavengers catalase and D-mannitol reduced the severity of infection by aggressive *B. cinerea* isolates (Tiedemann, 1997). Thus, what is an appropriate defence against one pathogen may in fact help another pathogen to cause disease, again highlighting a role for nonhost or basal resistances in combating plant pathogens.

1.1.2 Cell wall appositions and basal resistance

During pathogen attack, plants employ a complex of physical and chemical defence strategies to combat attempted invasions. Pathogen penetration attempts are often met with targeted cell wall fortification, and the formation of these localized cell wall appositions (CWAs) or papillae has long been recognized as a common plant response to fungal penetration attempts (de Bary, 1863). Because the occurrence of CWAs often correlates to increased penetration failure, CWA formation is considered an important resistance mechanism. CWAs form in both susceptible and resistant hosts, as well as in nonhosts, and therefore constitute an ancient or basal form of resistance, halting the early stages of fungal ingress into host cells. Basal resistance refers to the resistance, successful or not, that all plants deploy against all perceived pathogens (Van Loon, 1997). Since being bred into commercial barley lines over 25 years ago, recessive mutations in the *Mlo* gene of barley have provided durable broad spectrum resistance to penetration by most powdery mildew races, based largely on strong oversized CWAs (reviewed by Lyngkjær et al., 2000). Although CWA formation has been recognized for over a century, the phenomenon continues to challenge researchers and many questions remain unanswered. Below, I summarize the events leading up to CWA formation and in Chapter 2, I present data showing the role of iron in CWA formation and the oxidative burst.

1.1.2.1 Cytoplasmic and cytoskeletal reorganization

One of the earliest recognizable changes in an epidermal cell responding to attempted pathogen penetration is cytoskeletal rearrangement. Penetration attempts cause microtubules and microfilaments in host cells to become radially arranged around the site of attack (Gross et al., 1993; Kobayashi et al., 1992). Treatment of barley, onion, *Arabidopsis* or tobacco with cytochalasin, an actin polymerization inhibitor, partially compromises nonhost resistance at the penetration stage for fungal pathogens (Kobayashi et al., 1997; McLusky et al., 1999; Kobayashi and Hakuno, 2003; Yun et al., 2003, Liu et al., 2007). Concurrent to cytoskeletal rearrangement, cytoplasmic streaming towards the pathogen contact site accelerates, and small volumes of cytoplasm termed cytoplasmic aggregates, which hold rough endoplasmic reticulum and vesicles presumably containing precursors necessary for CWA formation, begin to accumulate beneath the pathogen-plant contact site (Kobayashi et al., 1992; Gross et al., 1993; Freytag et al., 1994; Koh et al., 2005, Liu et al., 2007). The polarization of the plant cell towards the point of pathogen attack gives rise to a dense region of cytoplasm, rich in peroxisomes and mitochondria (Koh et al., 2005). As the cell becomes poised for pathogen attack, the cell nucleus migrates towards the pathogen contact site and the cell begins to produce a CWA (Škalamera and Heath, 1998).

1.1.2.2 Vesicle traffic

Recently, the *Arabidopsis PEN1* (*PENETRATION1*) and barley *ROR2* (*REQUIRED FOR MLO RESISTANCE2*) genes were isolated and characterized as orthologous synaptome-associated protein receptors (SNAREs) (Collins et al., 2003; Assaad et al., 2004). *Arabidopsis* or barley plants with mutations in their respective SNARE genes show increased penetration by barley powdery mildew. In addition to ROR2, a SNAP-25 homologue was also shown to be required for full resistance in barley, and ROR2 and SNAP-25 interacted in yeast two hybrid experiments. Collins et al. (2003) suggested that the proteins may be involved in the facilitation of vesicle exocytosis or the homotypic fusion of vesicles as they carry cargo towards the CWA. Assaad et al. (2004) noted that while *pen1* plants had a delayed CWA response and were less resistant to powdery

mildew, mutations in *PEN1*'s closest homologue, *SYP122*, caused no change in resistance, suggesting that PEN1 is specifically involved in CWA formation. Interestingly, *pen1syp122* double mutants were dwarfed and necrotic, a feature not seen in either single mutant, suggesting that despite distinct roles in penetration resistance, the two proteins have some overlapping functions.

1.1.2.3 Cell wall modification

Although the structural rearrangements preceding CWA formation are now becoming clearer, the identity of the contents carried by CWA-destined vesicles remains somewhat mysterious. The structure and composition of CWAs show remarkable heterogeneity, but they commonly contain callose, pectic substances, phenolic derivatives, suberin, proteins, and some metal ions (reviewed by Smart, 1991). The synthesis, deposition, and assembly of these materials are apparently accompanied by the localized release of ROS, predominantly H_2O_2 (Thordal-Christensen et al., 1997). ROS are discussed below in more detail (1.2.2). Studies in the Wei lab have shown that ROS production beneath the germinating conidium can be detected as early as 3 h after inoculation, before an appressorium is formed by the fungus. Also, the presence of ROS in CWA-destined vesicles (Hückelhoven et al., 1999; Collins et al., 2003; Chapter 2) suggests that the means by which ROS are produced arrive at CWAs together with the CWA building materials.

1.2 Iron and Reactive Oxygen in Plant-Pathogen Interactions

1.2.1 Reactive oxygen species in plant-pathogen interactions

Reactive oxygen species (ROS) are formed through successive one electron reductions of molecular oxygen and include, from most oxidized to most reduced, superoxide ($O_2^{\bullet -}$), hydrogen peroxide (H_2O_2) and the hydroxyl radical ($OH^{\bullet}$) (Pierre and Fontecave, 1999). In addition to these ROS brought about by electron transfer, singlet oxygen ($^1O_2$) is a ROS produced when O_2 accepts energy from excited P680 of

photosystem II, a phenomenon common under high light situations (Fryer et al., 2002). ROS can be produced enzymatically or chemically in living organisms, and can have wide ranging deleterious effects on cells because of their extreme pro-oxidant character (Halliwell and Gutteridge, 1999).

Production of ROS is induced by various stresses (Dat et al., 2000), and ROS are thought to play a dual role as stress indicators and secondary messengers for the stress response in plant cells (Knight and Knight, 2001; Mittler, 2002; Mittler et al., 2004). Under normal conditions, cells control the relative levels of oxidants and reductants, resulting in redox equilibrium. Prominent contributors to ROS production in plants include the electron transport chains of photosynthesis in the chloroplasts during high light exposure (Hideg et al., 2000; Fryer et al., 2002), and of respiration in the mitochondria through the cytochrome c pathway (Maxwell et al., 1999). While mitochondrial and chloroplastic electron transport processes are the major contributors in the generation of ROS, a wide range of enzymatic ROS generators have also been identified in a number of subcellular compartments (Table 1.2), some of which are important in plant defence.

During pathogen attack, plants use ROS as a defence in at least 3 different ways. First, the localized, rapid, transient oxidative burst works to directly harm the pathogen. For example, the plant pathogenic bacterium *Erwinia chrysanthemi* requires the protein repair enzyme methionine sulfoxide reductase (MsrA) for full virulence, and *msrA* mutants are more sensitive to the oxidative stress inducer paraquat (El Hassouni et al., 1999). Second, ROS are used for the oxidative coupling of cell wall constituents surrounding sites of attempted invasion. Oxidative coupling is used to build and cross-link various components of the cell wall (Fry, 1986) and has been specifically demonstrated for several cell wall phenolics (Wallace and Fry, 1999), which are important components of CWAs (Kruger et al., 2002; Chapter 4). Third, ROS are important in creating and perpetuating an alarm signal within (and possibly outside of; see Thaler, 1999) the plant, allowing for the activation of a range of defence mechanisms. The role of ROS in plant signalling is dealt with in Section 1.2.1.1 below.

Table 1.2 Some enzymatic sources of non-electron transport ROS production and their subcellular location in plants (adapted from Mittler, 2002).

Enzyme	Location	ROS produced
Amine oxidase	**Apoplast**	**H_2O_2**
Glycolate oxidase	**Peroxisome**	**H_2O_2**
Lipoxygenase	**Peroxisome**	**H_2O_2**
NADPH oxidase	**Plasma membrane**	**$O_2^{\bullet-}$**
Oxalate oxidase	**Apoplast**	**H_2O_2**
Peroxidase	**Apoplast/Peroxisome**	**H_2O_2**
Quinone reductase	**Cytosol**	**$O_2^{\bullet-}$**
Xanthine oxidase	**Peroxisome**	**$O_2^{\bullet-}$**

In the model plant *Arabidopsis thaliana*, the respiratory burst oxidase homologues (RBOH) AtrbohD and AtrbohF are responsible for the majority of hydrogen peroxide (H_2O_2) production following inoculation with the avirulent bacterium *Pseudomonas syringae* pv *tomato* or the virulent oomycete *Hyaloperonospora parasitica* (Torres et al., 2002). Since the RBOHs are NADPH oxidases that produce $O_2^{\bullet-}$, this H_2O_2 arises via dismutation rather than being a direct product of the RBOHs. Likewise, *Nicotiana benthamiana* NbrbohA and NbrbohB, which are similar to AtrbohF and AtrbohD, respectively, are required for H_2O_2 production in response to *Phytophthora infestans* (Yoshioka et al., 2003). In addition to RBOHs, *Arabidopsis* type III peroxidases have recently been shown to generate significant levels of H_2O_2 in response to *Fusarium oxysporum* cell wall preparations (Bindschedler et al., 2006). Silencing of peroxidases, but not RBOHs, led to significantly increased susceptibility in *Arabidopsis* (Torres et al., 2002; Bindschedler et al., 2006). In monocots, the role of individual ROS generators is less clear. In wheat and barley, H_2O_2 is produced at defensive CWAs, while $O_2^{\bullet-}$ is produced in epidermal cells only in association with successful fungal penetration (Hückelhoven and Kogel, 2003; Trujillo et al., 2004).

Recently, Trujillo et al. (2006) found that silencing the barley *AtrbohF* homologue *HvrbohA* led to increased penetration resistance against the powdery mildew fungus *Blumeria graminis* f. sp. *hordei*, suggesting that $O_2^{\bullet -}$ is required for cellular accessibility in that system. Unlike $O_2^{\bullet -}$, H_2O_2 is produced at wheat and barley CWAs in response to successful or defeated host fungi as well as nonhost fungi, and is therefore linked to basal resistance, which is active in all plants against all pathogens.

1.2.1.1 Signalling through reactive oxygen

The ability of plants to produce massive amounts of ROS with regional (tissue, cellular, or organellar, for example) precision, combined with the oxidative power of the ROS themselves allows for plants to use ROS as signal molecules. Indeed, the ability of ROS signals to modify proteins and perpetuate a signal has led to calls for a comprehensive classification scheme for redox-based protein modifications (Forrester and Stamler, 2007).

The transcriptional regulator Yap1p controls transcription of up to 70 genes in response to H_2O_2 in yeast (Lee et al., 1999; Kuge et al., 2001). Recently, the structural mechanism by which Yap1p recognizes this redox stress was discovered. Under non-stress conditions, Yap1p is transported in and out of the nucleus through interactions between its C terminal nuclear export signal (NES) and the nuclear exporter Crm1p (Kuge et al., 2001; Wood et al., 2004). Once exposed to H_2O_2, two reduced cysteine moieties form a disulphide bridge that hides this export signal, allowing Yap1p to stay in the nucleus and direct transcription of ROS scavenging genes (Kuge et al., 2001). In *Arabidopsis*, a partial pathway leading to the recognition of ROS has also been reported (Kovtun et al., 2000). In response to H_2O_2 treatment, a mitogen activated protein kinase kinase kinase (MAPKKK), ANP1, becomes activated by an as yet unknown factor, and phosphorylates an unrecognized MAPKK, which in turn phosphorylates MPK3 and MPK6, leading to transcription of the ROS-responsive genes *GST6* and *HSP18.2*. Both *Arabidopsis* MAPKKs MKK4 and MKK5 are able to phosphorylate MPK3 and MPK6 in response to the bacterial flagellin signal flg22 (Asai et al., 2002). The H_2O_2-inducible serine/threonine kinase OXI1 is required for full activation of MPK3 and MPK6 as well

as basal resistance to *Peronospora parasitica* and root hair growth, highlighting the diversity of MAPK signalling processes in response to H_2O_2 (Rentel et al., 2004).

1.2.2 The relationship between iron and reactive oxygen

Iron is an essential element for most life, as it is required as a prosthetic group or cofactor for many enzymes across a wide array of metabolic pathways. Although essential, iron can also generate dangerous free radicals through its ability to donate and receive electrons. Free iron can produce ROS in the Fenton/Haber-Weiss reactions (Pierre and Fontecave, 1999), and is therefore bound to various chelators during storage and transport within organisms. In animals, iron is generally bound to the storage or transfer proteins ferritin, lactoferrin or transferrin, or within the heme or iron-sulphur groups of functional proteins (Schaible and Kaufmann, 2004). Plants also use ferritin to store iron, but transport iron mainly with the tripeptide chelator nicotianamine (Schmidt, 2003). Apart from free iron and iron bound to chelators for storage or transport, various oxidising and reducing enzymes use iron as a cofactor for electron donation or acceptance. Table 1.3 illustrates some of the ways that iron leads to the production or disarmament of ROS.

Because of its potent redox activity, iron has often been associated with the oxidative burst. Until very recently though, the role of iron in mediating the oxidative burst in plants has been associated with iron-containing proteins like peroxidases and iron superoxide dismutases (Thordal-Christensen et al., 1997; Bindschedler et al., 2006). Indeed, the first report of *in situ* H_2O_2 localisation in plants assumed that peroxidases were responsible for ROS production at CWAs (Thordal-Christensen et al., 1997). In *Arabidopsis*, the importance of peroxidases in the oxidative burst has since been shown (Bindschedler et al., 2006). In cereals, the significance of peroxidases in generating an oxidative burst has been inferred from immunolocalisation and large scale gene expression studies, both of which show a correlation between peroxidase expression and the oxidative burst (Scott-Craig et al., 1995; Liu et al., 2005). In chapters 2 and 3 of this thesis, I show a previously unrecognised role for iron in mediating the oxidative burst and cognate redox signalling.

Table 1.3 Redox reactions involving iron and oxygen (Adapted from Pierre and Fontecave, 1999).

Oxidising agent	Reaction	Example
O_2	$Fe^{(II)} + O_2 \rightarrow Fe^{(III)} + O_2^{\bullet-}$	Autoxidation
$O_2^{\bullet-}$	$Fe^{(II)} + O_2^{\bullet-} \rightarrow Fe^{(III)} + H_2O_2$	Iron SOD[a]
H_2O_2	$Fe^{(II)} + H_2O_2 \rightarrow Fe^{(III)} + OH^- + OH^{\bullet}$	Fenton reaction
$Fe^{(III)}$	$Fe^{(III)} + O_2^{\bullet-} \rightarrow Fe^{(II)} + O_2$	Haber-Weiss reaction
$Fe^{(IV)}=O$	$Fe^{(IV)}=O + D^{n+} \rightarrow Fe^{(III)} + D^{(n+1)+} + H_2O$	Peroxidase

[a]SOD: superoxide dismutase

1.3 Themes and Research Questions

This thesis is a compilation of projects focused on the roles of iron and reactive oxygen in plant-pathogen interactions. In order to understand the role of iron in plant ROS production during pathogen attack, I first examined the localisation and reactive properties of iron during powdery mildew infection of wheat. To investigate the consequences of iron loading on gene expression, I then evaluated the ability of apoplastic iron overloading to influence the expression of redox-related genes. To illustrate the ability of plants to disarm reactive oxygen during pathogen attack and thereby avoid self-injury, I investigated the role of quinone reductases in preventing runaway ROS production. Finally, to gain insight into the importance of iron in fungal pathogenesis, I created and characterised novel *Fusarium graminearum* iron uptake mutants. The goal of this thesis is to answer the following questions:

- What role does iron play in the production of plant ROS during fungal pathogen attack?
- How does free, reactive iron influence plant gene expression?
- How do plants prevent self-injury during the production of defensive ROS?
- How do fungi harvest plant iron during infection?

CHAPTER 2

TARGETED IRON ACCUMULATION MEDIATES THE OXIDATIVE BURST IN CEREALS[1]

[1]This chapter contains excerpts from the following paper:

Liu, G.*, Greenshields, D.L.*, Sammynaiken, R., Hirji, R., Selvaraj, G., and Wei, Y. (2007). Targeted alterations in iron homeostasis underlie plant defense responses. Journal of Cell Science *120*, 596-605. **Contributed equally*

I performed all of the experimental work except as noted below:

Guosheng Liu performed the histochemical staining collaboratively with me, wrote draft sections of the paper and contributed to experiments not described in this chapter.

Ramaswami Sammynaiken performed the EPR spectroscopy.

Rozina Hirji contributed to experiments not described in this chapter.

Gopalan Selvaraj planned experiments, contributed novel materials not described in this chapter, wrote draft sections of the paper, and acted in a supervisory role.

Yangdou Wei planned experiments, performed the histochemical staining collaboratively with me, wrote draft sections of the paper, and acted in a supervisory role.

Inductively coupled plasma mass spectrometry was performed through a fee-for-service arrangement with the Department of Geological Sciences, University of Saskatchewan.

2.1 Introduction

The establishment of cell wall appositions (CWAs) is associated with elevated levels of H_2O_2 at the site of infection (Thordal-Christensen et al., 1997; Wei et al., 1998). A variety of reactive oxygen species (ROS) producing enzymes have been suggested to participate in creating the oxidative burst (Bolwell et al., 2002; Hückelhoven and Kogel, 2003; Torres et al., 2002), but no single enzyme system can conclusively account for ROS production across the continuum of plant-microbe interactions. Beyond roles in fortifying CWAs and toxicity to the pathogen, mounting evidence suggests that H_2O_2 also regulates a number of signaling pathways in plants (Mittler et al., 2004), including local and systemic signaling essential for plant innate immunity (Alvarez et al., 1998; Levine et al., 1994).

Iron is essential for most life, but it readily engages in one-electron reduction-oxidation (redox) reactions between its ferric (3^+) and ferrous (2^+) states that can catalyze the generation of toxic free radicals through the Fenton reaction (Pierre and Fontecave, 1999). Iron accumulation or imbalance has been implicated in human diseases such as hemochromatosis, Friedreich's ataxia, Parkinson's and Alzheimer diseases (Hentze et al., 2004). Iron acquisition is a virulence factor for bacterial pathogens of animals, and animals withhold iron as a defence strategy (Schaible and Kaufmann, 2004). A role for iron has also been reported in some plant diseases, such as soft rot and fire blight incited by *Erwinia chrysanthemi* and *E. amylovora*, respectively (Expert, 1999), with a focus on iron acquisition by the pathogen. Unfortunately, aspects beyond this tug-of-war between plant and pathogen for iron as a nutrient, including the role of iron involvement in plant redox reactions, particularly in modulating oxidative stress, remain elusive.

To understand the basis for CWA resistance and to identify genes that mediate H_2O_2 metabolism, we had previously constructed an expressed sequence tag (EST) library from diploid wheat (*Triticum monococcum* L.) epidermis attacked by *Blumeria graminis* f. sp. *tritici* (*Bgt*) (described in Greenshields et al., 2004a and Liu et al., 2005). Unexpectedly, sequence alignments against gene databases showed that this library was noticeably rich in transcripts encoding products related to the metabolism of iron and ROS. Given the significance of iron in cellular redox regulation and the direct links

between iron perturbation and human pathology, further investigation of the role of iron in plant-microbe interactions appears to be justified.

2.2 Results

2.2.1 Fe^{3+} is secreted to CWAs during pathogen attack

To characterize iron homeostasis in pathogen-challenged plants at the tissue level, we used inductively coupled plasma mass spectrometry (ICPMS) to track any concentration changes in metals in the epidermis and mesophyll of wheat leaves inoculated with *Bgt*. We found that iron as well as other transition metals (Cu, Mn and Zn) accumulated in the infected epidermis 24 h post inoculation (hpi) (Figure 2.1a), a time-point where CWAs are mature and the success or failure of the attempted infection is distinguishable. In contrast to the epidermis, the mesophyll did not show any significant changes in Fe, Mn, or Zn concentrations. Cu levels, on the other hand, showed a significant decrease in the mesophyll following *Bgt* attack, but the overall Cu pool was small compared to the other accumulating metals, and was therefore not investigated further.

Since we had seen a 55% (w/w) increase in the iron content of wheat epidermis following inoculation with *Bgt* (Figure 2.1a), we wanted to determine where the iron was accumulating at the cellular level. To localize iron at the cellular level in *Bgt*-attacked wheat leaves, we adapted the Prussian blue staining technique, previously used to study iron accumulation in Alzheimer disease (Smith et al., 1997), for use in our wheat-*Bgt* pathosystem. Plant Fe^{2+} staining was only found in the nuclei of the epidermal cells and in the fungal tissues (Figure 2.1b). The Fe^{2+} staining of the fungal spores and germ tubes is consistent with a previous observation that ferric reductase activity is high in the spores and germ tubes of *B. graminis* f. sp. *hordei* (Wilson et al., 2003). In contrast to reduced Fe^{2+}, oxidized Fe^{3+} staining was intense at the CWAs and at the edges of halo areas (Figure 2.1c). Inoculated epidermal guard cells and trichomes also showed Fe^{3+} staining (Figure 2.1c), but no staining occurred in uninoculated leaves (data not shown), implicating pathogen-responsive iron accumulation in these structures as well. Fe^{3+} was found in the nuclei of epidermal cells with and without inoculation. We also found similar Fe^{3+} accumulation at CWAs in the other monocot crop plants

barley, corn, millet, oat and sorghum (Figure 2.1d), suggesting that the phenomenon is conserved throughout cereals. Together, these results show that in pathogen-attacked cereal leaves, Fe^{3+} is targeted to the epidermis where it accumulates in and around CWAs.

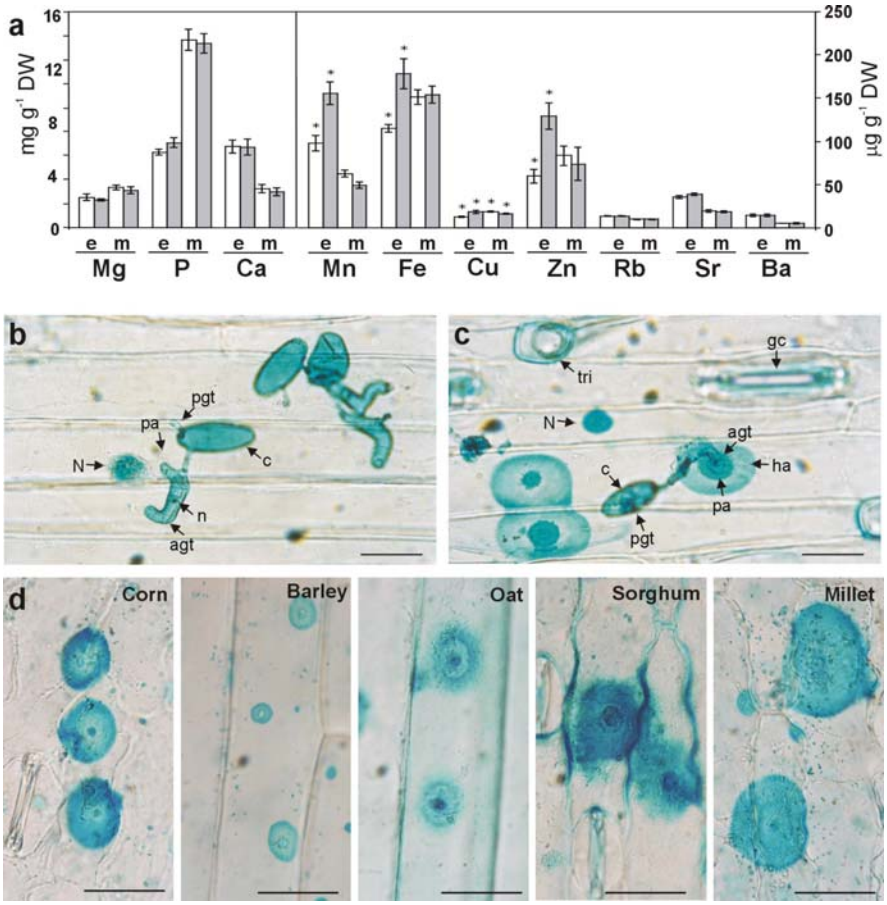

Figure 2.1 Targeted iron redistribution in wheat leaves after *Bgt* attack. c, conidium; pgt, primary germ tube; agt, appressorial germ tube; pa, papilla; ha, halo; gc, guard cell; tri, trichome; N, epidermal nucleus; n, fungal nucleus. Scale bar, 20 µm. **(a)** Concentrations of iron and other transition metals increase in *Bgt*-attacked tissue. Metal concentrations determined by ICPMS analysis of wheat leaf epidermis (e) and underlying mesophyll tissues (m) in response to *Bgt* attack, 24 h post-inoculation (hpi) (shaded bars), or before inoculation (open bars). The mean values (± SE) of three independent treatments are shown. Asterisks indicate significant difference ($p<0.01$) before and after inoculation, based on Student's t-test. **(b)** *In situ* Fe^{2+} Prussian blue staining of wheat epidermis 24 hpi with *Bgt*. **(c)** *In situ* Fe^{3+} Prussian blue staining of wheat epidermis 24 hpi with *Bgt*. **(d)** *In situ* Fe^{3+} Prussian blue staining of epidermal peels 24 hpi with *Bgt* in corn, barley, oat, sorghum and millet.

2.2.2 Fe^{3+} is secreted to CWAs guided by actin

Pathogen attack causes a rapid remodeling of the host cell cytoskeleton and active streaming of cytoplasm towards sites of contact in different pathosystems (Kobayashi et al., 1997; Ŝkalamera and Heath, 1998; Takemoto et al., 2003; Koh et al., 2005). Endoplasmic reticulum, peroxisomes and Golgi bodies aggregate and accumulate at the infection site, suggesting that production and secretion of cellular components including secondary metabolites and proteins are activated around the penetration site (Takemoto et al., 2003, Koh et al., 2005). To track the path of iron to the infection sites, we conducted an infection time course in which wheat leaves were stained with the Fe^{3+} Prussian blue reaction every 2 hpi with *Bgt* spores. Figure 2.2a shows that between 14 and 18 hpi, Fe^{3+} is transported to the infection sites in vesicle-like bodies and is then loaded into CWAs by fusion of these vesicle-like bodies to the plasma membrane. These vesicle-like bodies are made up of a mixture of small papillae and large multivesicular components, such as multivesicular bodies and paramural bodies (R. Hückelhoven, personal communication). Similar vesicle-like bodies have previously been shown to contain H_2O_2 in *B. graminis* f. sp. *hordei*-attacked barley cells (Hückelhoven et al., 1999; Collins et al., 2003). To further characterize the transport of Fe^{3+} to CWAs, we treated freshly inoculated leaves with the actin filament disruptor cytochalasin A (cytA). In leaves treated with 1 $\mu g ml^{-1}$ cytA, Fe^{3+} was present at 55% fewer appressorial germ tube-associated CWAs than in water treated control leaves (Figure 2.2b), suggesting that actin guides vesicle-like bodies destined for CWAs. While the majority of iron-positive sites following cytA treatment showed only weak iron accumulation centrally in the CWA, iron accumulation at the outer CWA haloes was completely abolished. CytA also blocked cytoplasmic aggregation and nuclear migration subjacent to sites of attack (Figure 2.2b). Together, these results show that in wheat leaves, cytosolic Fe^{3+} is transported to CWAs in vesicle-like bodies guided by actin polymerization.

2.2.3 The Fe^{3+} at CWAs is chelatable and redox-active

To examine whether the stained Fe^{3+} in CWAs was firmly bound to proteins, we treated infected epidermal tissues with 10 mM deferoxamine (DFO) prior to staining. DFO is a

Fe^{3+}-specific high-affinity bacterial siderophore with a stability constant for Fe^{3+} of 10^{31}, but does not remove iron from heme proteins in animal cells (Keyer and Imlay, 1996). Fe^{3+} staining in CWAs was completely abolished by DFO treatment, although the CWAs and associated cytoplasmic aggregations were still apparent beneath the fungal penetration attempts (Figure 2.3a). In contrast, DFO treatment did not eliminate Fe^{3+} staining in fungal tissues. To ensure that the observed chelatable iron accumulation in and around CWAs was not an artifact of our fixation and staining methods, we used the membrane-impermeable Fe^{3+}-binding fluorescent dye calcein to examine iron accumulation in fresh leaf samples. Calcein has a stability constant for Fe^{3+} of 10^{24}, which is lower than the stability of EDTA-Fe^{3+}, but higher than that of citrate-Fe^{3+}. Binding of Fe^{3+} to calcein quenches its fluorescence, providing a reliable indicator of labile iron in biological systems (Thomas et al., 1999). Figure 2.3b (upper panel) shows that prior to treatment with DFO, calcein fluorescence is quenched in the CWAs of wheat leaves 24 hpi, indicating the presence of labile or reactive iron in these structures. Following DFO treatment, however, there was enhanced calcein fluorescence at CWAs, indicative of iron removal, while the iron within the fungal structures remains unchanged (Figure 2.3b, lower panel).

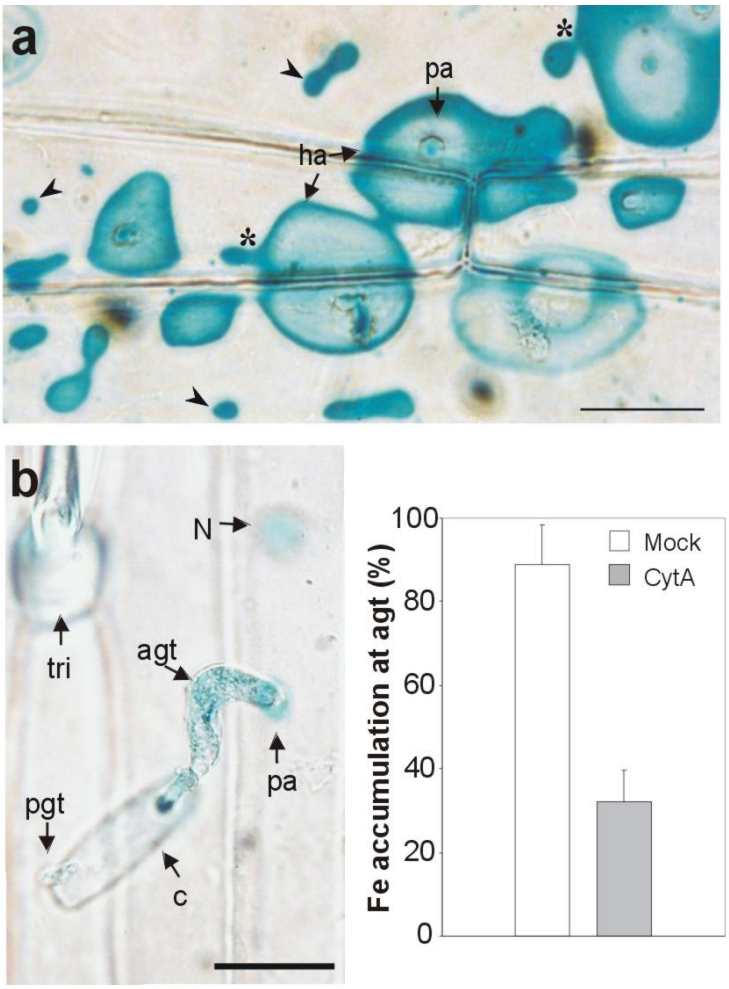

Figure 2.2. Fe^{3+} is secreted to CWAs through vesicles guided by actin polymerization. c, conidium; pgt, primary germ tube; agt, appressorial germ tube; pa, papilla; ha, halo; gc, guard cell; tri, trichome; N, epidermal nucleus; n, fungal nucleus. Scale bar, 20 µm. **(a)** Fe^{3+} stained secretory vesicle-like bodies in leaf epidermis 18 hpi with *Bgt*. Arrowheads show the Fe^{3+}-rich vesicle-like bodies. Asterisks show the point of vesicle-like body/CWA fusion. **(b)** Cytochalasin A (cytA) blocks nuclear migration and iron accumulation at CWAs. Graph shows a 55% (±SE) reduction in iron accumulation at appressorial germ tube-associated CWAs, based on 100 *Bgt* attack sites per leaf on 3 leaves.

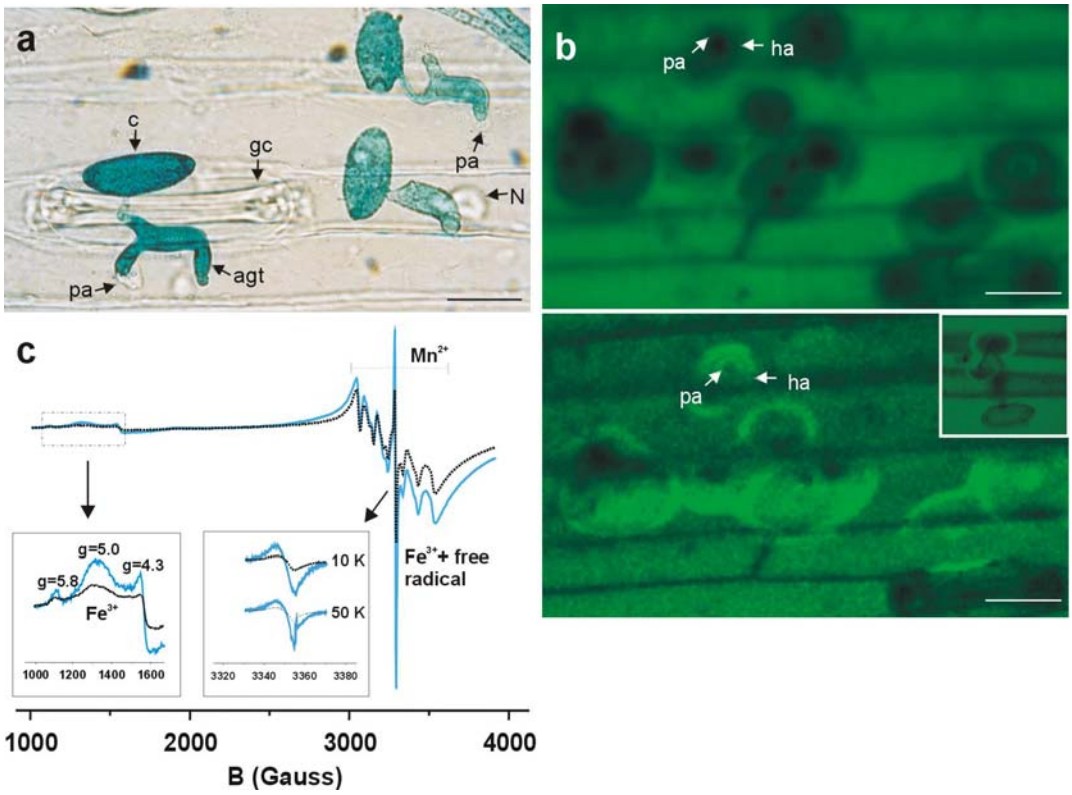

Figure 2.3 Chelatable, redox-active iron accumulation in wheat leaves after *Bgt* attack. c, conidium; agt, appressorial germ tube; pa, papilla; ha, halo; gc, guard cell; N, epidermal nucleus; Scale bar, 20 μm. **(a)** Wheat epidermis 24 hpi with *Bgt* stained for Fe^{3+} after pretreatment with the Fe^{3+} chelator DFO. **(b)** Wheat leaves 24 hpi with *Bgt* were preloaded with calcein for 20 min and then treated with 10 mM DFO for 30 min. The quenching (upper panel) and dequenching (lower panel) of calcein fluorescence were imaged using confocal microscopy. Inset in lower panel shows fluorescence dequenching in an appressorium-associated CWA. **(c)** Wheat leaves 24 hpi with *Bgt* (blue solid line) or uninoculated (black dotted line) were directly subjected to wide range X-band EPR detection. Peaks correspond to Fe^{3+}, free radicals, and Mn^{2+} (sextets), respectively. The insets are the enlarged high resolution scanning for high spin and low spin Fe^{3+}, respectively. The g values of high spin Fe^{3+} are indicated. Spectral intensities were normalized relative to sample weight. Two independent experiments showed similar results.

To further investigate the oxidation states and lability of the accumulating iron in pathogen-challenged wheat leaves, we compared intact leaves before and 24 hpi with *Bgt* using electron paramagnetic resonance (EPR) spectroscopy. The EPR spectra of control and inoculated leaves are shown in Figure 2.3c. The intensity of the Fe^{3+} signal at g = 4.3, 5.0 and 5.8, which represents a high spin state Fe^{3+}, as would be expected for a weakly bound system, was 4-5 times higher in leaves 24 hpi than in control leaves

(Figure 2.3c, left inset), indicating an increase in redox-active iron after *Bgt* attack. A strong signal with a single isotropic feature at g = 2.0 was also observed in both control and inoculated leaves, and yielded a more intense spectrum in inoculated leaves. High resolution scanning using variable temperatures revealed a broad feature of the mixture of low spin Fe^{3+} with free radicals (Figure 2.3c, right inset) (Clay et al., 2002). The dramatic increase in EPR-detectable Fe^{3+} following infection could reflect either the increased transport of Fe^{3+} into infected leaves, the oxidation of the iron pool in infected leaves, or a combination of both of these. These results demonstrate that in response to *Bgt* attack, Fe^{3+} is deposited and accumulates at CWAs in a redox-active form.

2.2.4 Apoplastic iron accumulation mediates H_2O_2 production

H_2O_2 can be detected *in planta* effectively by 3,3'-diaminobenzidine (DAB) staining, as demonstrated in a barley leaf-powdery mildew system (Thordal-Christensen et al., 1997). We found H_2O_2 accumulation, indicated by the strong reddish-brown color of oxidized DAB, in wheat leaf epidermis in response to *Bgt* in and around CWAs subjacent to the primary and appressorial germ tubes (Figure 2.4a). The DAB staining was also visible in trichomes and guard cells of the inoculated epidermis. To examine the interplay between the oxidative burst and iron in CWAs, we double stained wheat leaves 24 hpi, first by *in vivo* DAB uptake to indicate the presence of H_2O_2, and then with Prussian blue following fixation to show the accumulation of Fe. As shown in Figure 2.4b, both Fe^{3+} and H_2O_2 were present in the CWAs. Fe^{3+} staining was more intense along the edge of the haloes surrounding the DAB staining, whereas the DAB staining was more pronounced centrally in CWAs and the inner layer of the haloes. Fe^{2+} was found in double-stained epidermal nuclei and in fungal tissues but was not observed in CWAs, as in the single staining (Figure 2.4c). We also double stained leaves during an inoculation time course, and established that Fe^{3+} and H_2O_2 are always found together and accumulate at primary germ tube-associated CWAs as well (Figure 2.4d). At 24 hpi, vesicle-like bodies double stained for Fe^{3+} and H_2O_2 were found centrally in CWAs (Figure 2.4e).

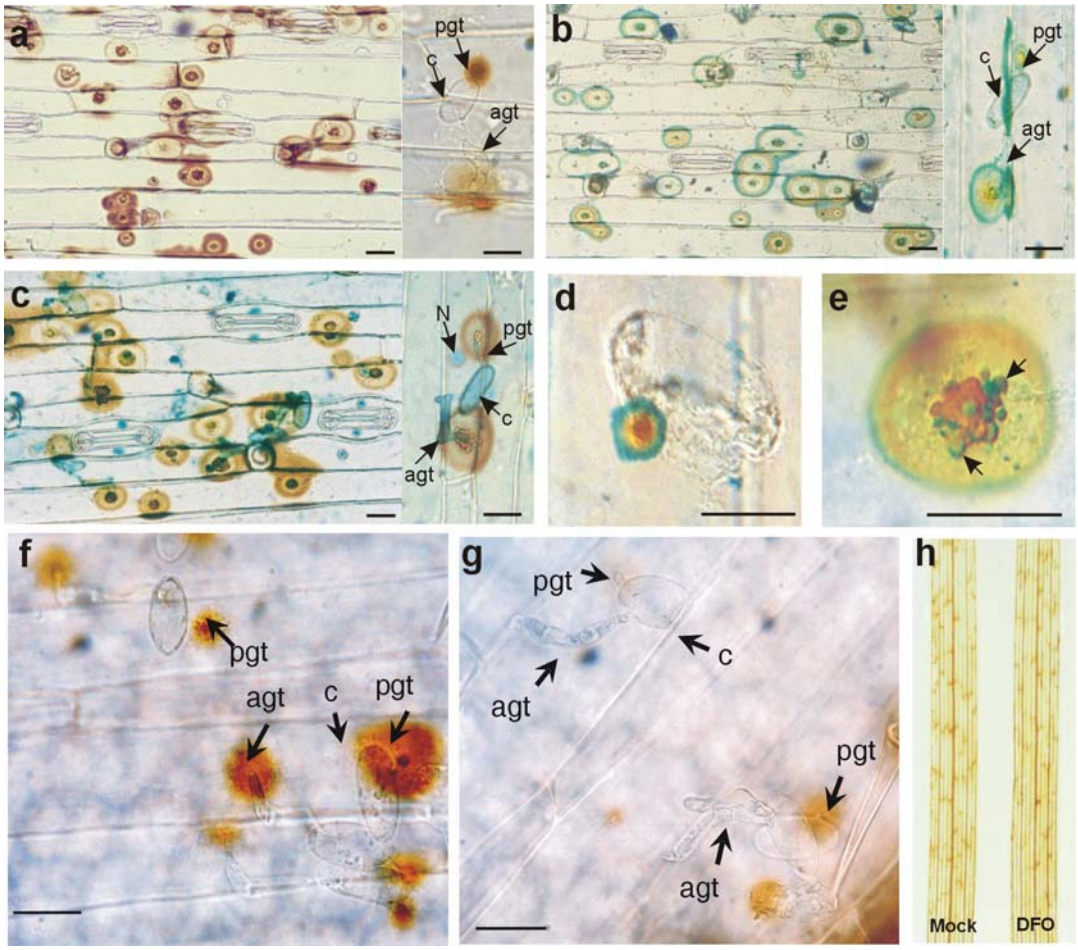

Figure 2.4 Fe^{3+} accumulation mediates H_2O_2 generation at CWAs. c, conidium; pgt, primary germ tube; agt, appressorial germ tube; N, host nucleus. Scale bar, 20 μm. **(a)** H_2O_2 accumulation in CWAs revealed by DAB staining 24 hpi. **(b)** Double staining for H_2O_2 and Fe^{3+} (blue) 24 hpi. **(c)** Double staining for H_2O_2 and Fe^{2+} (blue) 24 hpi. **(d)** Double staining for H_2O_2 and Fe^{3+} at a primary germ tube-associated CWA 5 hpi. **(e)** Vesicle-like bodies within a CWA double staining for H_2O_2 and Fe^{3+} 24 hpi. **(f)** H_2O_2 generation at appressorial germ tube-associated CWAs. **(g)** DFO pretreatment blocks H_2O_2 generation at primary germ tube-associated CWAs. **(h)** Wheat leaves with (right) or without (left) pretreatment of 1.5 mM DFO were stained using DAB and photographed 24 hpi.

To determine whether the accumulated Fe^{3+} actively participates in H_2O_2 generation, we pretreated inoculated wheat leaves with a range of DFO concentrations prior to H_2O_2 staining with DAB. As shown in Figures 2.4f and 2.4g, treatment of the inoculated leaves with 1.5 mM DFO blocks oxidative burst generation at both appressorial and primary germ tube-associated CWAs. Despite the lack of H_2O_2

accumulation at CWAs, cytoplasmic aggregation and nuclear migration were still apparent beneath sites of *Bgt* attack, suggesting that DFO treatment chelated iron without blocking other processes relevant to CWA formation. The efficacy of DFO in oxidative burst inhibition was concentration dependent and at concentrations above 5 mM, development of the *Bgt* appressorial germ tube was hindered. Interestingly, the overall macroscopic appearance of the DAB staining in DFO-treated leaves remained unchanged regardless of the DFO concentration (Figure 2.4h), suggesting that the role of iron in H_2O_2 generation is specific to sites of pathogen attack. The results show that the redox-active Fe^{3+} deposited at CWAs in response to fungal attack mediates production of H_2O_2 in the oxidative burst.

2.3 Discussion

2.3.1 Redistribution of iron in response to pathogen attack

We had initially noted an enrichment of iron- and H_2O_2 metabolism-related transcripts in an EST collection of *Bgt*-infected *T. monococcum* epidermis. We have now shown significant localized accumulation of iron in infected plants that is consistent with targeted redistribution. Since unregulated changes in iron concentrations can be dangerous (Hentze et al., 2004; Schaible and Kaufmann, 2004), this strategy employed by plants appears to avoid deleterious effects while providing a function with respect to plant defence. Our experiments reveal at least three separate phases in targeted redistribution of wheat iron during *Bgt* attack: (1) the tissue-level accumulation of iron in attacked epidermis; (2) the loading of iron into secretory vesicle-like bodies; and (3) the release of this iron to CWAs.

In animals, the best-studied route of iron uptake is the endocytosis of iron complexed with transferrin and the transferrin receptor, but non-transferrin-bound iron can also be taken up directly via the divalent metal transporter DMT-1 (Hentze et al., 2004; Schaible and Kaufmann, 2004). DMT-1 is also responsible for efflux of iron from the transferrin-iron uptake endosomes into the cytosol, while cytosolic iron is pumped out of the cell by the permease ferriportin. The loading of iron into secretory vesicles following *Bgt* attack might require a transporter, as no known transferrin homologues

exist in higher plants. Several types of iron transporters have been identified in plants, including the natural resistance-associated macrophage protein (NRAMP), ZRT/IRT-like protein, ATP-binding cassette (ABC) and yellow stripe families (Hall and Williams, 2003), but this knowledge is largely restricted to aspects of developmental iron acquisition and is complicated by the presence of multiple isoforms. Nevertheless, NRAMP-type transporters appear to be promising candidates for the role of pathogen-induced iron translocation, as *OsNramp3* is induced by both iron and pathogen infection in rice leaf tissue (Zhou and Yang, 2004).

Vesicle-like bodies containing H_2O_2 can be observed moving towards the CWAs in challenged host cells (Hückelhoven et al., 1999; Collins et al., 2003). Similarly, we showed iron-laden vesicle-like bodies in transit to and coalescing with CWAs. Recently, components of the SNARE complex have been identified as important mediators of CWA formation in barley and *Arabidopsis*, mediating exocytosis of CWA constituents to the apoplast (Collins et al., 2003; Assaad et al., 2004). To be soluble and transportable in living cells, iron must be chelated with ligands, which in plants include di- and tri-carboxylic acids, amino acids, amides, amines and especially nicotianamine (NA) (Curie and Briat, 2003; Mori, 1999; Ling et al., 1999). cDNA microarray analysis showed a correlation between the transcriptional regulation of NA synthesis and polar vesicle secretion (Negishi et al., 2002). The systemic acquired resistance (SAR) regulator NPR1, which is required for expression of *PR* genes, was also found to regulate the protein secretion pathway in *Arabidopsis*, revealing a link between these processes (Wang et al., 2005).

2.3.2 Apoplastic iron and the oxidative burst

It is generally believed that generation of ROS promotes cross-linking of cell wall components leading to the development of CWAs, localized physical barriers to pathogen invasion (Schulze-Lefert 2004; Thordal-Christensen et al., 1997). Beyond this, ROS production can take the form of so-called microbursts which perpetuate a signal leading to the development of SAR (Levine et al., 1994). In the model dicot plant *Arabidopsis*, superoxide (O_2^-) is produced by NADPH oxidase during hypersensitive cell death (Torres et al., 2002). It was previously shown that the localized burst of H_2O_2 at

barley CWAs is not sensitive to the NADPH oxidase inhibitor diphenyleneiodonium, and that superoxide is produced only in association with failed CWAs at successful penetration sites (Hückelhoven and Kogel, 2003). Like barley, the diploid wheat system used here is insensitive to diphenyleneiodonium. The difference between monocot and dicot pathogen-induced ROS generation systems is further supported by a lack of detectable Fe^{3+} at *Arabidopsis* CWAs (Greenshields et al., 2007). In Alzheimer disease-affected brains, Fe^{3+} is localized to lesions characteristic of the disease, where it participates in oxidative damage to the brain (Smith et al., 1997). We have now shown that the oxidative burst in cereals is reliant on iron accumulation at CWAs, in a manner similar to that seen in Alzheimer disease.

While in transit and after having been deposited to the apoplast, the iron we observed was in a "free" or "chelatable" form, as it was EPR-detectable and readily removed by DFO. In mammalian cells, free iron is recognized as a major cause of oxidative stress and toxicity in specific tissues and cell types (liver, macrophages and brain) (Hentze et al., 2004; Smith et al., 1997). Because of the overwhelming complexity of biological systems and the ability to analyze only limited aspects of a given system at one time, the role of transition metals in producing ROS in biological systems remains far from clear. The supposed role of iron in ROS production is often summarized by the Fenton/Haber-Weiss reactions (Pierre and Fontecave, 1999) as follows:

(1) $Fe^{3+} + O_2^{\cdot-} \rightarrow Fe^{2+} + O_2$

(2) $Fe^{2+} + H_2O_2 \rightarrow Fe^{3+} + OH^{\cdot} + OH^{-}$

Interestingly, only Fe^{3+} was found at CWAs, suggesting that H_2O_2 is in excess and the Fe^{2+} is rapidly oxidized to Fe^{3+} at CWAs. However, this explanation seems to be at odds with the ability of DFO, a free iron chelator, to prevent H_2O_2 production at CWAs by chelating the free Fe^{3+}. Neither Fe^{3+} nor H_2O_2 alone are capable of oxidizing DAB *in vitro*, but in combination, they produce the color reaction (Liu et al., 2007). This Fe^{3+}/H_2O_2-dependent process is responsible for the majority of the *in planta* DAB reaction, as DFO was able to abolish the stain, but had little effect on the peroxidase/H_2O_2-dependent DAB reaction (Liu et al., 2007). It also remains possible that the bulk of the H_2O_2 at CWAs is converted to $OH^{\cdot}$, and that the DAB is oxidized by $OH^{\cdot}$, rather than H_2O_2, to produce the observed color reaction. This line of reasoning is

supported by the EPR spectrum of inoculated wheat leaves, which showed a strong free radical peak mixed with low spin Fe^{3+}. While DFO is unable to chelate iron from iron-containing peroxidase, studies have shown increases in peroxidase gene transcription (Liu et al., 2005) and peroxidase protein localization (Scott-Craig et al., 1995) in powdery mildew-challenged epidermal tissue. These induced peroxidases are likely producing H_2O_2 in challenged plants, suggesting either that the peroxidase activity alone is not enough to oxidize a visible amount of DAB or that iron is loaded into peroxidases at the cell wall, a process necessary for enzyme activity (Passardi et al., 2004), and that DFO blocks this iron loading. Regardless of the chemistry by which it occurs, the blocking of CWA-associated H_2O_2 generation by DFO shows that iron is essential for the oxidative burst. Much of the power of this hypothesized system of ROS generation lies in the rigid localization of iron and H_2O_2 within CWAs; in response to *Bgt* attack, H_2O_2 accumulation is highly focused to the points of attack.

2.4 Materials and Methods

2.4.1 Plant and pathogen materials

The powdery mildew isolate (*Blumeria graminis* f. sp. *tritici*) was originally isolated from the hexaploid wheat field cultivar Conway in Saskatoon, SK and maintained on the same cultivar under greenhouse conditions. Over 150 accession lines of the diploid wheat *Triticum monococcum* L. (AA genome) were screened for susceptibility to the powdery mildew fungus. Plants were grown in a chamber with a cycle of 16 h light and 8 h dark at 20°C. One most susceptible line (Line 441) was used throughout this study. For inoculation, the first leaves of *T. monococcum* plants were placed on a plastic plate with the abaxial side up and mildewed plants were shaken above the leaf surface (Thordal-Christensen and Smedegaard-Petersen, 1988).

2.4.2 Metal element analysis

The metal contents were determined using a PQ II Turbo$^+$ quadrupole inductively coupled plasma mass spectrometer (ICPMS) (VG Elemental, Cambridge, UK) at the

University of Saskatchewan Geology Department. Samples 24 hpi with *Bgt* were powdered by grinding in liquid N_2, dried overnight at 70°C, and then digested completely in 70% (v/v) HNO_3 at 120°C. Before analysis, solutions were diluted by a factor of 100, and indium and bismuth were added to aliquots as internal standards for drift correction.

2.4.3 Histological staining and light microscopy

Staining of iron in *Bgt*-infected epidermal cells was adapted from the method described by Smith et al (1997), which is based on the Prussian blue reaction and has been used clinically for diagnosis of diseases characterized by iron overload within animal tissues. Briefly, epidermal peels from wheat and other monocot plants were fixed in methanol:chloroform:acetic acid at 4°C for 15 h, followed by an ascending ethanol dehydration. After rehydration through graded ethanol, leaf epidermal tissues were incubated for 15-30 h in 7% (w/v) potassium ferrocyanide (for Fe^{3+} detection) or 7% (w/v) potassium ferricyanide (for Fe^{2+} detection) in aqueous hydrochloric acid (3%). For detection of oxidative burst, mainly H_2O_2, we used the method described in Thordal-Christensen et al., (1997). For double detection of iron and H_2O_2, we performed DAB staining first and then Prussian blue staining. No obvious interference was found in this sequential double staining method.

2.4.4 Confocal microscopy for calcein fluorescence

For the determination of chelatable iron in CWAs, leaf epidermis 24 hpi was incubated in 1.5 mM calcein (Molecular Probes, Eugene, OR) for 20 min. The iron-mediated fluorescence quenching was recorded by confocal laser scanning microscopy (LSM 510, Zeiss, Oberkochen, Germany) (Petrat et al., 2001) with excitation/emission at 488/515 nm and 1 % argon laser output. Immediately after the fluorescence measurements, the labile iron was removed from calcein by adding 10 mM DFO to the sample and incubating for 30 min.

2.4.5 Electron paramagnetic resonance (EPR) spectroscopy

EPR experiments were performed on a Bruker EMX spectrometer equipped with an oxford cryostat (Billerica, MA) at the Saskatchewan Structural Sciences Centre (Saskatoon). Samples were packed into 3mm id quartz tubes that were screened for background signal. The 4.2 K EPR experiments were conducted with the spectrometer frequency at 9.39 GHz, sweep width 3000 G, modulation amplitude of 1 G, power 2 mW, 100 KHz modulation frequency, gain 2 x 10^4, and 12 scans at 335 sec/scan. High resolution EPR experiments were conducted at 10 K and at 50 K with the spectrometer frequency at 9.39 GHz, sweep width 40 G, modulation amplitude of 0.3 G, power 2 mW, 100 KHz modulation frequency, gain 2 x 10^5, and 12 scans at 83 sec/scan.

2.4.6 Cytochalasin A and DFO treatment for cytological observations

The cut ends of primary leaves of 7-day-old wheat leaves 0.5 hpi with *Bgt* were immersed in a solution of 0.1-10 μg/ml cytA for 24 h before staining for iron with Prussian blue; or in 0.1-10 mM DFO for 6 h before the addition of DAB for an additional 17.5 h.

CHAPTER 3

CHANGES IN IRON HOMEOSTASIS MEDIATE DEFENCE GENE TRANSCRIPTION[1]

[1]This chapter is based on supplementary data from the following paper:

Liu, G.*, Greenshields, D.L.*, Sammynaiken, R., Hirji, R., Selvaraj, G., and Wei, Y. (2007). Targeted alterations in iron homeostasis underlie plant defense responses. Journal of Cell Science *120*, 596-605. **Contributed equally*

I performed all of the experimental work except as noted below:

Guosheng Liu performed the RNA gel blots collaboratively with me and contributed to experiments not described in this chapter.

Ramaswami Sammynaiken contributed to experiments not described in this chapter.

Rozina Hirji contributed to experiments not described in this chapter.

Gopalan Selvaraj planned experiments, contributed novel materials not described in this chapter and acted in a supervisory role.

Yangdou Wei planned experiments and acted in a supervisory role.

3.1 Introduction

In order to effect changes in dynamic cellular processes, a signal must be perceived, relayed and recognized. In the previous chapter, I showed that during powdery mildew attack, free, reactive iron is secreted to the apoplast where it mediates the oxidative burst. Here, I examine the consequences of this massive redirection of cellular iron on host gene transcription.

Iron homeostasis in plants is regulated at both the organismal and cellular levels. In response to iron deficiency, graminaceous plants secrete phytosiderophores of the mugineic acid family, which bind soil iron and take it up for distribution throughout the plant (Mori, 1999). Recently, a mugineic acid transporter was cloned from barley and showed root epidermal cell-specific expression during growth under iron deficiency (Murata et al., 2006). Although the pathways leading to mugineic acid synthesis and transport are now well-characterised, little is known about plant responses to iron overload. In animals, iron toxicity is well-known and iron overload has been linked to several important diseases including Alzheimer and Parkinson's diseases (Molina-Holgado et al., 2007), as well as minor conditions like varicose veins (Zamboni et al., 2006). In neurodegenerative diseases, iron is toxic through its ability to produce reactive oxygen species (ROS) at sites where it accumulates (Smith et al., 1997; Hentze et al., 2004; Molina-Holdago et al., 2007). As shown in Chapter 2, iron accumulation is also responsible for localised ROS production in cereals.

To gain insights into the effects of iron-related diseases on human gene expression, Muckenthaler et al. (2003) designed a specialised cDNA microarray comprised of gene targets selected for their association with iron metabolism, or related pathways like oxidative stress and nitric oxide metabolism. Hybridisation of the array with hemin-, ferric ammonium citrate-, sodium nitroprusside-, H_2O_2- or deferroxamine-treated cell RNA revealed interesting links between oxidative and nitrosative stress and iron metabolism. We reasoned that by creating treatment conditions that mimicked the apoplastic iron accumulation observed following powdery mildew attack, we too could isolate iron-specific gene expression responses and gain insight into the transcriptional consequences of this mode of defence.

3.2 Results

3.2.1 Building the RedoxArray

To examine the effect of iron loading on gene expression in wheat, we searched for genes from several functional categories in a 3000 clone expressed sequence tag (EST) library that had been previously developed (described in Greenshields et al., 2004a; Liu et al., 2005). The genes were chosen based on EST homology to known genes in other species. We developed a nylon macroarray platform for analysis of gene expression because it allows for simultaneous examination of hundreds of samples; the array is referred to as RedoxArray hereafter. Because we specifically wanted a snapshot of redox- or iron homeostasis-related gene expression, genes from this functional category made up 52% of the RedoxArray targets. The other functional categories represented on the RedoxArray are listed in Figure 3.1. Together, 187 cDNAs were represented as 198 array features. Each cDNA was amplified from plasmid inserts with PCR, and these PCR products were spotted onto a nylon membrane as described in section 3.4.4.

3.2.2 Iron overload induces expression of defence- and iron homeostasis-related genes

To test the effects of iron accumulation on gene expression, we set up a regime of iron treatment that could mimic the accumulation of iron and the accompanying apoplastic H_2O_2 production in wheat leaves (Figure 3.2). Following 24 h of treatment with 500 μM Fe-EDTA, inductively coupled plasma mass spectrometry revealed that wheat leaves accumulated about 400 μg iron per-gram-dry-weight of wheat leaf tissue. This treatment also produced an oxidative burst restricted to the cell walls of treated plants. We harvested mRNA from the treated plants, labelled it with ^{32}P, and used it to probe the RedoxArray. As a control, we treated plants with 500 μM EDTA and used mRNA from that treatment to hybridise the RedoxArray. Table 3.1 shows the mean expression and induction of genes following iron treatments. As expected, several iron homeostasis-related genes including gene encoding ferritin, nicotianamine synthase and metallothionein were among the most highly induced genes following the iron overload

treatment. Interestingly though, several pathogenesis-related (*PR*) genes were also highly induced by the iron treatment; genes encoding PR-4, PR-5, glutathione S transferase and endochitinase were the four most highly induced transcripts.

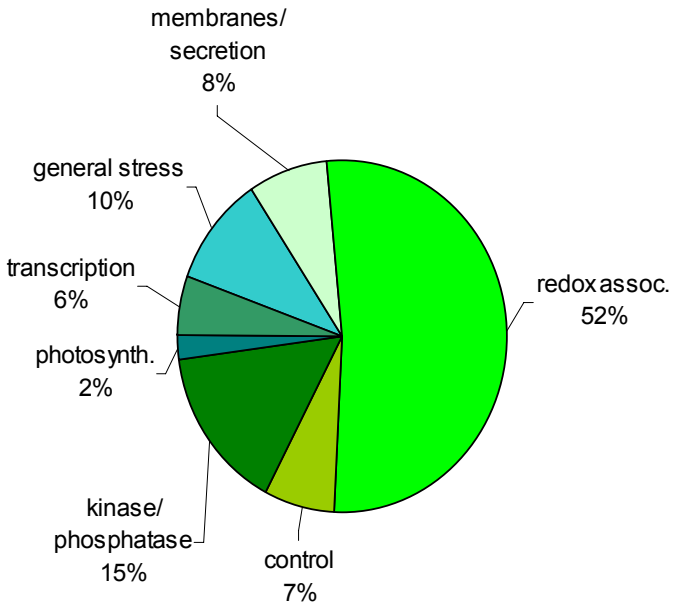

Figure 3.1 Functional categories of genes represented on the RedoxArray. One hundred eighty seven cDNAs from the indicated functional categories were identified from a powdery mildew-infected wheat epidermis EST collection, amplified from plasmids and spotted onto nylon membranes to create a 198-feature array.

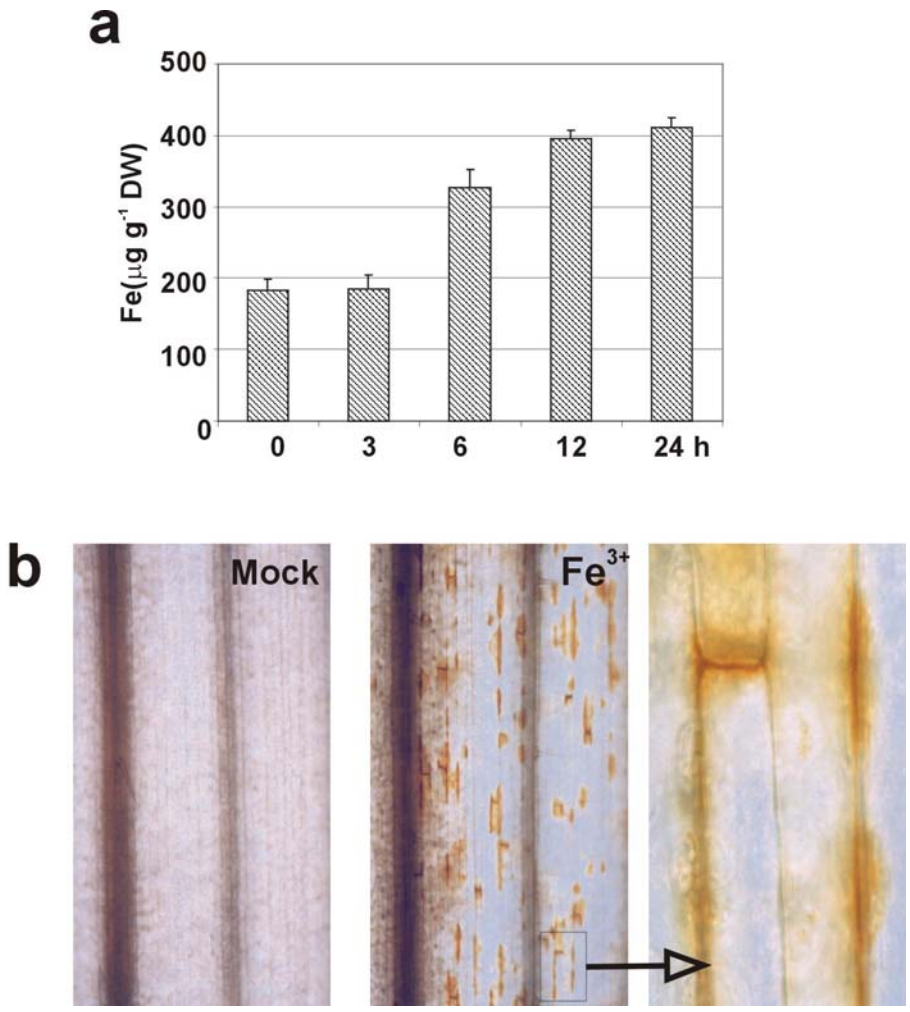

Figure 3.2 Iron overload induces an apoplastic oxidative burst. (a) Inductively coupled mass spectrometry analysis of Fe^{3+}-EDTA uptake in wheat seedlings. Values represent mean ± SE (n=3). DW=dry weight. **(b)** Diaminobenzidine staining for H_2O_2 in wheat leaves 12 h after treatment with either 500 μM Fe3+-EDTA (middle and right panels) or 500 μM EDTA (Mock, left panel). Arrow shows magnified view of box highlighting apoplastic H_2O_2.

Table 3.1 Gene expression in *Triticum monococcum* following iron loading.

Clone number	Accession number	Name	Expression level	Fold change[a]	Closest BLASTx hit	e-value
1561	DR432330	THAUMATIN-LIKE PROTEIN, PR-5	1.8	19.5 ± 5.4	T06790	3.00E-97
2990	DR432232	PR-4,	17.9	19.1 ± 1.3	AAT67050	2.00E-68
3007	DR432334	GLUTATHIONE S-TRANSFERASE	21.6	17.5 ± 1.6	CAC94005	1.00E-52
569	DR432293	ENDOCHITINASE	1.9	16.6 ± 1.8	CAA53626	1.00E-67
461	DR432282	FERRITIN	5.1	15.3 ± 1.7	AAT67051	2.00E-116
2535	DR432205	NICOTIANAMINE SYNTHASE	23.0	13.5 ± 0.2	Q9XFB7	2.00E-46
2853	DR432223	GERMIN-LIKE PROTEIN 4	4.3	12.6 ± 1.8	AAT67049	1.00E-95
669	DR432302	METALLOTHIONEIN	34.7	10.6 ± 0.3	AAT99566	4.00E-12
2534	DR432204	BAX INHIBITOR	3.4	9.7 ± 2.2	CAC37797	1.00E-16
2381	DR432196	PR-2, B-1,3-ENDOGLUCANSE	17.6	9.5 ± 0.9	CAA77085	2.00E-77
2732	DR432218	GERMIN-LIKE PROTEIN 4	10.7	9.5 ± 2.2	AAT67049	4.00E-67
2534	DR432204	BAX INHIBITOR	17.3	8.6 ± 1.5	CAC37797	1.00E-16
3283	DR432247	PR-1B	26.4	8.4 ± 0.1	CAA07473	1.00E-78
1029	DR432310	BARLEY STEM RUST RESISTANCE PROTEIN	14.9	8.0 ± 0.8	AAM81980	3.00E-42
420	DR432280	METALLOTHIONEIN	28.0	8.0 ± 0.2	AAT99566	4.00E-12
2135	DR432193	PEROXIDASE 8	6.7	7.4 ± 1.5	AAW52722	3.00E-75
825	DR432305	UDP-GLUCOSE: FLAVONOID 7-O-GLUCOSYLTRANSFERASE	4.7	7.1 ± 2.1	BAB17061	3.00E-92
1098	DR432326	CALMODULIN	12.6	7.0 ± 0.5	P62162	1.00E-67
886	DR432173	SAM DECARBOXYLASE	41.2	6.8 ± 0.3	CAC09522	5.00E-25
1262	DR432177	DISULPHIDE ISOMERISE	9.2	6.7 ± 0.9	CAC21230	4.00E-52
3086	DR432335	GLYCOGENIN	6.8	6.3 ± 1.5	BAD23777	3.00E-34
2296	DR432195	CATALASE	12.5	6.1 ± 0.7	Q43206	1.00E-125
620	DR432298	PEROXIDASE 6	5.4	6.1 ± 0.4	AAW52720	2.00E-177
2692	DR432215	MULTIDRUG RESISTANCE-ASSOCIATED PROTEIN	10.0	5.8 ± 0.5	AAL47686	5.00E-28
1012	DR432309	PROTEIN KINASE	10.8	5.8 ± 0.2	AAK02024	2.00E-29
BD6	DR432266	HEAT SHOCK PROTEIN COGNATE 70	27.2	5.6 ± 0.4	XP_470141	2.00E-98
201	DR432274	GERMIN LIKE PROTEIN 4	6.8	5.5 ± 1.9	AAT67049	1.00E-77
BA6	DR432261	BETA-D-GLUCAN EXOHYDROLASE	25.7	5.5 ± 0.4	AAD23382	4.00E-78
1102	DR432327	PEROXIDASE 2	6.6	5.5 ± 1.2	AAW52716	7.00E-161
1003	DR432307	SERINE/THREONINE KINASE RECEPTOR PRECURSOR	11.9	5.2 ± 0.1	BAC83192	8.00E-53
3027	DR432234	RECEPTOR-LIKE KINASE	27.6	5.1 ± 0.9	BAD53342	6.00E-55
3153	DR432242	RICE MAPK2 HOMOLOGUE	20.5	5.1 ± 0.4	AAF61238	4.00E-89
2812	DR432221	THAUMATIN-LIKE PROTEIN	11.7	5.1 ± 0.8	CAA41283	5.00E-88
1036	DR432314	BLUE COPPER-BINDING PROTEIN	13.6	5.0 ± 0.6	AAD10251	5.00E-47
1309	DR432183	PM ATPASE	19.6	4.9 ± 0.2	AAN15220	3' UTR
3314	DR432250	CYTOCHROME P450	15.1	4.9 ± 0.3	AAK38092	1.00E-76
3556	DR432253	PM ATPASE	14.7	4.8 ± 0.8	AAV71150	1.00E-130
2274	DR432194	GLYCOLATE OXIDASE	36.3	4.8 ± 0.3	AAB82143	9.00E-14
1043	DR432316	NTPRP27-LIKE SECRETED PROTEIN	16.2	4.8 ± 0.6	AAD46133	4.00E-67
3522	DR432252	PM ATPASE	21.0	4.7 ± 0.4	P83970	8.00E-63
1009	DR432308	SENESCENCE-ASSOCIATED PROTEIN-LIKE	20.0	4.7 ± 0.3	BAD28022	2.00E-27
2980	DR432228	33KD SUBUNIT OF OXYGEN EVOLVING COMPLEX OF PSII	21.0	4.6 ± 0.2	BAB64069	3.00E-94
607	DR432296	CYTOCHROME C1 PRECURSOR	2.7	4.6 ± 1.1	BAB64199	7.00E-44
24	DR432269	XANTHINE DEHYDROGENASE	3.3	4.5 ± 0.9	AAT81740	7.00E-48
2017	DR432191	PUTATIVE ACONITASE	11.1	4.4 ± 0.2	BAD05751	3.00E-91
399	DR432277	PEROXIDASE 7	13.8	4.4 ± 1.0	AAW52721	0.00E+00
491	DR432289	PLASTIDIC 2-OXOGLUTARATE/MALATE TRANSPORTER	6.9	4.4 ± 0.4	BAD06219	9.00E-28
194	DR432273	HEAT SHOCK FACTOR RHSF3	3.3	4.3 ± 0.7	AAQ23057	2.00E-78
389	DR432276	CALNEXIN	5.4	4.3 ± 1.0	T03251	1.00E-87
2616	DR432207	PR1-B	10.9	4.3 ± 0.6	CAA07473	3.00E-77
2661	DR432211	SAM SYNTHASE	4.4	4.3 ± 1.2	P50299	7.00E-98
1079	DR432322	ACONITASE	8.3	4.3 ± 0.6	AAL13084	9.00E-109
2508	DR432203	PHOSPHORIBULOKINASE	5.4	4.3 ± 0.2	S16585	3.00E-66
674	DR432304	PSEUDO-RESPONSE REGULATOR 1	22.9	4.1 ± 0.2	BAD38854	2.00E-61
1093	DR432325	METALLOTHIONEIN	25.0	4.0 ± 0.1	AAP80616	2.00E-08
AC8	DR432255	GLUTATHIONE PEROXIDASE	39.0	3.9 ± 0.1	AAQ64633	1.00E-90
2930	DR432225	PEROXIDASE 5	10.4	3.9 ± 0.4	AAW52719	5.00E-99
655	DR432301	GLUTATHIONE S-TRANSFERASE	12.2	3.8 ± 0.2	CAC94005	1.00E-104
1072	DR432320	ACTIN-DEPOLYMERIZING FACTOR 5	12.0	3.8 ± 0.0	AAM63761	4.00E-38
2595	DR432206	FERREDOXIN	50.9	3.8 ± 0.1	P00228	7.00E-35
962	DR432306	PEROXIDASE 3	20.0	3.7 ± 0.1	AAW52717	3.00E-159
BA12	DR432260	GLUTATHIONE S-TRANSFERASE	15.3	3.7 ± 0.4	P30110	4.00E-67
1077	DR432321	PROTEIN KINASE-LIKE	10.0	3.5 ± 0.9	BAD73350	2.00E-57

Clone number	Accession number	Name	Expression level	Fold change[a]	Closest BLASTx hit	e-value
1067	DR432319	NODULIN 3	15.6	3.4 ± 0.2	CAA69976	3.00E-42
384	DR432275	CYDOPHILIN A	34.9	3.3 ± 0.1	AAK49428	4.00E-89
2779	DR432220	AAC OXIDASE	19.7	3.2 ± 0.2	AAC28488	5.00E-97
464	DR432283	LRR-CONTAINING F-BOX PROTEIN, COI1-LIKE	5.7	3.2 ± 0.2	AAU90110	5.00E-52
3045	DR432239	PROTEIN PHOSPHATASE 2C	13.5	3.1 ± 0.2	CAE03557	7.00E-54
3180	DR432243	FERULATE-5-HYDROXYLASE	5.3	3.1 ± 0.4	AAG13555	4.00E-43
1279	DR432180	LRR RECEPTOR-LIKE PROTEIN KINASE	6.0	3.1 ± 1.0	BAD27618	2.00E-62
480	DR432286	MITOGEN-ACTIVATED PROTEIN KINASE ERK1-LIKE	4.9	3.1 ± 1.0	BAD72351	1.00E-118
1284	DR432181	CHLOROPHYLL A/B BINDING	48.0	3.1 ± 0.0	CAA44777	2.00E-92
1313	DR432184	SEC24, OXIDATIVE STRESS PROTECTION	12.8	3.0 ± 0.2	Q9M291	5.00E-20
1064	DR432318	CALCIUM-DEPENDENT PROTEIN KINASE, ISOFORM 2	17.7	2.9 ± 0.3	P53683	3.00E-98
BC2	DR432264	CYTOCHROME P450, IN DIBOA BIOSYNTHESIS	10.2	2.9 ± 0.2	BAD08937	1.00E-60
481	DR432287	ANTIOXIDANT CEO PROTEIN	9.1	2.9 ± 0.5	AAL58179	3.00E-71
473	DR432284	RECEPTOR-LIKE PROTEIN KINASE	7.9	2.9 ± 0.2	AAP52678	2.00E-09
S-15	DR432337	PEROXIDASE 10	11.3	2.8 ± 0.3	AAW52724	2.00E-177
3198	DR432245	GLUTATHIONE PEROXIDASE	29.0	2.7 ± 0.0	AAQ64633	9.00E-76
498	DR432290	LEA-LIKE	8.1	2.7 ± 0.2	AAS07355	4.00E-51
2669	DR432214	METHYLENETETRAHYDROFOLATE REDUCTASE	10.3	2.7 ± 0.3	AAD51733	2.00E-85
403	DR432278	CLATHRIN HEAVY CHAIN	11.2	2.7 ± 0.4	T06779	2.00E-117
2224	DR432333	GLUTATHIONE S-TRANSFERASE	21.9	2.6 ± 0.1	AAK66773	6.00E-107
3308	DR432249	METALLOTHIONEIN, ALUMINUM INDUCIBLE	89.4	2.6 ± 0.0	P43400	1.00E-12
2643	DR432209	NADH MONOHYDROASCORBATE REDUCTASE	10.5	2.6 ± 0.1	BAD09086	2.00E-84
1246	DR432176	PR-2, B-1,3-ENDOGLUCANASE	10.2	2.5 ± 0.2	BAB85436	4.00E-47
1268	DR432179	ATPASE	8.9	2.5 ± 0.2	AAT44305	2.00E-42
1263	DR432178	CALCINURIN-B LIKE	8.7	2.4 ± 0.2	AAM91028	1.00E-71
482	DR432288	PUTATIVE MULTIPLE STRESS-RESPONSIVE ZINC-FINGER PROTEIN	7.1	2.4 ± 0.5	BAD35553	4.00E-75
670	DR432303	CLASS III CHITINASE RCB4	5.6	2.4 ± 0.6	AAK26395	5.00E-49
2490	DR432202	HR PROTEIN HIR1	6.9	2.4 ± 0.1	AAN17457	1.00E-118
1031	DR432312	COATOMER PROTEIN COMPLEX, SUBUNIT BETA 2	11.7	2.4 ± 0.0	BAD25014	7.00E-95
553	DR432291	PEROXIREDOXIN Q	16.7	2.4 ± 0.2	AAV66923	9.00E-44
1173	DR432188	GP91PHOX, ARABIDOPSIS GP91PHOX-D	11.3	2.4 ± 0.2	BAB70751	3.00E-74
645	DR432300	GTPASE ACTIVATOR	7.2	2.3 ± 0.3	BAD33761	3.00E-22
626	DR432299	CHLOROPHYLL A/B BINDING	32.0	2.3 ± 0.1	CAA44777	1.00E-87
172	DR432271	HSP70-LUMENAL BINDING	6.0	2.3 ± 0.2	T05741	3.00E-34
414	DR432279	PEROXIDASE 9	7.0	2.2 ± 0.2	AAW52723	1.00E-113
3043	DR432238	UBIQUITIN-CONJUGATING ENZYME	6.4	2.2 ± 0.4	NP_566563	3.00E-75
1286	DR432182	14-3-3 PROTEIN, WPK4(SNF1) BINDING PROTEIN	7.1	2.1 ± 0.7	BAB11739	9.00E-98
2943	DR432227	PROTEIN PHOSPHATASE TYPE2C	7.6	2.1 ± 0.1	BAC16709	6.00E-86
586	DR432294	CALMODULIN	7.9	2.1 ± 0.1	AAC49583	3.00E-45
2410	DR432197	COLBALAMIN-INDEPENDENT MET-SYNTHASE	10.0	2.0 ± 0.3	BAD34660	2.00E-37
BF1	DR432267	PEROXIDASE 4	29.8	1.9 ± 0.1	AAW52718	6.00E-63
2865	DR432224	GLUTATHIONE REDUCTASE	18.1	1.9 ± 0.4	AAQ64632	1.00E-113
842	DR432172	CHALCONE SYNTHASE	0.1	1.9 ± 0.5	AAQ19322	4.00E-90
BD4	DR432265	GLUTAREDOXIN	20.7	1.9 ± 0.0	BAD89485	3.00E-43
1189	DR432190	PEROXIDASE 1	10.6	1.8 ± 0.1	AAW52715	1.00E-81
1174	DR432189	NUCLEOTIDE PYROPHOSPHATASE	10.4	1.8 ± 0.2	CAE46394	1.00E-129
1159	DR432187	CHAPERONE	6.1	1.8 ± 0.3	NP_910052	1.00E-65
1087	DR432324	ZINC FINGER PROTEIN	9.6	1.8 ± 0.2	BAD13036	4.00E-61
601	DR432295	BASAL TRANSCRIPTION FACTOR SNAPC	3.0	1.8 ± 0.5	XP_476599	4.00E-61
1040	DR432315	ABA INDUCED PROTEIN KINASE	7.3	1.7 ± 0.3	AAW49219	2.00E-68
2987	DR432230	WCI5	75.1	1.7 ± 0.0	T06278	4.00E-20
1032	DR432313	SERINE/THREONINE-SPECIFIC PROTEIN KINASE -LIKE	11.5	1.6 ± 0.2	BAD61459	9.00E-99
3295	DR432248	FATTY ACID ALPHA-OXIDASE	4.6	1.6 ± 0.2	AAF64042	1.00E-102
2696	DR432216	PEROXIDASE 1	25.2	1.6 ± 0.1	AAW52715	9.00E-84
1033	DR432174	QUINONE REDUCTASE 2	20.7	1.5 ± 0.0	NP_916411	7.00E-79
2981	DR432229	WRKY TRANSCRIPTIONAL FACTOR 39	10.3	1.5 ± 0.4	AAK96198	3.00E-37
2663	DR432213	QUINONE REDUCTASE 1	18.3	1.5 ± 0.1	AAX81879	9.00E-35
AF1	DR432256	CYTOSOLIC PYRUVATE KINASE	8.6	1.5 ± 0.1	AAN31877	5.00E-56
2989	DR432231	PUTATIVE DEVELOPMENTAL PROTEIN SINAT5	20.6	1.5 ± 0.1	BAD30685	1.00E-100
3504	DR432251	CU/ZN SUPEROXIDE DISMUTASE	21.4	1.5 ± 0.1	AAB67990	4.00E-55
476	DR432285	BRASSINOSTEROID INSENSITIVE 1 PRECURSOR	7.3	1.4 ± 0.1	XP_479008	1.00E-30
3233	DR432246	NADPH-CYTOCHROME P450 REDUCTASE	7.8	1.4 ± 0.1	AAG17471	1.00E-132
1047	DR432317	DNAJ	16.1	1.4 ± 0.1	AAT75262	5.00E-83
1120	DR432328	SEC61	7.8	1.4 ± 0.2	AAF80449	6.00E-105
2662	DR432212	LIPOXYGENASE	5.4	1.3 ± 0.4	BAD10665	1.00E-65
2126	DR432192	PAL	9.7	1.3 ± 0.1	CAA89007	1.00E-125
1130	DR432186	METAL-TRANSPORTING P-TYPE ATPASE	45.6	1.3 ± 0.0	XP_483048	3.00E-62
2938	DR432226	ALTERED RESPONSE TO GRAVITY	0.1	1.2 ± 0.4	XP_467717	3.00E-67

Clone number	Accession number	Name	Expression level	Fold change[a]	Closest BLASTx hit	e-value
BB9	DR432263	IRON-PHYTOSIDEROPHORE TRANSPORTER PROTEIN	15.0	1.2 ± 0.1	CAE05719	1.00E-107
3566	DR432254	FERREDOXIN-DEPENDENT GLUTAMATE SYNTHASE	15.5	1.2 ± 0.1	S67499	1.00E-106
1085	DR432323	PROTEIN KINASE XA21	9.4	1.2 ± 0.1	BAD12988	2.00E-41
154	DR432270	ARIADNE-LIKE PROTEIN ARI2	7.8	1.2 ± 0.2	CAD52884	1.00E-56
421	DR432281	GAMYB-BINDING PROTEIN	8.3	1.2 ± 0.1	AAO25540	8.00E-125
2448	DR432199	THIOREDOXIN PEROXIDASE	19.0	1.1 ± 0.1	AAC78473	1.00E-77
3028	DR432235	WRKY TRANSCRIPTIONAL FACTOR	14.8	1.1 ± 0.0	DAA05110	7.00E-28
1202	DR432329	GLUTATHIONE S-TRANSFERASE	13.6	1.1 ± 0.2	AAM12304	1.00E-37
3065	DR432240	CALRECTULIN	14.7	1.1 ± 0.1	BAC06263	6.00E-47
3148	DR432241	ZINC FINGER PROTEIN	11.1	1.0 ± 0.1	BAD46368	2.00E-83
3507	DR432336	GLUTATHIONE S-TRANSFERASE	11.2	1.0 ± 0.1	CAC94004	4.00E-32
BB5	DR432262	FERRIDOXIN-DEPENDENT GLUTAMATE SYNTHASE	15.7	0.9 ± 0.1	BAD31105	1.00E-110
2832	DR432222	SEC13	2.8	0.9 ± 0.2	BAB83081	1.00E-112
615	DR432297	PENTAMERIC POLYUBIQUITIN	39.6	0.9 ± 0.0	CAA54603	5.00E-83
3032	DR432236	PROTEIN KINASE FAMILY PROTEIN	12.3	0.9 ± 0.1	NP_189116	3.00E+74
3038	DR432237	LRR-CONTAINING F-BOX PROTEIN (COI1)	9.0	0.9 ± 0.2	AAO38719	6.00E-25
2211	DR432332	DISULPHIDE ISOMERISE	21.1	0.8 ± 0.2	AAV32227	6.00E-63

[a]Fold change: mean ± standard deviation

3.2.3 Iron overload induces gene expression through iron-dependent and iron-independent pathways

To validate the RedoxArray data, we performed RNA gel blots using a group of the iron-responsive genes from the array, including iron homeostasis-related (*TmFer1* and *TmNAS3*) and *PR* (*TmPR1b, TmPR5* and *TmGLP4*) genes (Figure 3.3a). To examine the dependence of gene induction on iron concentration, we used the same set of iron-responsive genes to probe RNA from wheat leaves incubated in increasing concentrations of iron. Figure 3.3b shows that while the iron homeostasis-related genes are up-regulated gradually in response to each increase in iron concentration, the defence-related *PR* genes required 500 μM Fe^{3+}-EDTA for activation. To investigate the specificity of iron homeostasis and defence-related gene expression by metal treatments we substituted the iron with calcium, magnesium, copper, or zinc (Figure 3.3b). While *TmFER1* and *TmNAS3* expression was induced by magnesium, the *PR* genes were induced mainly by copper. Because the *PR* genes assayed were expressed in high concentrations of copper and iron, we hypothesized that it was the metal treatment-induced production of ROS, rather than the metals themselves, which was responsible for the gene induction. To evaluate this hypothesis, we pretreated plants with the redox buffer glutathione (GSH) for 6 h before treating them with either iron or H_2O over a 24 h time course. Figure 3.3c shows that iron-mediated induction of *TmFER1* and *TmNAS3* expression occurs regardless of the redox status of the plants, whereas *PR* gene

expression is abolished by suppressing the iron-mediated oxidative burst. Together, these results show that iron overload regulates gene expression through both direct (Fe-dependent) and indirect (ROS-dependent) pathways.

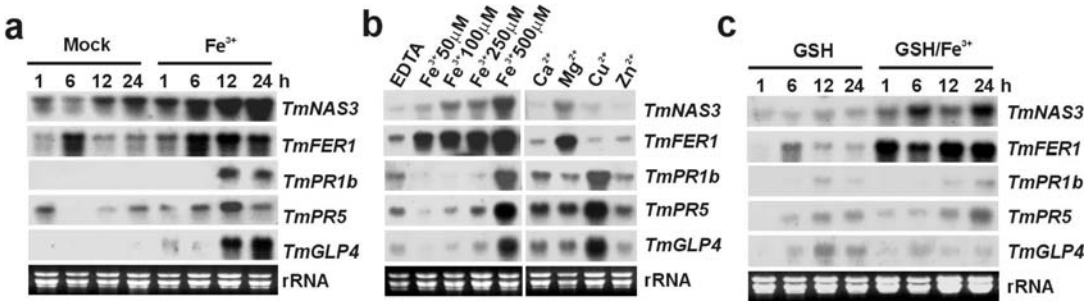

Figure 3.3 Iron loading controls gene expression through iron- and redox-specific pathways. (a) RNA gel blot analysis of time-dependent induction of iron homeostasis- and defence-related genes following loading with 500 µM EDTA (Mock) or 500 µM Fe-EDTA at the time points indicated. Even loading of total RNA was monitored by ethidium bromide staining of RNA. **(b)** RNA gel blot analysis of iron concentration- and metal-dependent gene expression. **(c)** RNA gel blot analysis of iron-dependent and ROS-dependent gene expression. GSH = reduced glutathione.

3.3 Discussion

3.3.1 The RedoxArray

cDNA and oligonucleotide arrays have become widely accepted tools in gene expression experiments. Although commercially available glass microarray chips are more commonly used than larger nylon macroarrays, the sensitivity and accuracy of either platform is comparable (Bertucci et al., 1999), and the latter can be prepared in-house without specialised equipment or expertise. We chose to construct the targeted RedoxArray because of an overrepresentation of redox-related transcripts in our EST collection and previous findings concerning iron accumulation during powdery mildew attack.

Before spotting onto the nylon membrane, concentrations of the PCR products were equalised to ensure even signals between treatments. Despite this precaution, the

mean expression levels of a given gene within replicates of a treatment were sometimes different, and we interpreted this as a difference in target concentration. For example, *PR-4* expression varied by about 16% between the four EDTA treatments. When there is an excess of target, as one would expect when using 20 ng of target per feature, the hybridisation signal varies linearly with target amount (Bertucci et al., 1999). To reduce the effect of these differences, we applied a mean shifting normalisation technique to the replicate data of a single treatment. By using this technique, the means of each array are centred and the expression value of a given gene in each replicate is thereby centred towards the mean expression value of all replicates within a treatment.

Nearly all of the genes on the array were induced following iron treatment. This could be accounted for in several ways. It is possible, however unlikely, that we did an excellent job in selecting gene targets that respond to iron. A more likely scenario is that the control (EDTA) and iron (Fe-EDTA) treatments are in fact opposing treatments; EDTA is an iron chelator, which could work to lower the overall free iron status of the treated plant. This could be investigated further by adding a distilled water treatment control to compare to the EDTA and iron treatments.

3.3.2 Transcriptional regulation by iron overloading

Extensive work in animal systems has revealed a complex regulatory network for iron homeostasis at the cellular and systemic levels (Muckenthaler et al., 2003; Hentze et al., 2004). Cellular iron uptake and storage are coordinately controlled by binding of Fe-regulatory proteins (IRP), IRP1 and IRP2, to iron-responsive elements (IREs) within the mRNAs (5'- or 3'-UTR) encoding ferritin and the transferrin receptor (TfR), thus mediating regulation at post-transcriptional level. In plants, no such a regulation system has yet been found and iron-homeostasis genes appear to be both transcriptionally and post-transcriptionally controlled (Briat et al., 1999; Petit et al., 2001). Here, we showed that iron overload controls the expression of many *T. monococcum* genes. Interestingly, some of the most highly induced genes following iron treatment were related to defence against pathogens. While the iron homeostasis-related genes *FER1* and *NAS3* showed gradual, concentration-dependent induction, the defence-related genes were only expressed when the plants were exposed to high concentrations of iron, suggesting that

iron itself is not directing transcription of this latter class of genes. The ability of copper loading to induce defence-related gene expression to similar levels as the iron treatment also suggested that defence gene induction by iron could be related to iron-mediated ROS, rather than as a response to the iron itself. Indeed, copper and iron are both able to participate in Fenton/Haber-Weiss chemistry leading to the production of ROS (Schützendübel and Polle, 2002; Valko et al., 2005). The role of copper in ROS production *in vivo* remains unclear because the amount of free copper within plants has not been established; in yeast, it has been estimated that there is less than one free copper ion per cell (Rae et al., 1999), suggesting that copper itself has little effect on ROS production. Using a differential display technique, Hamel et al. (1998) found that expression of defence-related genes was induced following aluminum treatment of *T. aestivum* roots. As in our iron treatment, a germin-like gene was also among the most highly expressed following this aluminum treatment. While aluminum itself does not participate in ROS-generation, it has been shown to exacerbate iron-induced ROS production (Alexandrov et al., 2005; Kapiotis et al., 2005) and this could account for the overlapping gene induction.

The most definitive evidence for the role of iron-mediated ROS in defence gene induction shown here was the absence of iron induction when plants were pre-treated with GSH. GSH is a redox buffer that has been shown to limit the toxic effects of ROS (Noctor et al., 2002; Noctor, 2006). We reasoned that by increasing the cellular (and possibly extracellular) reductant pool by treating the plants with an excess of GSH, we could disarm the majority of the ROS produced during iron overload. GSH provides the reducing power used by ROS consuming enzymes including peroxidases and it can be coupled to other reactive molecules through the action of glutathione-S-transferase (Noctor, 2006). Metallothioneins, small cysteine-rich metal binding proteins, have been shown to scavenge reactive oxygen species (Wong et al., 2004), presumably through a disulfide bridge formation mechanistically similar to GSH/GSSG cycling. Two metallothionein ESTs (DR432280 and DR432302) representing the same gene and similar to a cadmium-binding metallothionein from *T. durum* (Bilecen et al., 2005), were expressed at over 8-times control levels following the iron treatment. The dual metal

binding and ROS scavenging properties of metallothioneins make it unclear which exact function this protein is playing during iron overload.

In Chapters 2 and 3, I showed that: powdery mildew attack causes iron accumulation in the epidermal apoplast; accumulation of apoplastic iron mediates the H_2O_2 production during pathogen attack; and iron accumulation directs the transcription of defence-related genes through H_2O_2 production. It remains unclear how the iron-mediated production of H_2O_2 acts as a signal to direct transcription of defence-related genes.

In *Arabidopsis* root hairs, a Rho-like GTPase is essential for activation of NADPH oxidase activity, which in turn promotes growth at the root hair tip (Carol et al., 2005). In response to H_2O_2, the *Arabidopsis* kinases ANP1 and OXI1 become activated and initiate kinase cascades leading to transcription of stress- and defence-related genes (Asai et al., 2002; Rentel et al., 2004). In *Arabidopsis*, the importance of peroxidases in the oxidative burst has been implicated in activation of NADPH oxidases during plant defence responses (Bindschedler et al., 2006). Very little work has been done to uncover related pathways in cereal pathosystems, and the steps between production of H_2O_2 and defence-related gene transcription remain obscured by a lack of experimental evidence.

3.4 Materials and Methods

3.4.1 Plant materials and treatment

Triticum monococcum L. line 441 (accession # TG13182) was grown in a chamber with 16 h light and 8 h dark at 20°C. The chemicals were purchased from Sigma-Aldrich (Oakville, Canada). For iron loading and time-course studies, 7-day-old plants were cut at the crown, transferred to 500 μM Fe-EDTA or 500 μM EDTA and sampled at 1, 6, 12 and 24 h. For iron concentration-dependent assays, the plants were transferred to solutions containing various concentrations of Fe-EDTA or 500 μM EDTA. For iron specificity assays, the plants were treated with 500 μM Na_2-EDTA, $CaCO_3$-EDTA, $MgSO_4$-EDTA, $CuSO_4$-EDTA or $ZnSO_4$-EDTA as described previously (Pekker et al., 2002). For the effect of reduced glutathione (GSH) on the iron-induced gene expression,

the plants were treated with 5mM GSH for 6 h followed by 24 h treatment with 500 μM Fe-EDTA.

3.4.2 Iron loading-induced oxidative burst

Seven-day-old wheat seedlings were treated with 500 μM Fe^{3+}-EDTA for 6 h. The occurrence of oxidative burst was detected by 3,3'-diaminobenzidine (Sigma) staining and observed under light microscopy.

3.4.3 RNA extraction and RNA gel analysis

Plant and fungal materials were ground under liquid nitrogen and transferred to extraction buffers. Total RNA was extracted according to Wilkins and Smart (1996).

3.4.4 Array filter construction and hybridization

The cDNA targets were amplified from bacterial stocks containing pBluescript (Stratagene, La Jolla, USA) with known inserts. Ten μl of bacterial stock was diluted 10X and heat shocked at 95°C for 10 min. Each 25 μl reaction contained: 1 μl heat shocked bacterial stock, 65 mM Tris–HCl, 16.6 mM $(NH_4)_2SO_4$, 3.1 mM $MgCl_2$, 0.01% (v/v) Tween 20, 1 U *Taq* polymerase, 0.6 μM primers (T3/T7 primer set), and 25 μM each of ATP, TTP, CTP and GTP at pH 8.8. Following quantitation of the PCR products with ethidium bromide and gel electrophoresis using the AlphaImager (Alpha Innotech, San Leandro, USA), 20 ng of the amplified plasmid inserts were spotted onto Hybond N nylon membranes (Amersham Biosciences, Piscataway, USA) in a 96 well-format grid.

Total RNA was extracted as above from wheat leaves cut at the crown and placed in either 500 μM EDTA or 500 μM Fe^{3+}-EDTA for 24 h. Poly(A)$^+$RNA was isolated using the PolyATtract® mRNA Isolation System (Promega) according to the manufacturer's instructions, and the mRNA was labelled with α-^{32}P-dCTP using Superscript II and the accompanying protocols (Invitrogen, Carlsbad, USA). Labelled cDNAs were purified through Sephadex G-50 (Amersham Biosciences) columns before RedoxArray hybridization at 60°C overnight in 5X Denhardt's, 5X SSC and 0.5% SDS.

Following hybridization, the filters were washed twice at room temperature in 1X SSC and 0.1% SDS for 15 min, and once at 60°C in 0.1X SSC and 0.1% SDS for 30 min.

3.4.5 Data treatment

A Storm phosphorimager (Amersham Biosciences) was used to obtain tiff images of the hybridized filters, which were then used to quantify gene expression using the ImageQuant software. Following background subtraction, the data from the filters were normalized using the mean centring procedure in the Avadis Prophetic program package (Strand Genomics, Bangalore, India). Four biological replicates were performed for each treatment. Expression data for a given gene was accepted if the standard deviation was <35% of the mean expression of the four replicates.

CHAPTER 4

DIFFERENTIAL REGULATION OF WHEAT QUINONE REDUCTASES IN RESPONSE TO POWDERY MILDEW INFECTION[1]

[1] This chapter is based on the following paper:

Greenshields, D.L., Liu, G., Selvaraj, G., and Wei, Y. (2005). Differential regulation of wheat quinone reductases during powdery mildew infection. Planta *222*, 867-875.

I performed all the experimental work, wrote the first draft and edited the final draft of the paper.

Guosheng Liu acted in a supervisory role and commented on the first draft of the paper.
Gopalan Selvaraj planned experiments, acted in a supervisory role and commented on drafts of the paper.
Yangdou Wei planned experiments, acted in a supervisory role and commented on drafts of the paper.

4.1 Introduction

Previously, I showed that reactive iron is secreted to the apoplast where it mediates reactive oxygen species (ROS) generation and defence gene transcription. Despite the apparent benefits of the ROS in plant defence, the plant must still protect itself from the inevitable oxidative stress associated with this form of defence, and plants have several enzymatic and nonenzymatic ROS scavenging systems in their arsenal (Mittler 2002). One such oxidative stress protection mechanism, as yet unevaluated in plant-pathogen interactions, is the action of the DT-diaphorase-like quinone reductases (QR2s), which catalyze the obligate divalent reduction of quinones to hydroquinones (Trost et al., 1995; Sparla et al., 1996; Sparla et al., 1999; Laskowski et al., 2002; Wrobel et al., 2002). Quinones are redox active compounds that can oxidize the thiol groups of proteins and glutathione, and undergo one electron reduction through the action of ζ-crystallin-like QRs (QR1s; Mano et al., 2000) to form unstable semiquinones, which rapidly auto-oxidize to form superoxide and the parent quinone (O'Brien 1991). QR2s are considered phase II enzymes, enzymes that act in the metabolism of xenobiotics, and have received considerable attention in humans because of a perceived role in preventing tumorigenesis (Rauth et al., 1997). Unlike semiquinones, the hydroquinones produced by two electron reduction of quinones are generally stable and can be removed from the quinone redox cycle through conjugation (Harborne 1979), making QR2s a tool of the plant cell's antioxidant repertoire. Thus, the univalent reducing ability of QR1 and the divalent reducing ability of QR2 put these two enzymes opposite one another in terms of quinone redox cycling. In this chapter, I report the isolation of genes encoding a QR1 and a QR2 from *Triticum monococcum* and show that while *TmQR1* is downregulated, *TmQR2* is induced specifically in the epidermis during powdery mildew infection. I also characterize TmQR2 through heterologous expression, and localize QR2 activity in and around infected epidermal cells.

4.2 Results

4.2.1 Sequence analysis and genomic organization of *T. monococcum* QR genes

To identify wheat genes induced by *Bgt*, Drs. Yangdou Wei and Gopalan Selvaraj developed a cDNA library from *Bgt*-infected diploid wheat leaf epidermis and have currently sequenced ~3000 ESTs from this library (described in Greenshields et al., 2004a). Sequence analysis of these ESTs identified one clone similar to plant *QR1*s and two identical clones similar to plant *QR2*s. The library is made up largely of pathogenesis related genes and these three were the only *QR*-like genes in the EST collection. The *QR1*-like clone was sequenced fully and named *TmQR1* after the ζ-crystallin-like *QR1* gene *TvQR1* from *Triphysaria versicolor* (AAG53945; Matvienko et al., 2001), that it is 62% identical to at the amino acid (aa) level. *TmQR1* contains a 1002 bp ORF that putatively codes for a 334 aa 35.1 kDa polypeptide with a pI of 9.23. TmQR1 also has similarity to the ζ-crystallins from guinea pig and yeast, and shares a conserved NAD(P)H binding motif with these proteins (Fig. 4.1a). One of the *QR2*-like clones was also sequenced fully and named *TmQR2* after the diaphorase-like QR2 gene *TvQR2* from *Triphysaria versicolor* (AAG53945; Matvienko et al., 2001), with which it shares 74% identity at the aa level. *TmQR2* has a 609 bp ORF, encoding a 203 aa polypeptide with a calculated molecular mass of 21.7 kDa and pI of 6.36. At the aa level, TmQR2 also shares high identity with QR2 *Phanerochaete chrysosporium* and the trp repressor binding protein of *E. coli*, as reflected in the alignment in Figure 4.1b. Neither of the deduced aa sequences of TmQR1 and TmQR2 contain elements suggesting of targeting sequences or membrane domains, and are therefore likely cytosolic.

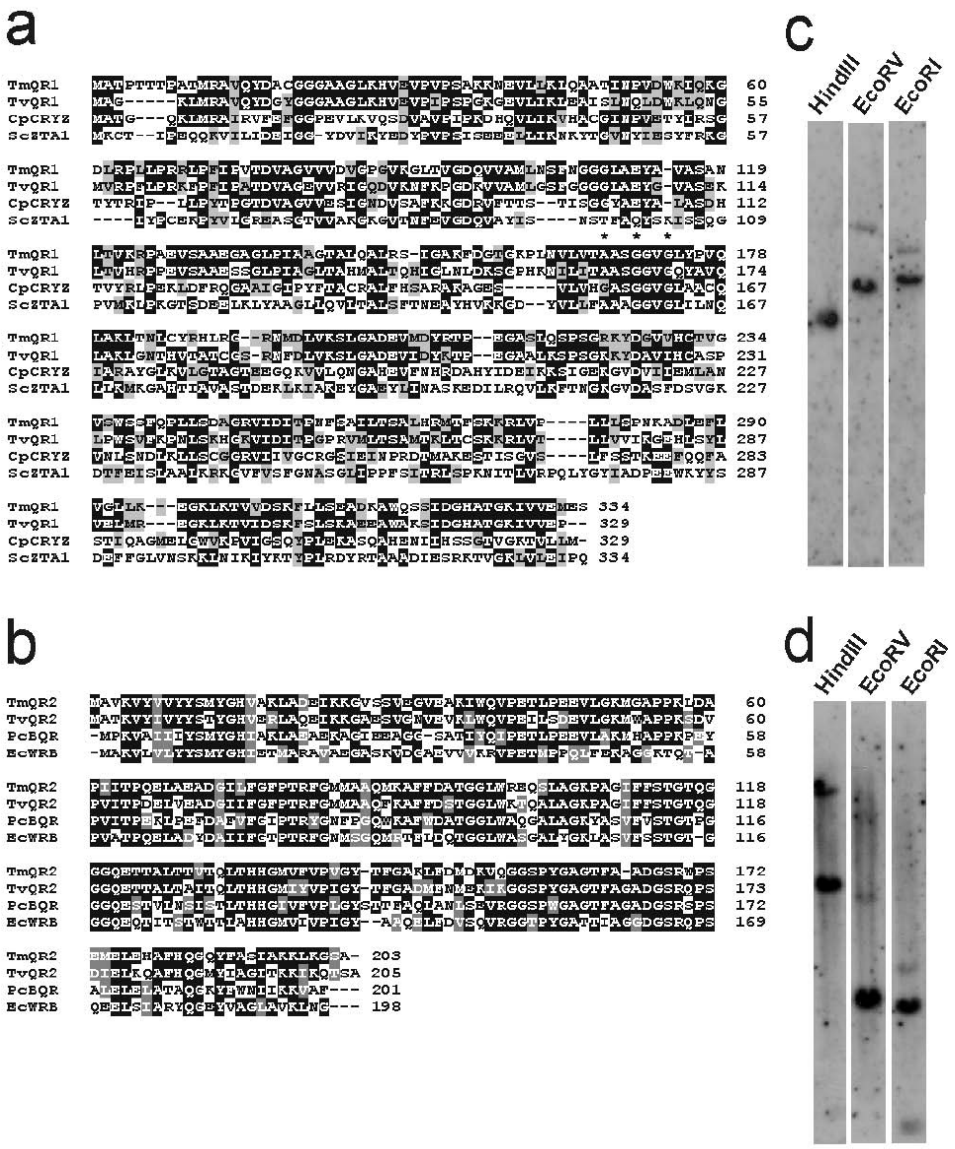

Figure 4.1 Single copy *TmQR1* and *TmQR2* genes in T. monococcum. (a) ClustalW alignment of the *TmQR1* deduced amino acid sequence against TvQR1 of *Tr. versicolor* (AF304462), CpCRYZ of guinea pig (P11415), and ScZTA1 of *Saccharomyces cerevisiae* (CAA84988). Gaps within the sequences were introduced to maximize the alignment. **(b)** ClustalW alignment of the *TmQR2* deduced amino acid sequence against QR2s TvQR2 of *Tr. versicolor* (AAG53945), PcBQR of *P. chrysosporium* (AAD21025), and the *E. coli* trp repressor binding protein WrbA (AAA24759). **(c)** DNA gel blot analysis of *TmQR1* and **(d)** *TmQR2* in *T. monococcum*. DNA digested with *Hind*III, *Eco*RV or *Eco*RI was separated on agarose gel, transferred to a nylon membrane, and probed with the ^{32}P-labeled full length cDNA.

To investigate the genomic organization of the *TmQR1* and *TmQR2* genes in *T. monococcum*, we performed DNA gel blot analyses with *T. monococcum* DNA digested with the restriction enzymes *Hind*III, *Eco*RV and *Eco*RI and probed with either the full length *TmQR1* (Fig. 4.1c) or *TmQR2* (Fig. 4.1d) cDNA. The probes hybridized to reveal either one or two strong bands in each of the digested DNAs, suggesting that the genes are represented by single copies in the *T. monococcum* genome. However, the presence of other weaker bands following hybridization of the blots suggests that additional homologue(s) of the genes may be present in the *T. monococcum* genome.

4.2.2 Enzymatic activity of recombinant TmQR2

To ensure that *TmQR1* and *TmQR2* encoded a functional QR1 and QR2, respectively, we expressed the genes in an *E. coli* expression system. The *TmQR1* and *TmQR2* ORFs were cloned into the pQE60 vector that contains an IPTG inducible promotor and an in frame C-terminal 6X-His tag, and the resulting vectors were used to transform *E. coli*. As shown in Figure 4.2a, expression of TmQR1 was lethal to the cells and we were unable to purify enough protein for further analysis. TmQR2, however, was not toxic to *E. coli* and the total protein and nickel-nitrilotriacetic acid agarose purified protein from transformed *E. coli* cells were analyzed by SDS-PAGE; the purified protein showed a single band corresponding to a 23 kDa polypeptide, which is consistent with the calculated MW of 22.6 kDa for the TmQR2 protein and the six extra His residues (Fig. 4.2b). Using an established in-gel activity stain based on the reduction of MTT tetrazolium to a blue formazan dye by quinones reduced by QR2 (Wrobel et al., 2002), we confirmed the QR activity of TmQR2 using both NADH and NADPH as electron donors (Fig. 4.2c). To investigate the inhibition of TmQR2 by dicumarol, a QR2 inhibitor (Trost et al., 1995; Wrobel et al., 2002), we incubated the protein in 100 µM dicumarol for 30 min prior to running the non-denaturing PAGE, and added 100 µM dicumarol to the gel staining buffer. As revealed in Figure 4.2c, no menadione reduction was observed in the presence of dicumarol. Together these results show that *TmQR2* encodes a dicumarol inhibitable QR2 that can use either NADH or NADPH as an electron donor. To determine the enzymatic activity of the recombinant TmQR2, we followed the oxidation of NADH in the presence of the enzyme and menadione and

found that for menadione, TmQR2 has a K_m of 3.36 µM and V_{max} of 639 nmol min^{-1} $µg^{-1}$ (Fig 4.2d). Similarly high affinities for quinones have also been reported for the QR2s of *Gloeophyllum trabeum* and *S. cerevisiae* (Kim and Suk 1999; Jensen et al., 2002).

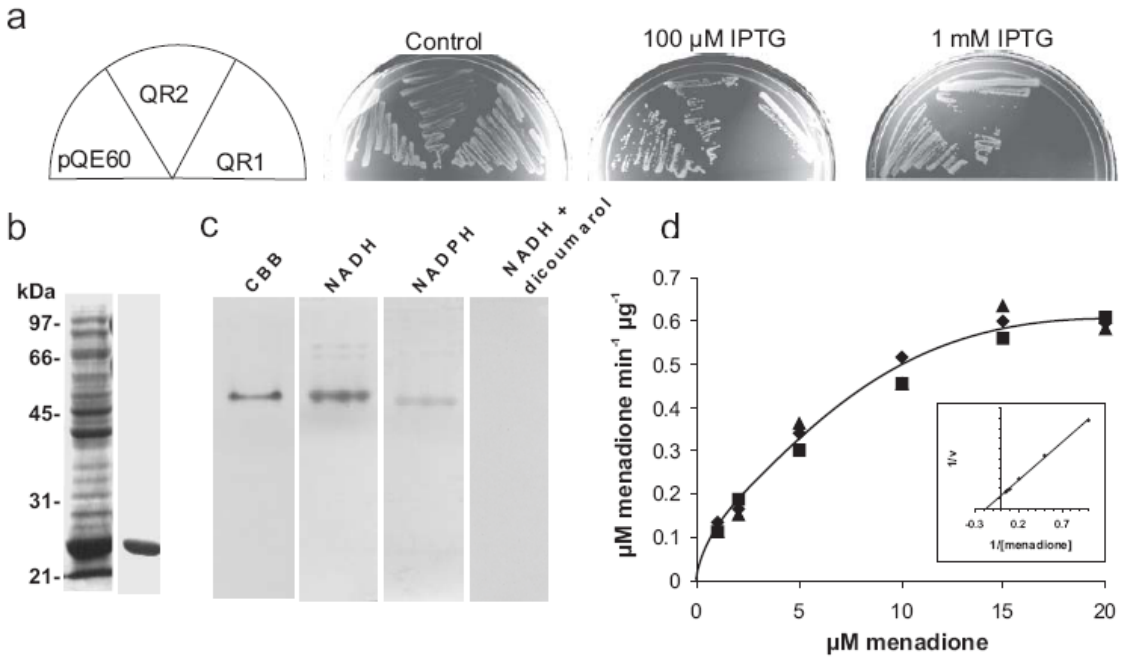

Figure 4.2 Characterization of recombinant TmQR2. (a) *E. coli* transformed with pQE60 either empty or harboring *TmQR1* or *TmQR2* and plated on LB agar containing either 0 (control), 100 µM or 1 mM IPTG to induce protein expression. TmQR1 expression was toxic to the cells. (b) Coomassie brilliant blue (CBB) stained SDS-PAGE gel of total protein from *E. coli* following induction with IPTG (left lane) and nickel-nitrilotriacetic acid agarose purified recombinant TmQR2 (right lane). The molecular mass standards are shown on the left side. (c) In-gel QR2 activity of the purified recombinant TmQR2. One microgram of TmQR2 was run per lane of a 10% non-denaturing gel. The proteins were separated and stained with CBB or assayed for QR activity using either NADH or NADPH as an electron donor. Inhibition by dicumarol was achieved by incubating the protein in 100 µM dicumarol for 30 min at 4°C prior to gel loading and by adding 100 µM dicumarol to the QR reaction buffer. (d) Activity of purified recombinant TmQR2 as a function of menadione concentration (1-20 µM). Inset: Lineweaver-Burke plot of TmQR2 activity.

4.2.3 QR gene expression during pathogen attack

To investigate the transcriptional regulation of *TmQR1* and *TmQR2* during *Bgt* infection, we followed mRNA accumulation of the two genes over 144 h using RNA gel blots

(Fig. 4.3a). The *T. monococcum-Bgt* pathosystem used here has an infection process similar to that seen in the well characterized barley-*B. graminis* f. sp. *hordei* interaction. The fungal primary germ tube appears between 3 and 6 hpi and is met simultaneously by a cell wall apposition (CWA) formed subjacent to this point of contact. The appressorial germ tube forms a penetration peg between 12 and 16 hpi and is met by a second larger CWA, but haustoria develop in successfully penetrated cells 24-32 hpi. Secondary hyphae begin to appear around 48 hpi with secondary haustoria developing by 72 hpi and conidiation and dispersal at 96-144 hpi. Although the majority of penetration attempts on this wheat line lead to pathogen infection and establishment, some attempted penetrations fail due to papilla-based or basal resistance. Interestingly, the two genes showed strikingly opposite expression patterns during this infection time course. *TmQR1* was expressed more strongly than *TmQR2* initially but showed no detectable expression after 3 hpi, whereas *TmQR2* was induced beginning at this time point. Following the 6 h time point, where expression of *TmQR1* is low and expression of *TmQR2* is high, neither of the genes showed any major change in expression level. Figure 4.3b shows that for 24 h following a mock inoculation, the genes show no major expression changes, thereby confirming that pathogen attack alters the expression of *TmQR1* and *TmQR2*. Because *Bgt* resides exclusively in the epidermis of its host, we investigated transcriptional changes of *TmQR1* and *TmQR2* in the epidermis and mesophyll separately using RT-PCR to see whether or not the spatial exclusivity of the pathogen influenced where these genes were expressed (Fig. 4.3c). We included the germin-like protein gene *TmGLP4* (Christensen et al., 2004) and the peroxidase gene *TmPOX6* (Liu et al., 2005) as positive controls for epidermis- and mesophyll-specific gene induction, respectively. As in the RNA gel blots, *TmQR1* was downregulated while TmQR2 was upregulated. Interestingly though, *TmQR2*'s induction was exclusively epidermal and *TmQR1*, although downregulated in both tissues, was expressed more strongly in the mesophyll than the epidermis. Together, these results suggest that TmQR2 could play a role in protecting the infected epidermis.

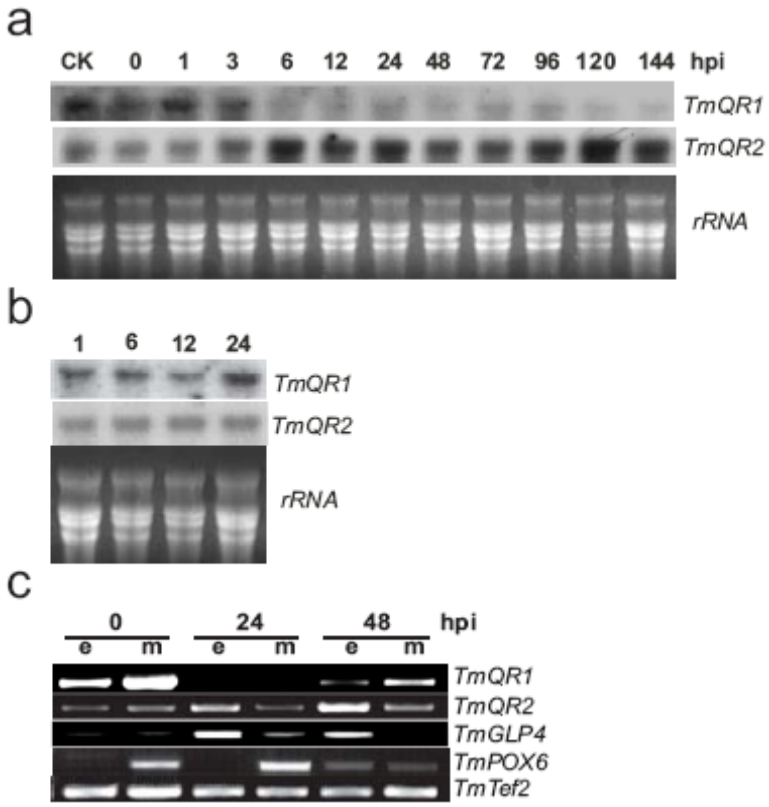

Figure 4.3 Differential regulation of *TmQR1* and *TmQR2* during powdery mildew infection. (a) RNA gel blot analyses of *TmQR1* and *TmQR2* before (CK) and 0-144 h post inoculation (hpi); ethidium bromide staining of RNA was used to confirm even loading. (b) RNA gel blot analyses of *TmQR1* and *TmQR2* 1-24 h after mock treatment; RNA was stained with ethidium bromide to confirm even loading. (c) RT-PCR of *TmQR1* and *TmQR2* in the epidermis (e) or mesophyll (m) of *T. monococcum* leaves 0, 24, and 48 hpi with *Bgt*. *TmGLP4* was included as a positive control for epidermal expression, *TmPOX6* was included as a positive control for mesophyll expression, and *Tmtef2* was included as a constitutively expressed loading control.

4.2.4 QR2 activity in infected epidermal cells

To investigate whether or not transcriptional activation of *TmQR2* leads to an accumulation of QR2 activity in the infected leaf epidermis, we adapted histochemical QR activity staining techniques previously used in mammalian brains (Hope and Vincent 1989; Murphy et al., 1998; Wang et al., 2000). Histochemistry was used instead of quantitative *in vitro* techniques because of problems with false positive activity associated with fungal tissues in the leaves, and because it allows for simultaneous

localization of the activity. The technique is based on the reduction of menadione, a quinone, to its hydroquinone form by QR2 and the subsequent spontaneous reduction of NBT by the hydroquinone to a blue formazan dye precipitate, thereby regenerating the quinone. Because NBT is also used to stain superoxide (Frahry and Schopfer 2001; Hückelhoven and Kogel 2003), we included the SOD mimetic MnTBAP (Patel and Day 1999) to control staining due to superoxide production. A similar technique using the SOD mimetic manganese desferal abolishes superoxide-mediated NBT staining in maize coleoptiles (Frahry and Schopfer 2001). Figure 4.4a shows the QR2 activity staining pattern in an infected epidermal cell 24 hpi with *Bgt*. QR2 activity is seen especially against the walls of infected cells and to some degree in neighboring cells, as well as in the fungal germ tube. The inset photo in Figure 4.4a shows another infection site at 48 hpi, where the activity has spread around the cell and is more pronounced in the adjacent cell. Interestingly, strong QR2 activity was observed only surrounding successful penetration attempts. No activity was associated with primary germ tube CWAs and although some light staining occurred at failed penetration attempts, it was never as strong as the staining seen where fungal haustoria had formed. Figure 4.4b shows the stain precipitate accumulation in a cell containing a haustorium 48 hpi. The addition of 100 μM dicumarol to the incubation and reaction buffers abolished most of the staining reaction in the epidermal cells, but did not change the staining of fungal structures (Fig. 4.4c). Finally, to ensure that the staining reaction was reliant on the menadione acceptor, we omitted menadione from reactions containing MnTBAP, and found that most of the staining of plant structures was abolished (Fig. 4.4d). Fungal structures were stained to some degree in all of these assays, suggesting either that NBT is able to permeate the fungal wall while the other reagents are not, that the fungus has a QR activity not inhibited by dicumarol, or that the fungus has NBT reductase activity.

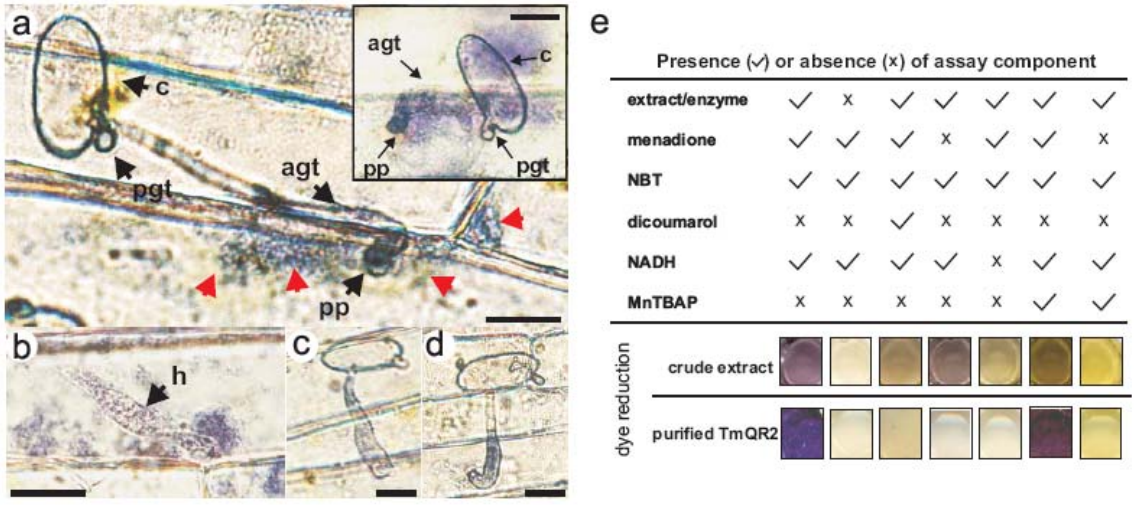

Figure 4.4 QR2 activity is associated with *Bgt* infection sites. (a) Infection site stained for QR2 activity 24 h post inoculation (hpi) as described in the Materials and Methods section. Red arrows highlight formazan accumulation. c: conidium, agt: appressorial germ tube, pgt: primary germ tube, pp: penetration peg. Inset: QR2 activity stained infection site 48 hpi (b) *Bgt* haustorium inside infected cell stained for QR2 activity 48 hpi. (c) Infection site stained with complete reaction buffer containing 100 µM dicumarol. (d) Infection site stained with reaction buffer without menadione. Scale bars correspond to 10 µm. (e) *In vitro* QR2 staining reaction. Two hundred microlitres of reaction buffer containing either crude protein extracts from wheat leaves 48 hpi with *Bgt* or 1 µg purified recombinant TmQR2 was dispensed into the wells of ELISA plates with the addition or omission of the indicated components and NBT dye reduction was monitored. No effort was made to quantify the dye reduction.

To verify the results observed *in situ*, we conducted similar trials *in vitro* using the same reaction buffers and component concentrations, but with or without the addition of either 5 µl crude protein extracts from *T. monococcum* leaves 48 hpi or 1 µg purified recombinant TmQR2. After 15 min incubation, a dark blue precipitate had formed in reactions containing the enzyme or extract, dye, NADH, and menadione (Fig. 4.5d). The reaction catalyzed by the recombinant protein generally produced a much darker stain than the crude protein extract reactions. In the absence of enzyme of crude extract there was no color reaction. When NADH was omitted from the crude extract reaction, some staining remained, but no staining was present in the recombinant protein reaction, and this difference could be due to NAD(P)H present in the crude extracts. While the omission of menadione from the crude extract-containing reactions without

MnTBAP lessened the staining intensity only slightly, reactions with MnTBAP but without menadione showed no staining, confirming both the presence of a superoxide generating system in infected leaves and the efficacy of the SOD mimetic. When dicumarol was added, some staining was evident, but it was of greatly diminished intensity compared to reactions lacking dicumarol. Because MnTBAP did not block either the *in situ* or *in vitro* NBT reduction, it seems that menadiol (hydroquinone) can donate electrons directly to NBT without using a superoxide intermediary.

4.3 Discussion

At least two major types of QRs exist in plants: the ζ-crystallin-like QR1s (Mano et al., 2000; Matvienko et al., 2001), which catalyze one electron reductions of quinones to semiquinone radicals, and the DT-diaphorase like QR2s (Trost et al., 1995; Sparla et al., 1996; Sparla et al., 1999; Laskowski et al., 2002; Wrobel et al., 2002), which catalyze two electron reductions of quinones to hydroquinones. Semiquinone radicals are rapidly autooxidized back to quinone, forming superoxide concurrently. In plants, the classification of QR2 as an antioxidant enzyme arises mainly from its ability to produce hydroquinones that can be converted to their arbutin monoglucosides, and hence removed from redox cycling (Harborne 1979). The antioxidant role of QR2 also has support from studies of its mammalian functional homologue, NQO1 (reviewed by Talalay and Dinkova-Kostova 2004). Here, we isolated and partially characterized genes representing both types of QR in *T. monococcum*. Our data suggest that QR2s are involved in detoxifying quinones in infected epidermal cells.

Approximately1.5% of all of the ESTs sequenced so far from our *T. monococcum* epidermal library encode type III peroxidases (Liu et al., 2005). We were therefore surprised to see transcriptional downregulation of *TmQR1* because superoxide production at the plant pathogen interface is a well known phenomenon (Hückelhoven and Kogel 2003). The activity of other enzymes able to carry out univalent quinone reductions does not seem to have a major effect on superoxide production in wheat though, given that most of the quinone-based NBT staining present in Fig. 4.4 can be explained without superoxide production. In the parasitic plant *Tr. versicolor*, the

TmQR1 and *TmQR2* homologues *TvQR1* and *TvQR2* were both highly upregulated by quinone treatments (Matvienko et al., 2001). We also sprayed *T. monococcum* leaves with ferulic acid or benzoquinone, but found no change in the transcript levels of *TmQR1* or *TmQR2* in RNA gel blots (data not shown), suggesting that the regulation seen during pathogen attack requires more than just the accumulation of quinones. Interestingly, *TvQR1* is induced solely in parasitic plants and is therefore considered to be involved in haustorium development in parasitic plants (Matvienko et al., 2001). In *Arabidopsis*, the QR1 gene *P1-ZCr* is induced by a number of oxidative stress treatments, including quinone application (Babiychuk et al., 1995). Unlike the situation observed in these other plants, in *T. monococcum* we found that *TmQR1* is constitutively expressed under normal conditions (Fig. 4.2b) and during quinone treatment, but downregulated during pathogen attack. Thus, the physiological role of TmQR1 remains unclear, although it might be involved in the regulation of the redox status of the NAD(P)H pool, as has been suggested for guinea pig ζ-crystallin (Rao et al., 1992). Regardless of its role in normal metabolism, TmQR1 is transcriptionally repressed in response to pathogen attack, and is therefore probably not an oxidative stress protection enzyme like P1-ZCr in *Arabidopsis*.

Unlike *TmQR1*, *TmQR2* was induced in the leaf epidermis upon pathogen attack. Following *Bgt* attack, QR2 activity was also localized to the infected epidermal cells, around the infection sites. Because QR2 activity was seen only in penetrated cells, it seems likely that the activity is a response to infection of susceptible cells. One possibility is that TmQR2 and/or its functional homologues, like related proteins in plants (Sparla et al., 1996; Matvienko et al., 2001), fungi (Jensen et al., 2002) and animals (Talalay and Dinkova-Kostova 2004), is involved in detoxifying intracellular quinones. Absolute characterization of the role of QR2s in relation to resistance and susceptibility, however, will require further study using approaches like reverse genetics. Figure 4.5 shows a hypothetical scheme for the regulation of cytosolic quinone reduction during *Bgt* infection. During normal conditions, QR1 reduces quinones to semiquinones, possibly to regulate the redox status of the NAD(P)H pool. The semiquinones are immediately oxidized back to quinones, giving rise to superoxide, which can be handled by one of the cell's various ROS scavenging pathways. When faced with pathogen

challenge, however, extracellular oxidative defence against the pathogen increases the demand for ROS scavenging pathways inside the cell, and QR1 is accordingly downregulated transcriptionally. Simultaneously, *QR2* transcription is upregulated and QR2 accumulates in epidermal cells where it reduces quinones to hydroquinones so that they can be removed from redox cycling through conjugation.

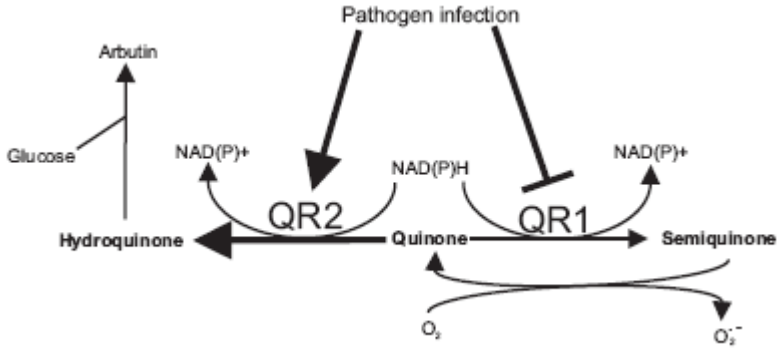

Figure 4.5 A proposed scheme for cytosolic quinone reduction and its regulation by pathogen attack. Details of the reactions are discussed in the text.

4.4 Materials and Methods

4.4.1 Plant and fungal materials

The powdery mildew isolate (*Bgt*) was originally isolated from the hexaploid wheat (*Triticum aestivum*) cultivar Conway in Saskatoon, Canada and maintained on the same cultivar. Plants were grown in a chamber with a cycle of 16 h light and 8 h dark at 20°C. One highly susceptible *T. monococcum* line (Line 441, accession # TG13182) was used throughout this study. Inoculation was performed on 7 day old *T. monococcum* leaves as previously described (Thordal-Christensen and Smedegaard-Petersen 1988) using fresh conidia from heavily infected plants.

4.4.2 Nucleic acid isolation and cDNA library construction

Total RNA was extracted as described in Chapter 3 and DNA was isolated by ethanol precipitation of the supernatant following LiCl precipitation of the RNA. cDNA library construction was performed as previously described (Liu et al., 2005), and DNA sequencing was performed by the Plant Biotechnology Institute (Saskatoon) DNA Technology Unit. tBLASTx analysis of initial EST batches against the GenBank non-redundant database revealed one clone similar to *QR1* sequences and two identical clones similar to *QR2* sequences. The *QR1*-like clone and one of the *QR2*-like clones, harboring the genes designated *TmQR1* (accession number: AY965347) and *TmQR2* (accession number: AY880319), respectively, were used for further study.

4.4.3 Gel blot and RT-PCR analyses

DNA and RNA gel blots on GeneScreen Plus membranes (PerkinElmer, Wellesley, USA) were prepared as described by Sambrook and Russell (2001). Probes were prepared from full length cDNAs using the Megaprime DNA labelling system (Amersham Biosciences, Piscataway, USA). Hybridization was performed as described by Sambrook and Russell (2001), with 2 x 20 min washing performed in 1X SSC, 0.1% SDS at 65°C, and 1 x 20 min washing in 0.1X SSC, 0.1% SDS. RT-PCR was performed using poly(A)$^+$RNA isolated from peeled *T. monococcum* abaxial epidermis and the remaining underlying mesophyll separately at 0, 24, and 48 hpi with *Bgt* as previously described (Liu et al., 2005). The primers QR1F (5'gccatggccaccccaaccacg) and QR1R (5'gagatctgctctccatctcaacgac) were used to amplify *TmQR1*, and QR2F (5'gccatggcggtcaaggtctatg) and QR2R (5'gagatctagcagatcccttgagtttc) were used to amplify *TmQR2*. The primers germinF (5'gccatcatccccttccttcc) and germinR (5'gcgggctggttggatgtgac) were used to amplify the epidermis-specific gene *TmGLP4* (accession number: AY650052), the primers 620F (5'gtagctagatagatttgtgag) and 620R (5'tcgaaccaaacggctcttatt) were used to amplify the mesophyll-specific gene *TmPOX6* (accession number: AY857760; Liu et al., 2005), and the primers Tef2F (5'cgtgccaagtctgatcctatgg) and Tef2R (5'gatgccgcgcatgttctcctcac) were used for

amplification of the constitutively expressed elongation factor gene *Tmtef2* (accession number: AY880320).

4.4.4 Heterologous expression and purification

Qiagen's (Mississauga, Canada) QIAexpressionist kit was used to express the TmQR1 and TmQR2 proteins in *E. coli*. The TmQR1 and TmQR2 coding regions were amplified by PCR using the QR1 and QR2 primer sets and then cloned into pBluescript (Stratagene, La Jolla, USA), digested with *Nco*I and *Bgl*II, and then subcloned into the *Nco*I and *Bgl*II sites of the expression vector pQE-60 (Qiagen) as translational fusions to the 6XHIS tag. DNA sequencing showed that the inserts had correct open reading frames (ORFs). The resulting plasmids were transformed into M15 *E. coli* cells (Qiagen) using the provided protocol for protein expression and purification. Expression of TmQR1 proved toxic to the cells, making it impossible to purify enough recombinant protein for further assays. Protein purity was verified using SDS-PAGE and Coomassie staining according to standard protocols (Sambrook and Russell, 2001). Protein concentration was determined using the Bradford method with BSA as a standard.

4.4.5 Recombinant TmQR2 activity assays

All chemicals were purchased from Sigma (St. Louis, USA) unless otherwise noted. In-gel QR assays were conducted in 10% non-denaturing polyacrylamide gels as described by Wrobel et al., (2002) using 1µg of purified recombinant TmQR2. Inhibition of in-gel QR2 activity by dicumarol was achieved by incubating the protein in 100 µM dicumarol in 50 mM Tris-HCl pH 7.5 (a 10 mM dicumarol stock was prepared in 0.1 N NaOH) for 30 min at 4ºC. Samples without dicumarol inhibition were incubated in 50 mM Tris-HCl pH 7.5 prior to loading. Following electrophoresis, the gels were stained in 50 mM Tris-HCl pH 7.5, 0.3 mg ml^{-1} MTT, 1 mM NADPH or NADH and 30 µM menadione with or without 100 µM dicumarol. Kinetic parameters of purified recombinant TmQR2 were determined by following the oxidation of NADH at 340 nm (ε_{340} nm = 6.22 mM^{-1} cm^{-1}) in a Beckman-Coulter (Fullerton, USA) DU-530 spectrophotometer for 1 min in kinetic mode. Reaction mixtures contained 50 mM Tris-HCl pH 7.5, 200 µM NADH, 1 µg

TmQR2, and 0.1-100 μM menadione. Control consisted of the reaction mixture without the enzyme.

4.4.6 QR2 activity assays of mildewed wheat

QR activity staining in *Bgt*-challenged epidermal cells was performed based on previous reports (Hope and Vincent 1989; Murphy et al., 1998; Wang et al., 2000), with some modification. A similar technique has also been used to detect superoxide in maize coleoptiles (Frahry and Schopfer 2001). Peeled epidermal strips of *T. monococcum* 24-48 hpi with *Bgt* were incubated for 30 min at 25ºC in reaction buffer [25 mM Tris-HCl pH 7.5, 0.01% Triton X-100, 1 mg/ml BSA, SOD mimetic 100 μM MnTBAP (Calbiochem, San Diego, USA)] with or without 100 μM dicumarol. This solution was then replaced with reaction buffer containing 300 μM NBT, 20 μM menadione and 1 mM NADH. Controls consisted of the reaction buffer with menadione, NBT, NADH, and the QR inhibitor 100 μM dicumarol (QR control) or the reaction buffer with NBT and NADH but without menadione (background superoxide control). The reaction was allowed to proceed up to 1 h at room temperature in the dark before photography. *In vitro* verification of *in situ* staining was performed using the same concentrations of all reagents as the *in situ* staining assays, but in a 200 μl final volume and with the addition of either a 5 μl aliquot of crude protein extract or 1 μg purified TmQR2. Crude protein extracts were obtained from the supernatant remaining following homogenization of 50 mg (fresh weight) wheat leaves 48 hpi in 100 μl ice cold extraction buffer (25 mM Tris-HCl pH 7.5, 0.01% Triton X-100, 1 mg/ml BSA) and centrifugation at 14000 rpm for 20 min at 4ºC. A no enzyme control was included for the complete reaction buffer. The *in vitro* assays were run for 15 min at room temperature in the dark in the wells of ELISA plates before being scanned on a flatbed scanner. All of the assays were performed several times and showed consistent results.

CHAPTER 5
IRON UPTAKE IN FUSARIUM GRAMINEARUM[1]

[1]This chapter is based on the following paper:

Greenshields, D.L., Liu, G., Feng, J., Selvaraj, G., and Wei, Y. (2007). The siderophore biosynthetic gene *SID1*, but not the ferroxidase gene *FET3*, is required for full *Fusarium graminearum* virulence. Molecular Plant Pathology *8*, 411-421.

I performed all of the experimental work, and wrote the first and final drafts of the paper.

Guosheng Liu acted in a supervisory role and commented on the first draft of the paper.

Jerry Feng constructed the plasmid *pBS-HPH* and commented on the first draft of the paper.

Gopalan Selvaraj planned experiments, acted in a supervisory role and commented on drafts of the paper.

Yangdou Wei planned experiments, acted in a supervisory role and commented on drafts of the paper.

5.1 Introduction

In the previous chapters, I focused on the roles of iron and reactive oxygen species (ROS) in plant defence, and how the plant defends itself against ROS. In this chapter, I explore how pathogens are able to acquire iron from their plant hosts.

In order to strip enough iron from the host to survive, fungal pathogens have evolved at least two iron acquisition systems. One system is hinged on the secretion and subsequent uptake of low molecular weight ferric iron (Fe^{3+}) specific chelators termed siderophores, while the other uses iron reductases at the pathogen cell wall to free bound or insoluble ferric iron by reducing it to ferrous (Fe^{2+}) for uptake (Haas, 2003; Philpott, 2006). The reductive iron uptake system requires a reductase, Fre1p or Fre2p (Georgatsou and Alexandraki, 1994), which can "labilize" ferric and make it available for uptake through divalent metal ion transporters like the SMF family of transporters (Cohen et al., 2000), or through the Fet3p ferroxidase/Ftr1p iron permease complex (Stearman et al., 1996). The siderophore iron uptake system involves the synthesis and excretion of siderophores, which then bind environmental iron and are taken up by a range of specific ferri-siderophore transporters (Haas, 2003). Most fungi produce hydroxymate siderophores, but are able to take up other types of siderophores as well. For example, *Saccharomyces cerevisiae*, which does not produce siderophores, is able to take up both fungal and bacterial ferri-siderophores (Philpott et al., 2002). The first committed step to hydroxymate siderophore biosynthesis is achieved through the action of SidA (Sid1 in *Ustilago maydis*; DffA in *Aspergillus oryzae*), an ornithine N^5-oxygenase, which N^5-hydroxylates ornithine (Eisendle et al., 2003). After the addition of an acyl moiety to N^5-hydroxyornithine, hydroxymate groups are linked together by nonribosomal peptide synthases (NPSs) like *U. maydis* Sid2 (Yuan et al., 2001) or *Cochliobolus heterostrophus* NPS6 (Oide et al., 2006). Different NPSs appear to be responsible for producing different siderophores. Disruption of *F. graminearum NPS2*, for example, leads to a loss of ferricrocin production (Tobiasen et al., 2007), while *C. heterostrophus* Δ*nps6* mutants cannot produce coprogen (Oide et al., 2006). Following iron binding, transporters recognize and take up specific ferri-siderophores; for instance, *S. cerevisiae* Arn4p recognizes enterobactin, while Arn3p recognizes ferrioxamines and ferrichromes (Philpott et al., 2002).

The ascomycete *Fusarium graminearum* is a cereal pathogen causing head blight in wheat and barley and ear rot in maize. *F. graminearum* also produces the toxin deoxynivalenol (vomitoxin) which renders wheat and barley unusable as food or feed, impairs germination, and alters the milling, malting, and baking qualities of the grain (Dexter et al., 1996). The importance of *F. graminearum* as a plant pathogen is also highlighted by the recent efforts in *F. graminearum* genomics. Through the efforts of a USDA funded project, a 36 Mb assembly has been released by the Broad Institute at MIT based on ~10X genome coverage from the shotgun sequencing of *F. graminearum* (Xu et al., 2006). Recently, genes for the *FTR1* and *FTR2* iron permeases and the *SIT1* ferrichrome transporter were characterized in *F. graminearum* (Park et al., 2006a; Park et al., 2006b). Loss of *FTR1* or *FTR2* did not affect *F. graminearum* pathogenicity on barley, however, and no report was made on the effect of *SIT1* deletion on pathogenicity of the fungus. Another recent report, however, has shown that the nonribosomal peptide synthase gene *NPS6* is a virulence determinant in several ascomycetes including *F. graminearum* (Oide et al., 2006). Interestingly, loss of the *U. maydis* ornithine N^5-oxygenase gene *Sid1* did not affect corn smut development on maize (Mei et al., 1993), but loss of the reductive iron uptake system reduced pathogen virulence (Eichhorn et al., 2006). Here we show, using *F. graminearum* strains with mutations at either *SID1* or *FET3*, that siderophore production, but not reductive iron uptake, is required for full virulence of *F. graminearum* on wheat.

5.2 Results

5.2.1 Identification and cloning of iron-responsive genes in *F. graminearum*

To identify iron uptake-related genes in *F. graminearum*, we searched the relevant literature and found characterized iron uptake-related genes in other fungal species. We then used these genes as BLAST queries for comparison to the *F. graminearum* genome at http://mips.gsf.de/genre/proj/fusarium/. Having identified putative iron uptake-related gene homologues in *F. graminearum*, we used them to query *F. graminearum* expressed sequence tag (EST) databases available from http://mips.gsf.de/genre/proj/fusarium/. If a single copy *F. graminearum* gene matched a known, characterized iron uptake-related

gene from another species (≥50% identical at the amino acid level) and was found in EST databases, it was investigated further. Five genes matched these parameters and are described in Table 5.1. To clone these putative iron uptake-related genes, mRNA was isolated from *F. graminearum* strain PH-1 grown in liquid medium without iron and containing casamino acids as the sole carbon source. This medium was used previously to produce an EST library containing all of these iron uptake-related genes (EST library Fg09, Bob Watson, Agriculture and Agri-Food Canada). The cDNAs representing the five genes were amplified by RT-PCR.

To test whether or not transcription of the five identified genes is controlled by iron, we grew *F. graminearum* strain PH-1 in minimal medium (MM-Fe) containing 0, 0.01, or 1 mM ferric ($FeCl_3$) or ferrous ($FeSO_4$) iron, and monitored expression of the genes using RNA gel blots (Fig. 5.1). Expression levels of all of the genes responded to iron concentration changes in a similar manner, showing the highest expression levels in the absence of iron and lower expression levels in higher iron concentrations regardless of whether the iron was in ferric or ferrous form.

Table 5.1 Iron uptake-related genes identified from *F. graminearum*.

Gene name	Putative function	MIPS entry	Protein accession number	Closest characterised BLAST hit	Percent identity[a]	Reference
ATX1	Copper chaperone, metal homeostasis factor	FG10854	XP_391030	*Trametes* AAN75572	57%	Uldschmid et al. (2002)
FET3	Cell surface ferroxidase	FG05159	XP_385335	*Aspergillus* AAT84595	58%	Schrettl et al. (2004)
MIR1	Triacetylfusarinine C permease	FG00539	XP_380715	*Aspergillus* AAN10149	58%	Haas et al. (2003)
SID1	L-ornithine N^5 monooxygenase	FG05371	XP_385547	*Aspergillus* BAC15565	50%	Yamada et al. (2003)
SIT1	Ferrioxamine transporter	FG05848	XP_386024	*Cryptococcus* XP_567138	51%	Tangen et al. (2007)

[a]Percent identity between the deduced amino acid sequences of the identified gene and the closest characterised BLAST hit.

5.2.2 Targeted disruption of *SID1* and *FET3*

Using split marker disruption vectors (de Hoogt et al., 2000) and PEG-mediated protoplast transformation (Proctor et al., 1997), we created mutants affected in either of the two iron uptake pathways by disrupting *FET3* (Fig. 5.2a) or *SID1* (Fig. 5.2b), respectively. Five hygromycin resistant Δ*fet3* mutants (Δ*fet3-1* to Δ*fet3-5*) and 3 hygromycin resistant Δ*sid1* mutants (Δ*sid1-1* to Δ*sid1-3*) were recovered and disruption of the genes was verified by PCR. Single copy insertions of the *Escherichia coli* hygromycin phosphotransferase gene (*HPH*) into the coding regions of *FET3* and *SID1* were confirmed by Southern blotting (Fig. 5.2c, d).

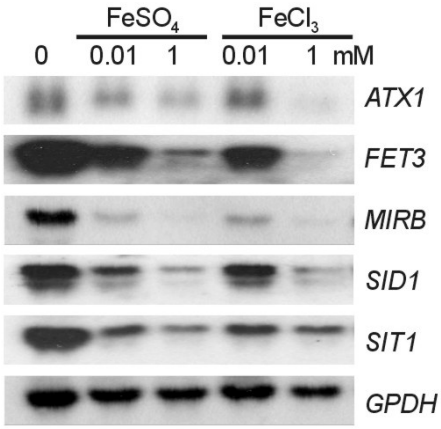

Figure 5.1 Transcriptional control of iron uptake-related genes by growth medium iron concentration. Total RNA was isolated from wild-type *F. graminearum* strain PH-1 grown without iron for 2 d and then transferred into minimal medium containing the indicated iron source and concentration. The RNA was separated by electrophoresis, transferred to nylon membranes and probed with ^{32}P-labeled cDNAs representing the iron uptake-related genes. The constitutively expressed glycerol 3-phosphate dehydrogenase gene GPDH was used to monitor even loading of the RNA.

5.2.3 *FET3* encodes a functional cell surface ferroxidase

For clarity, the *F. graminearum FET3* gene will be referred to as *FgFET3* in this section. To confirm that *FgFET3* encodes a functional ferroxidase, we expressed it in the yeast *fet3fet4* mutant, which lacks the ability to assimilate iron through the reductive pathway (Dix et al., 1994). As shown in Fig. 5.3, the *fet3fet4* mutant grew only in the presence of

1 mM free $FeCl_3$, but not when the iron was chelated with EDTA or citrate. The *fet3fet4* strain harbouring the *pYES2-FgFET3* construct was able to grow like wild type except when seeded at low concentration on a medium without iron. The results show that *FgFET3* encodes a ferroxidase able to complement the iron uptake deficiencies of the yeast *fet3fet4* mutant.

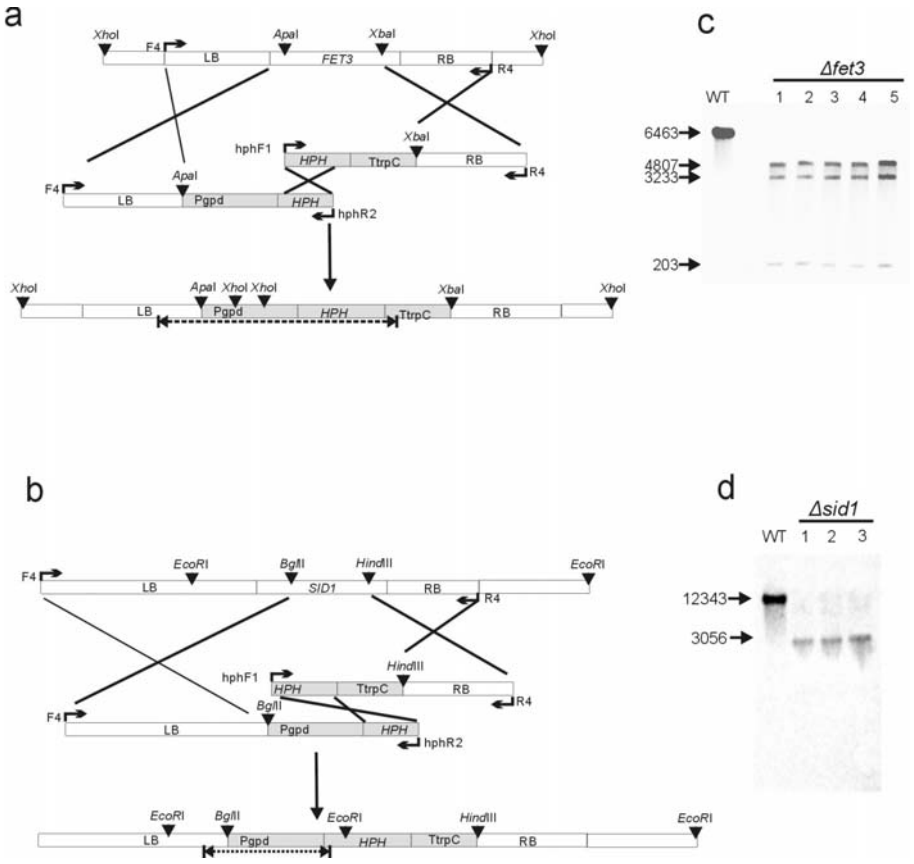

Figure 5.2 Targeted disruption of *F. graminearum FET3* and *SID1*. The disruption strategy for *FET3* **(a)** or *SID1* **(b)**, showing the native (top) and recombinant (bottom) genomic regions of the respective genes. Restriction sites for genomic DNA/hygromycin resistance cassette ligation and for Southern digestion are shown. Dashed double-headed arrows below the disrupted gene represent the region used to probe the Southern blots. **(c** and **d)** Southern blots showing single copy insertion of the hygromycin resistance cassette into *FET3* **(c)** and *SID1* **(d)**. The DNA of *F. graminearum* strain PH-1 (WT) or putative Δ*fet3* and Δ*sid1* mutants was digested with *Xho*I or *Eco*RI, respectively, separated on a 0.7% (w/v) agarose gel, transferred to a nylon membrane, and probed with a ^{32}P-labeled region of the disruption vector. The expected fragment sizes are indicated on the left.

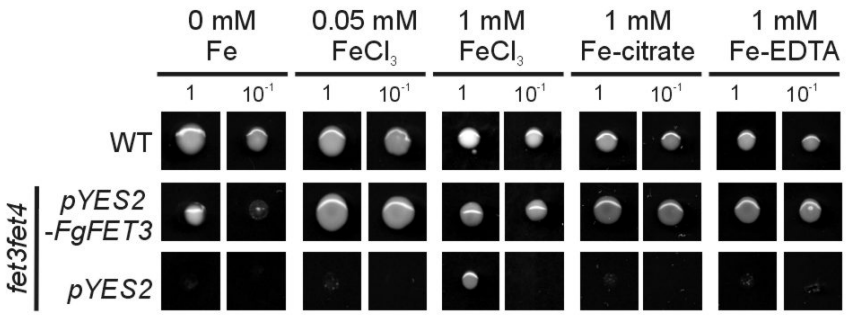

Figure 5.3 *FET3* complements the yeast iron uptake mutant *fet3fet4*. Wild-type *S. cerevisiae* (WT) or *fet3fet4* yeast harbouring either the complementation vector *pYES2-FgFET3*, or the empty vector *pYES2* were grown overnight in synthetic defined (SD) medium (-ura, pH 4.0) and adjusted to an OD of 0.2. One microlitre of this culture, either before (1) or after (10^{-1}) a ten-fold dilution, was spotted onto SD plates with galactose replacing glucose as the carbon source and containing the iron sources indicated, and the plates were incubated for 2 d.

5.2.4 *SID1* is required for siderophore production and iron uptake

To test the role of *F. graminearum SID1* and *FET3* on siderophore production, we grew Δ*fet3*, Δ*sid1* and wild-type *F. graminearum* strains in MM-Fe with 0, 0.01, or 1 mM $FeCl_3$ or $FeSO_4$ and assayed siderophore excretion using the chrome azurol S liquid assay (Schwyn and Neilands, 1987; Payne, 1994). While both the Δ*fet3* and wild-type strains excreted similar amounts of siderophores, no siderophore production was evident in the Δ*sid1* strains (Fig. 5.4). We then examined the impact of *FET3* or *SID1* disruption on fungal growth by growing Δ*fet3*, Δ*sid1* and wild-type *F. graminearum* strains on MM-Fe plates containing 50 μM of the ferrous chelator bathophenanthrolinedisulfonic acid, or 0.01 or 1 mM $FeSO_4$, and measuring daily radial colony growth for 2 d (Table 2). Bathophenanthrolinedisulfonic acid was added to the iron-free medium to ensure that any trace iron was unavailable to the fungus. All three genotypes were able to grow without iron, but Δ*sid1* grew significantly slower than either wild type or Δ*fet3*. When iron was added to the media, however, there were no significant differences between the growth of either mutant and the wild type.

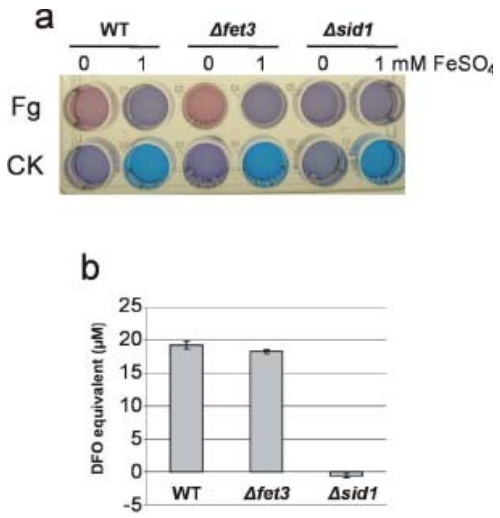

Figure 5.4 *SID1* is required for siderophore biosynthesis. Siderophore production in wild-type (WT), Δ*fet3* and Δ*sid1 F. graminearum* strains was measured in the culture supernatant of MM-Fe liquid culture using the chrome azurol S assay. **(a)** Color change of the chrome azurol S assay solution and supernatants before (CK) or after (Fg) addition of the fungus. Change from blue to pink indicates the presence of siderophores. **(b)** The data were transformed to deferrioxamine (DFO) equivalent by comparison to a standard curve. Bars represent the mean ± standard deviation of three biological replicates.

To examine the loss of siderophore production on the ability of Δ*sid1* to take up and store iron, we grew the wild-type and mutant strains on MM-Fe plates containing 0.01 mM $FeSO_4$ and then transferred them into liquid MM-Fe containing 1 mM $FeCl_3$ for 1.5 h and examined the iron content of the hyphae using the fluorescent iron dye calcein. Non-fluorescent calcein-AM can enter cells freely, but is converted to membrane-impermeable fluorescent calcein inside the cells, where the binding of free iron quenches its fluorescence (Thomas et al., 1999). Calcein fluorescence is quenched much more efficiently by ferric iron than by ferrous iron and is therefore mainly indicative of free ferric iron. The hyphae of Δ*sid1* contained much less free iron than wild-type *F. graminearum* (Fig. 5.5a). Interestingly, the Δ*fet3* mutant had a much higher amount of free iron than wild type, suggesting either that the Δ*fet3* strain takes up more iron than the wild-type fungus, or that the iron it does take up remains free intracellularly. We observed differences in the free iron pools of wild-type and mutant *F. graminearum* conidia by harvesting conidia from the three strains after growth in 0.01

mM $FeSO_4$ and again staining with calcein-AM. Fig. 5.5b shows that conidial iron deposition mirrored the free iron content of the hyphae.

Table 5.2 Impact of iron concentration on wild type, Δ*fet3* and Δ*sid1* growth.

Iron concentration	Strain	Radial growth/day (mm)[a]
0 mM+BPS[b]	PH-1	**9.0 ± 0.7**
	Δ*fet3*	**9.3 ± 0.3**
	Δ*sid1*	**6.8 ± 0.8** [c]
0.01 mM $FeSO_4$	PH-1	**8.6 ± 0.6**
	Δ*fet3*	**9.4 ± 0.8**
	Δ*sid1*	**7.5 ± 0.6**
1 mM $FeSO_4$	PH-1	**8.6 ± 0.9**
	Δ*fet3*	**7.8 ± 0.6**
	Δ*sid1*	**10.1 ± 0.6**

[a]Data presented are mean values of three replicates ± standard deviations
[b]BPS: 0.05 mM Bathophenanthrolinedisulfonic acid
[c]Significant difference compared to PH-1 ($p<0.01$ with Student's T-test)

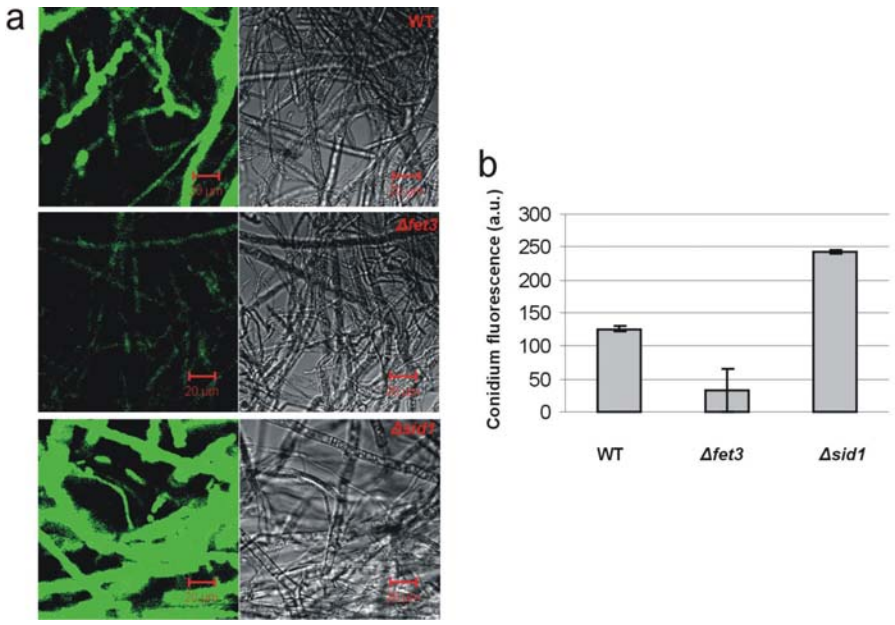

Figure 5.5 Disruption of *FET3* or *SID1* alters the intracellular iron pool. (a) Free intracellular iron was measured with a laser scanning microscope using the fluorescent iron-binding dye calcein-AM in wild-type (WT), Δ*fet3* and Δ*sid1 F. graminearum*. Red bars represent 20 µm. **(b)** Free intracellular iron in *F. graminearum* conidia. Bars represent the mean fluorescence of calcein ± standard deviation in three biological replicates. a.u.: arbitrary units.

5.2.5 Loss of *SID1*, but not *FET3*, alters iron-related gene expression

To examine the effect of the loss of *SID1* or *FET3* on iron uptake-related gene expression, we grew *F. graminearum* Δ*sid1* or Δ*fet3* in MM-Fe containing 0, 0.01, or 1 mM $FeCl_3$ or $FeSO_4$, and monitored expression of *ATX1*, *FET3*, *MIRB*, *SID1* and *SIT1* using RNA gel blots (Fig. 5.6). *ATX1* putatively encodes a copper chaperone/metal homeostasis factor, and *MIRB* and *SIT1* putatively encode triacetylfusaranine C and ferrioxamine transporters, respectively (Lin and Culotta, 1995; Lin et al., 1997; Haas et al., 2003; Park et al., 2006b). When compared to wild-type gene expression under the same conditions (Fig. 5.1), the Δ*fet3* mutant showed no alteration in iron uptake-related gene expression, except the loss of *FET3* expression, which confirmed the disruption of that gene and creation of a null-mutant. The Δ*sid1* mutant on the other hand, showed higher levels of iron-related gene expression than either the wild type or Δ*fet3* mutant when iron was added to the growth medium, suggesting that the Δ*sid1* mutant is iron-starved regardless of the medium iron concentration. These results suggest that siderophore-mediated iron uptake is preferred over FET3/FTR1-mediated iron uptake in *F. graminearum*.

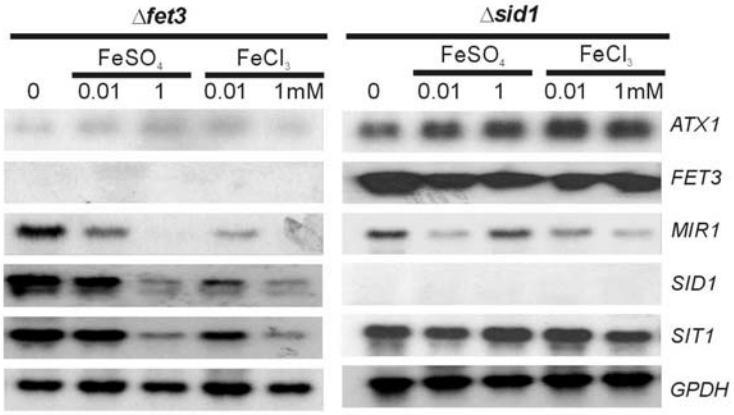

Figure 5.6 Δ*sid1* mutants show higher expression of iron-related genes. Total RNA was isolated from the Δ*fet3* or Δ*sid1* mutants grown in MM-Fe containing the indicated iron sources. Following electrophoresis and transfer to nylon membranes, the RNA was probed with ^{32}P-labeled cDNAs representing *FET3* or *SID1*. The constitutively expressed gene *GPDH* was used to monitor even loading of the RNA.

5.2.6 *SID1*, but not *FET3*, is required for full virulence on wheat

To study the involvement of *FET3* and *SID1* in pathogenicity, we first followed expression of the five iron uptake-related genes during a 7-d infection time course of wild-type *F. graminearum* on wheat spikes (Fig. 5.7a). Beginning at 3 d post inoculation (dpi), both *ATX1* and *SID1* were expressed to detectable levels, while *FET3*, *MIR1* and *SIT1* showed no detectable expression.

We then examined the impact of the loss of *FET3* or *SID1* on *F. graminearum* virulence by inoculating wheat spikes with Δ*fet3*, Δ*sid1*, or wild-type PH-1 strains, and followed the disease progress over a 9-d time course (Fig. 5.7b). To improve the contrast between infected and uninfected spikelets, we cleared the spikes with a solvent solution. In cleared, fixed spikes, slight browning of the inoculated spikelet was evident beginning at 3 dpi when either PH-1 or the Δ*fet3* mutant was used as inoculum. Spikelets inoculated with the Δ*sid1* mutant, however, did not begin to brown until 5 dpi. Both PH-1 and Δ*fet3* mutant inoculated spikes showed similar disease progression, with spikelets above, below and on the opposite side of the rachis to the inoculated spikelet becoming heavily infected by 7 dpi. After 9 dpi, symptoms on spikes inoculated with the Δ*sid1* mutant were still restricted to the inoculated spikelet. To compare the spread of PH-1 and Δ*sid1* strains through the rachis, we removed the spikelets from the cleared, fixed spikes and examined the rachis nodes for the browning characteristic of fungal invasion. Fig. 5.7c shows that at 9 dpi, symptoms caused by the Δ*sid1* mutant were still confined to within the inoculated spikelet, while the spike inoculated with the wild-type fungus showed heavy infection on both sides of the rachis and above and below the inoculated spikelet. To ensure that the Δ*sid1* mutant was confined within the inoculated spikelet, rather than spreading asymptomatically, we sectioned the rachis surrounding the spikelets inoculated with the Δ*sid1* mutant or wild type PH-1 and stained the tissue with trypan blue. As shown in Fig. 5.7d, no hyphal growth was evident in the rachis of the Δ*sid1*-inoculated spike, while abundant hyphal growth was visible in the parenchymatic tissues of the rachis of the PH-1-inoculated spike. These results show that *SID1* is required for full virulence of *F. graminearum* on wheat.

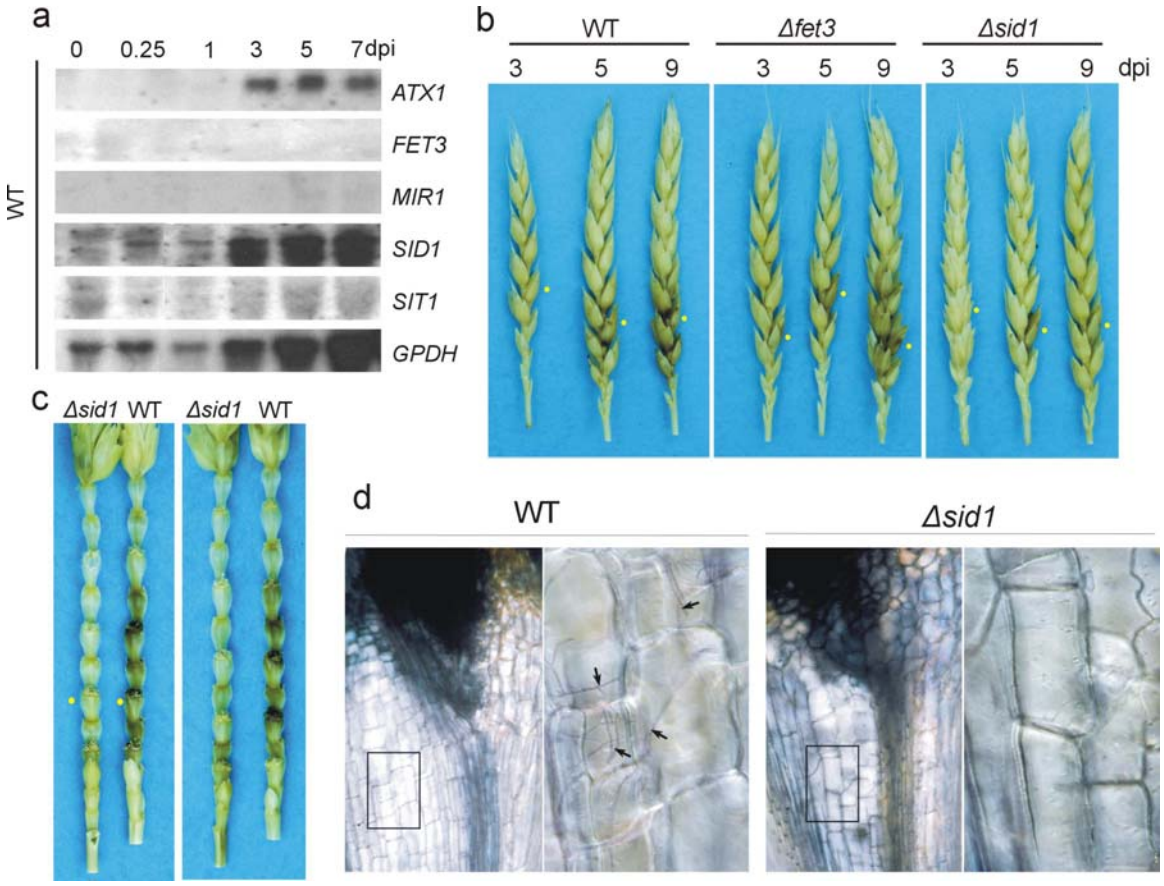

Figure 5.7 *SID1* is required for full *F. graminearum* virulence on wheat. (a) Transcription of iron uptake-related genes during infection of wheat spikes. Total RNA was isolated from spray-inoculated spikes at the time points indicated and was probed with ^{32}P-labeled cDNAs representing the iron uptake-related genes *ATX1*, *FET3*, *MIR1*, *SID1* or *SIT1*, or the constitutively expressed gene *GPDH*. **(b)** Disease progress in wheat spikes inoculated with Δ*fet3*, Δ*sid1* or wild-type (WT) strains of *F. graminearum*. Inoculated wheat (cv. CDC Teal) spikes were cleared, fixed and photographed 3, 5 and 9 days post inoculation (dpi). The Δ*sid1* mutant was restricted to the inoculated spikelet, limiting infection of adjacent spikelets. Yellow dots indicate inoculation points. **(c)** Infection patterns of Δ*sid1* and wild-type strains in the wheat rachis. Spikelets were detached from wheat spikes inoculated with Δ*sid1* or wild-type (WT) strains 9 dpi. Infection caused by the wild type spreads into several adjacent rachis nodes, while no visible infection appears within the rachis node (yellow dot) attached to the spike inoculated with Δ*sid1* mutant. The right panel shows the opposite side of the rachis. **(d)** Micrographs of longitudinal hand sections of wheat rachis and adjacent nodes, showing that intracellular hyphae (arrows) of the wild-type strain colonize the parenchyma tissue, whereas the Δ*sid1* mutant is absent from the rachis 9 dpi. The right panels show close-up views of the parenchyma cells of rachises.

5.3 Discussion

Iron is an essential nutrient for fungi; it is required for a range of enzymes and structural proteins. Iron is likely a limiting factor for pathogen growth inside of the host because it is sequestered by storage and transport peptides in plants and animals. Indeed, iron sequestration is a major anti-pathogen defence mechanism in some animal and plant systems (Alford et al., 1991; Expert, 1999; Schaible and Kaufmann, 2004). In *Arabidopsis*, ferritin withholds iron from the bacterial pathogen *Erwinia chrysanthemi*, suggesting that iron sequestration is also important in that pathosystem (Dellagi et al., 2005). We have also found that iron is an important defence factor in wheat, where it participates in generation of the oxidative burst and in regulating defence gene expression (Liu et al., 2007). We have now shown that siderophore production and virulence in *F. graminearum* requires *SID1*, which putatively encodes an ornithine N^5-oxygenase.

In an effort to characterize iron uptake in *F. graminearum*, we cloned iron uptake-related genes with homologues that had previously been studied in other fungi. These included *ATX1*, *FET3*, *MIR1*, *SID1* and *SIT1*, which putatively encode a copper chaperone/metal homeostasis factor, a cell surface ferroxidase, a triacetylfusarinine C transporter, an ornithine N^5-oxygenase, and a ferrichrome transporter, respectively. As expected, all of these genes were induced under low iron conditions. Surprisingly though, only *ATX1* and *SID1* were expressed *in planta*, suggesting that these genes are likely more important during infection. Our infection time courses using wild type PH-1, Δ*fet3* and Δ*sid1* strains certainly showed that this is true for *SID1*. In yeast, *ATX1* is required for resistance to superoxide and H_2O_2 (Lin and Culotta, 1995). Interestingly, *ATX1* is also required for high affinity iron uptake in yeast, as Atx1p provides copper to the multicopper ferroxidase Fet3p (Lin et al., 1997). In *F. graminearum*, the apparent lack of importance of *FET3* in virulence suggests that the *in planta* expression of *ATX1* could have more to do with antioxidant functions than copper delivery to FET3. The *SID1* RNA gel blot hybridization showed a doublet associated with this transcript. This doublet is interesting because *SID1* appears to be a single copy gene in *F. graminearum*, based on the available genome sequence. However, because both transcripts are absent

in the Δ*sid1* mutant, the second band could represent an alternatively spliced version of the gene.

The functional complementation of the yeast *fet3fet4* mutant showed that *F. graminearum FET3* does encode a functional cell surface ferroxidase. Unfortunately, the low overall levels of detectable ferroxidase activity precluded biochemical analysis of *FET3* disruption in *F. graminearum*. Interestingly though, using the fluorescent iron dye calcein, we showed that the Δ*fet3* strain had significantly higher levels of free intracellular iron than wild-type *F. graminearum*. In *A. nidulans*, deletion of *SidA* led to an increase in the intracellular free iron pool (Eisendle et al., 2003). Here, we showed that SID1 was responsible for the production of extracellular siderophores, but that the Δ*sid1* strain contained less free intracellular iron than wild type. Eisendle et al. (2003) germinated the *A. nidulans* cultures in 1.5 mM ferrous iron, whereas ferric iron was used in our uptake study, and this may explain the observed differences in calcein fluorescence. We hypothesize that siderophore-mediated iron uptake is responsible for the bulk of *F. graminearum* iron uptake, and that the observed decrease in intracellular free iron reflects the Δ*sid1* strain's impairment in iron uptake. Although the Δ*fet3* mutant was not impaired in siderophore biosynthesis and export, it remains possible that up-regulation of an unidentified siderophore exporter, like *E. chrysanthemi* YchA (Franza et al., 2005) or *E. coli* EntS (Furrer et al., 2002), could lead to lower intracellular siderophore concentrations and the observed increase in the free iron pool. Further work is needed to characterize this aspect of the mutant.

The two major types of resistance to *Fusarium* head blight in wheat are type I resistance, which prevents infection of the initially contacted floret, and type II resistance, which prevents spikelet-to-spikelet spread of the fungus (Schroeder and Christensen, 1963). The Δ*sid1* mutant was able to initiate a similar level of infection as the wild-type strain within the inoculated spikelet, but was unable to spread through the rachis. There are several possible explanations for this change in virulence, but we favour the view that the developing seed provides a ready source of nutrients that are not available within the rachis. Indeed, the iron content of all parts of the wheat plant except the grain drop over time, as the plant redirects its iron to the grain during maturation (Garnett and Graham, 2005). Also, while the phloem and xylem sap are relatively rich in

iron (Cataldo et al., 1988; Stephan et al., 1994), we did not detect much wild-type hyphae in the vascular tissues of the rachis, but rather found mostly intercellular hyphae in the parenchyma. This distinction may be cultivar-specific though, as Jansen et al. (2005) found hyphae both intracellularly in the vasculature and intercellularly in the parenchyma of the rachis of spring wheat cv. *Nandu* as early as 6 dai. Regardless of the wild-type growth pattern, however, the Δ*sid1* mutant was not found in either of these rachis cell types.

Our recent work on the role of iron in plant defence showed that while free, reactive iron is secreted to infection sites, where it mediates H_2O_2 production, host intracellular iron deficiency promotes the transcription of pathogenesis-related genes (Liu et al., 2007). This iron-dependent defence mechanism suggests that siderophores secreted by invading fungi may also trigger these defences. Siderophores could therefore act as pathogen-associated molecular patterns (PAMPs), and may alert the host to the pathogen's presence. Indeed, all of the plant pathogenic fungi that have been identified as requiring extracellular siderophores are necrotrophs (Oide, 2006), and are not likely hindered by a PAMP-triggered hypersensitive response (Govrin and Levine, 2000). The biotroph *U. maydis* requires reductive iron uptake rather than siderophores to sequester host iron (Eichhorn et al., 2006) and *Blumeria graminis* exhibits iron reductase activity during infection (Wilson et al., 2003), further suggesting separate strategies between biotrophs and necrotrophs. Our data suggest that in *F. graminearum*, siderophore-mediated iron uptake is more important than reductive iron uptake: First, there was no impairment in low iron growth in the Δ*fet3* strain, while the Δ*sid1* strain grew significantly more slowly than wild type. Second, the Δ*sid1* strain had a significantly smaller intracellular iron pool than the wild-type strain, while the Δ*fet3* strain iron pool was significantly larger than the wild-type iron pool. Third, disruption of *FET3* had no effect on the iron-dependent transcription of the other iron uptake-related genes, but disruption of *SID1* led to induction of all of the iron uptake-related genes. Finally, *SID1*, but not *FET3*, was required for full virulence of *F. graminearum* on wheat.

5.4 Materials and Methods

5.4.1 Fungal material and culture conditions

The wild-type *Fusarium graminearum* (*Gibberella zeae*) strain PH-1, obtained from the Fungal Genetics Stock Centre (Kansas City, MO), was used throughout. The fungus was routinely maintained on potato dextrose agar, containing 100 μg ml^{-1} hygromycin-B if needed, at room temperature and kept under long term storage in 30% (v/v) glycerol at -80°C. For cDNA cloning, wild type PH-1 was grown in an iron-free medium with casamino acids as the carbon source [containing (g/L): KH_2PO_4, 1.0; KNO_3, 1.0; $MgSO_4.7H_2O$, 0.5; KCl, 0.5; CH_3COONa, 1.0; casamino acids, 20]. For iron source assays of gene expression and siderophore production, the fungus was first grown for 4 d in minimal medium (Correll et al., 1987) without iron (MM-Fe) to which 0.01 mM $FeSO_4$ had been added, using a mycelium-covered 5 mm^2 plug as the inoculum. After 4 d, the mycelium was collected by filtration, washed twice with distilled water, and placed in MM-Fe for 2 d before being transferred to MM-Fe containing the indicated iron source for an additional 2 d. For radial growth assays, 5 mm^2 MM-Fe plugs were placed in the centre of MM-Fe plates containing either 50 μM of the iron chelator bathophenanthrolinedisulfonic acid (Sigma-Aldrich, St. Louis, MO), 0.01 mM $FeSO_4$ or 1 mM $FeSO_4$, and radial growth was measure from the centre of the colonies at 1, 2 and 3 d. To produce conidia, the fungus was grown in mung bean medium (Bai and Shaner, 1996) for 4 d, and the conidia were collected from the supernatant by filtration and centrifugation.

5.4.2 Siderophore determination and intracellular iron pool measurement

Siderophore secretion was determined by measuring siderophores in the growth medium using the chrome azurol S liquid assay as described (Schwyn and Neilands, 1987; Payne, 1994). Siderophore production was measured in the mutant strains Δ*sid1-1* and Δ*sid1-2,* and Δ*fet3-1,* Δ*fet3-2* and Δ*fet3-3*. The intracellular free iron pool was measured using calcein-AM (Molecular Probes, Eugene, OR) using an adaptation of Eisendle and colleagues' (2003) protocol. Δ*fet3-1* to Δ*fet3-3* , Δ*sid1-1* to Δ*sid1-3*, or wild type PH-1 *F. graminearum* was grown on solid MM-Fe containing 0.01 mM $FeSO_4$, and small

pieces of the mycelial mats were incubated in MM-Fe with 1.5 mM $FeCl_3$ for 1.5 h. Ferric $FeCl_3$ was used for measuring uptake because it is a substrate for both the reductive and siderophore uptake pathways. Conidia were harvested from mung bean medium containing 0.01 mM $FeSO_4$. The mycelia and conidia were then washed with water and transferred to 2 μM calcein-AM for 2 h before examination with a laser scanning microscope (Zeiss, Jena, Germany) with excitation/emission at 488/515 nm and 1 % argon laser output. For conidial iron storage measurements, the fluorescence was quantified using the Zeiss LSM Imaging software package.

5.4.3 DNA and RNA isolation and analysis

RNA and DNA were isolated as described in Chapters 3 and 4. DNA and RNA gel blots on GeneScreen Plus membranes (PerkinElmer, Wellesley, MA) were prepared as described by Sambrook and Russell (2001). Poly(A)$^+$RNA was isolated using the PolyATtract mRNA Isolation System (Promega, Madison, WI) according to the manufacturer's instructions. DNA from wild type PH-1 and the putative mutants was cut with *Xho*I and *Eco*RI for the Δ*fet3* and Δ*sid1* DNA gel blots, respectively. Probes for RNA gel blots were prepared from cDNAs using the Megaprime DNA labeling system (Amersham, Bucks, UK). The Δ*fet3* DNA gel blot probe was a *Hin*dIII/*Sac*I fragment of the Δ*fet3* ligation transformation construct. The Δ*sid1* DNA gel blot probe was a *Sma*I/*Nhe*I fragment of the Δ*sid1* ligation transformation construct. Hybridization was performed as described by Sambrook and Russell (2001), with 2 x 20 min washing performed in 1X SSC, 0.1% SDS at 65°C, and 1 x 20 min washing in 0.1X SSC, 0.1% SDS.

5.4.4 Targeted gene disruption

To construct the gene replacement vector for *FET3* disruption, a 3.2-kb fungal expression cassette governing *E. coli* hygromycin-B phosphotransferase gene expression (*HPH*) was cut from pGC1-1 (Rikkerink et al., 1994) by *Eco*RI/*Hin*dIII and inserted into the same site of *pBluescript* (Stratagene, La Jolla, CA) to create *pBS-HPH*. *FET3* was amplified from genomic DNA with the Expand high fidelity PCR kit (Eppendorf,

Hamburg, Germany) using primers fetF4 (5'-ctacagcctaacactggctcatcc) and fetR4 (5'-ccaccgttacggttggtgcatctg), cut with *Apa*I/*Xba*I, and the left and right gene borders were ligated to a *Apa*I/*Xba*I *HPH* fragment cut from *pBS-HPH*. The resulting 5421 bp ligation product was amplified in two sections using primers fetF4 and hphR2 (5'-ctacacagccatcggtccagacg) for the 5' end, and primers hphF1 (5'-cgccgatagtggaaaccgacgc) and fetR4 for the 3' end, resulting in left and right fragments which shared a 844 bp region of the *HPH* gene that were used for transformation. *SID1* was amplified using primers sidF4 (5'-cttcatcgtcagagtcaggccctg) and sidR4 (5'-cctgcccaatgataccttgcttgc), cut with *Bgl*II/*Hind*III, and the left and right gene borders were ligated to a *Bgl*II/*Hind*III *HPH* fragment cut from *pAN7-2* (Punt et al., 1987). The resulting 5798 bp product was amplified in two sections by sidF4 and hphR2, and sidR4 and hphF1, respectively. Protoplast preparation and fungal transformation were carried out as described by Proctor et al. (1997).

5.4.5 Yeast complementation

The yeast strains used in this study were wild-type DY1457 (*MAT*α, *ade6*, *can1*, *his3*, *leu2*, *trp1*, *ura3*) and *fet3fet4* DEY1433 (*MAT*α, *ade2, can1, his3, leu2, trp1, ura3, fet3*::*HIS3, fet4*::*LEU2*). The yeast strains were a kind gift from David Eide (University of Wisconsin-Madison). *F. graminearum FgFET3* was amplified from MM-Fe mRNA with the Expand high fidelity PCR kit (Eppendorf) using primers fetF2 (5'-ctgtccagagtgtgtccgg) and fetR2 (5'-ggggctgtgcgttggcgttgc), TA-cloned into plasmid *pBluescript*, confirmed by sequencing, cut with *Sac*I and *Xho*I, and subcloned into *Sac*I/*Xho*I-digested *pYES2* (Invitrogen, Carlsbad, CA) behind the GAL promoter to make *pYES2-FgFET3*. The GAL promoter of plasmid *pYES2* drives expression of the inserted gene when the yeast is grown in the presence of galactose. Wild-type and *fet3fet4* strains were transformed with either *pYES2* or *pYES2-FgFET3* using standard procedures (Schiestl and Gietz, 1989) and plated onto SD medium (0.67% (w/v) yeast nitrogen base without amino acids, 2% (w/v) glucose or galactose, required auxotrophic supplements, and 2% (w/v) agar for plates) containing 50 µM bathophenanthrolinedisulfonic acid and the iron sources and concentrations indicated in

the figure legend. Bathophenanthrolinedisulfonic acid is a ferrous iron chelator and was added to chelate any trace ferrous iron that would allow the *fet3fet4* mutant to grow.

5.4.6 Inoculation and pathogenicity tests

The susceptible wheat (*Triticum aestivum*) cultivar CDC Teal was used for virulence tests (Feng et al., 2005). Plants were grown in 10 cm pots in a growth chamber with day/night temperatures of 22°C/18°C and a 16 h photoperiod. Wheat spikes at anthesis were point-inoculated with the *F. graminearum* wild-type strain PH-1 or transformants by placing a droplet (10 µl) of conidial suspension (10^6 ml^{-1}) within the palea and lemma of one floret of the fourth spikelet from the bottom of the spike tested, and were kept at 100% humidity for 2 d after inoculation. The inoculations were repeated four times independently using all of the Δ*sid1* mutant strains and Δ*fet3-2,* Δ*fet3-3* and Δ*fet3-4*. Each mutant was used to inoculate at least five spikes per experiment and similar results were obtained between strains of either mutant. Spikes were cleared in 60:30:10 methanol:chloroform:acetic acid and rehydrated through an ethanol gradient before photography or dissection and staining in trypan blue. For RNA isolation from infected plants, spikes were sprayed with a 10^4 ml^{-1} suspension of conidia, kept at 100% humidity for the first 2 d and harvested at the time points specified.

CHAPTER 6

GENERAL DISCUSSION

It had previously been suggested that the pathogen-induced oxidative burst, a rapid, transient burst of reactive oxygen species (ROS), was the product of enzymatic processes at the site of pathogen attack (Thordal-Christensen et al., 1997; Torres et al., 2002; Yoshioka et al., 2003; Bindschedler et al., 2006; Trujillo et al., 2006). The widespread use of *Arabidopsis thaliana* as a model research organism in plant biology has reinforced this view. In *Arabidopsis*, silencing of respiratory burst oxidase homologues or peroxidases can abrogate indicator dye-detectable production of ROS (Torres et al., 2002; Torres et al., 2005; Bindschedler et al., 2006). Because stable monocot transformation is difficult and unreliable, research into ROS production during monocot-pathogen interactions has borrowed heavily from investigations in *Arabidopsis*. Unfortunately, reliance on data from this distant plant system has further obscured progress into ROS-based defences in monocot plants. In Chapter 2, I showed that during powdery mildew attack, diploid wheat plants launch a targeted redistribution of cellular iron to the apoplast. Apoplastic iron accumulation was also shown to occur following attack of maize, oat, barley, sorghum and millet, suggesting that this defence phenomenon is common to cereal crops. It is important to note that no non-cereal monocots were tested in this work, so the results may not apply to all monocots. Once in the apoplast, the accumulated iron mediates production of H_2O_2. How the free, reactive iron leads to H_2O_2 production remains unknown. Interestingly, Smith et al. (1997) found a nearly identical phenomenon in Alzheimer disease-affected brains, suggesting that this mode of ROS production has evolved independently in different kingdoms.

Although the oxidative burst can be an effective defence strategy, in terms of cell wall strengthening, defence gene signalling and damage to the pathogen, the plant cell must still protect itself from this potentially harmful mode of protection. The relative amount of oxidized and reduced constituents of these couples (e.g. NADP:NADPH) determines the overall redox state of the cell, and buffers its relative oxidizing or reducing potential. It should be noted that measurements of ROS therefore reflect a shift in redox balance, and that when ROS are detected, it shows that the cellular balance has shifted and that ROS-scavenging mechanisms are unable to keep up with ROS production. Several ROS-scavenging mechanisms occur in plants and are hinged on enzymatic cycling of redox couples. An entry point for much of this scavenging is

through the reduction of $O_2^{\bullet-}$ to H_2O_2 via the action of superoxide dismutase (SOD, Bowler et al., 1991). H_2O_2 can then be disarmed by conversion to water by catalase (Willekens et al., 1997). H_2O_2 can also be converted to water by oxidation of glutathione (GSH) to glutathione disulfide (GSSG) through the action of glutathione peroxidase (Noctor et al., 2002). The GSSG can then be re-reduced to GSH by glutathione reductase, using NAD(P)H. Another means of converting H_2O_2 to water is through cycling of the redox couple ascorbate and monodehydroascorbate (MDA), which are cycled by ascorbate peroxidase and MDA reductase (Shigeoka et al., 2002). The importance of ascorbate and glutathione in redox cycling is evident from the lowered oxidative stress tolerance in transgenic plants with altered ascorbate (Conklin et al., 1996) or glutathione (Creissen et al., 1999) levels. In Chapter 4, I demonstrated a new ROS-scavenging pathway that relies on the quinone reductase QR2. QR2 does not disarm ROS on its own, but rather prevents the futile cycling of quinones and concomitant $O_2^{\bullet-}$ production by QR1s, and in this way is comparable to the ascorbate and glutathione cycles.

In Chapter 3, I showed that iron accumulation leads to the induction of defence gene expression through ROS production. In *Arabidopsis*, two kinases ANP1 and OXI1 have been shown to lead a signalling cascade following exposure to H_2O_2 (Asai et al., 2002; Rentel et al., 2004). As above though, drawing parallels between *Arabidopsis* and wheat is sometimes inaccurate. Interestingly, further work in the Wei lab has shown that the apoplastic accumulation of cellular iron leaves the cytoplasm in a state of iron depletion, which works synergistically with ROS to promote defence gene expression (Liu et al., 2007). This iron depletion-driven defence gene induction is especially interesting when considering the results presented in Chapter 5, which show that *Fusarium graminearum* requires siderophore production for full virulence. Recently, Oide et al. (2006) described the role of the non-ribosomal peptide synthase NPS6 in extracellular siderophore production and showed that it was required for full virulence in the ascomycetes *Cochliobolus heterostrophus*, *C. miyabeanus*, *F. graminearum* and *Alternaria brassicicola*. Siderophore production is not required for virulence in the basidiomycetes *Ustilago maydis* (Mei et al., 1993) and *Microbotryum violaceum* (Birch and Ruddat, 2005), but loss of the ferroxidase/permease system of reductive iron uptake

leads to a reduction in *U. maydis* virulence (Eichhorn et al., 2006). On the surface, it seems convenient to attribute these different modes of infection-related iron uptake to the taxonomic distance between ascomycetes and basidiomycetes. However, neither *Saccharomyces cerevisiae* nor *Candida albicans* can produce or secrete siderophores (Philpott, 2002) and *B. graminis* f. sp. *hordei* spores show abundant ferric reductase activity (Wilson et al., 2003). Also, *B. graminis* f. sp. *hordei* condia express the multicopper oxidase gene *FET3* (Thomas et al., 2001), which is required for full virulence in *U. maydis* (Eichhorn et al., 2006). In light of data showing the induction of wheat defence-related genes following siderophore treatments (Liu et al., 2007), it is tempting to consider that pathogen-produced siderophores may in fact work as pathogen-associated molecular patterns (PAMPS) in triggering host defences. All of the plant pathogenic fungi that require siderophore production for virulence are necrotrophs (Oide et al., 2006), which are not as sensitive to recognition by the host as biotrophs (van Kan, 2006). Also, *U. maydis*, the only biotrophic pathogen characterised with respect to iron uptake, uses the reductive uptake system, thus avoiding secretion of potentially recognisable siderophores. Similarly, what little evidence that exists suggests that biotrophic *B. graminis* f. sp. *hordei* also uses the reductive iron uptake system. It will be interesting to explore this relationship further and to understand how fungal siderophores are recognised and handled by host plants. Figure 6.1 represents the themes presented in this thesis.

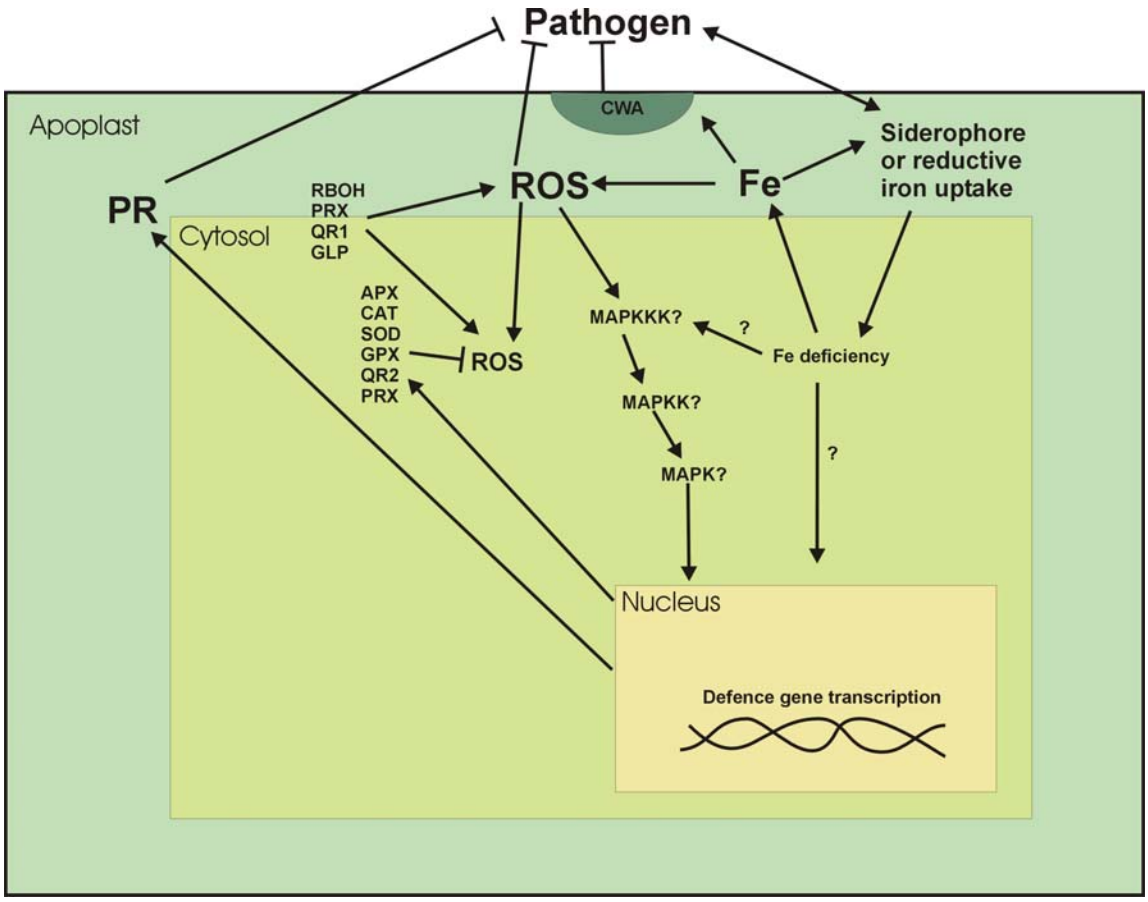

Figure 6.1 Iron and reactive oxygen in wheat-pathogen interactions. When pathogens attack, wheat plants mount a number of related defences. The production of reactive oxygen species (ROS) is controlled by either the apoplastic accumulation of reactive iron (Fe) or by enzymatic means. Cell wall appositions (CWAs) are fortified barriers formed beneath sites of attack and are major sites of iron and ROS accumulation. The production of ROS in the apoplast can trigger defence gene expression, possibly through an as yet unidentified kinase signalling cascade. Plants defend themselves against the negative effects of ROS using a number of enzymatic ROS scavengers. The secretion of cellular iron can lead to a state of intracellular iron deficiency, which can also promote defence gene transcription. This iron deficiency can be exacerbated by secretion of iron-binding siderophores by the pathogen. Defence gene transcription leads to yet another mode of defence through the production and secretion of pathogenesis-related (PR) proteins. RBOH: respiratory burst oxidase homologue; PRX: peroxidase; QR: quinone reductase; GLP: germin-like protein; APX: ascorbate peroxidase; CAT: catalase; SOD: superoxide dismutase; GPX: glutathione peroxidase; MAPK: mitogen-associated protein kinase.

While some progress has been made towards understanding the roles of iron and ROS during plant-pathogen interactions, questions still remain. How do cereals sense and relay the ROS signal to the nucleus to promote defence gene transcription? How is iron deficiency sensed by the plant cell, and how is this signal relayed to the nucleus? Increased focus on important cereal crops will surely unravel much of what remains unknown. In particular, the development of high-throughput techniques for screening defence responses *in planta* will help to fill the gaps in what is now a fragmented picture.

LITERATURE CITED

Able, A.J. (2003). Role of reactive oxygen species in the response of barley to necrotrophic pathogens. Protoplasma *221,* 137-143.

Agrios, G. N. (1999). Plant Pathology. Academic Press, Toronto.

Akileswaran, L., Brock, B.J., Cereghino, J.L., and Gold, M.H. (1999). 1,4-Benzoquinone reductase from *Phanerochaete chrysosporium*: cDNA cloning and regulation of expression. Applied and Environmental Microbiology *65,* 415-421.

Alexandrov, P.N., Zhao, Y., Pogue, A.I., Tarr, M.A., Kruck, T.P.A., Percy, M.E., Cui, J., and Lukiw, W.J. (2005). Synergistic effects of iron and aluminum on stress-related gene expression in primary human neural cells. Journal of Alzheimer's Disease *8,* 117-127.

Alford, C.E., King Jr., T.E., and Campbell, P.A. (1991). Role of transferrin, transferrin receptors, and iron in macrophage listericidal activity. Journal of Experimental Medicine *174,* 459-466.

Alvarez, M.E., Pennell, R.I., Meijer, P., Ishikawa, A., Dixon, R.A., and Lamb, C. (1998). Reactive oxygen intermediates mediate a systemic signal network in the establishment of plant immunity. Cell *92,* 773-784.

An, Q., Hückelhoven, R., Kogel, K.-H., and van Bel, A.J.E. (2006). Multivesicular bodies participate in a cell wall-associated defence response in barley leaves attacked by the pathogenic powdery mildew fungus. Cellular Microbiology *8,* 1009-1019.

Asai, T., Tena, G., Plotnikova, J., Willmann, M.R., Chiu, W., Gomez-Gomez, L., Boller, T., Ausubel, F.M., and Sheen, J. (2002). Map kinase signalling cascade in *Arabidopsis* innate immunity. Nature *415,* 977-983.

Assaad, F.F., Qiu, J., Youngs, H., Ehrhardt, D., Zimmerli, L., Kalde, M., Wanner, G., Peck, S.C., Edwards, H., Ramonell, K., Somerville, C.R., and Thordal-Christensen, H. (2004). The PEN1 syntaxin defines a novel cellular compartment upon fungal attack and is required for the timely assembly of papillae. Molecular Biology of the Cell *15,* 5118-5129.

Atkinson, M. M., Midland, S. L., Sims, J. J., and Keen, N. T. (1996). Syringolide 1 triggers Ca^{2+} influx, K+ efflux, and extracellular alkalization in soybean cells carrying the disease-resistance gene *Rpg4*. Plant Physiology *112,* 297-302.

Babiychuk, E., Kushnir, S., Belles-Boix, E., Van Montagu, M., and Inze, D. (1995). *Arabidopsis thaliana* NADPH oxidoreductase homologs confer tolerance of yeasts toward the thiol-oxidizing drug diamide. Journal of Biological Chemistry *270,* 26224-26231.

Bai, G.H., and Shaner, G. (1996). Variation in *Fusarium graminearum* and cultivar resistance to wheat scab. Plant Disease *80,* 975-979.

Bertucci, F., Bernard, K., Loriod, B., Chang, Y.-C., Granjeaud, S., Birnbaum, D., Nguyen, C., Peck, K., and Jordan, B.R. (1999). Sensitivity issues in DNA array-based expression measurements and performance of nylon microarrays for small samples. Human Molecular Genetics *8,* 1715-1722.

Bilecen, K., Ozturk, U.H., Duru, A.D., Sutlu, T., Petoukhov, M.V., Svergun, D.I., Koch, M.H.J., Sezerman, U.O., Cakmak, I., and Sayers, Z. (2005). *Triticum durum* metallothionein: Isolation of the gene and structural characterization of the protein using solution scattering and molecular modeling. Journal of Biological Chemistry *280,* 13701-13711.

Bindschedler, L.V., Dewdney, J., Blee, K.A., Stone, J.M., Asai, T., and Plotnikov, J. et al. (2006). Peroxidase-dependent apoplastic oxidative burst in *Arabidopsis* required for pathogen resistance. Plant Journal *47,* 851-863.

Birch, L.E., and Ruddat, M. (2005). Siderophore accumulation and phytopathogenicity in *Microbotryum violaceum*. Fungal Genetics and Biology *42,* 579-589.

Bolwell, G.P., Bindschedler, L.V., Blee, K.A., Butt, V.S., Davies, D.R., Gardner, S.L., Gerrish, C., and Minibayeva, F. (2002). The apoplastic oxidative burst in response to biotic stress in plants: A three-component system. Journal of Experimental Botany *53,* 1367-1376.

Briat, J.-F., Lobréaux, S., Grignon, N., and Vansuyt, G. (1999). Regulation of plant ferritin synthesis: How and why. Cellular and Molecular Life Sciences *56,* 155-166.

Bowler, C., Slooten, L., Vandenbranden, S., De Rycke, R., Botterman, J., Sybesma, C., Van Montagu, M., and Inze, D. (1991). Manganese superoxide dismutase can

reduce cellular damage mediated by oxygen radicals in transgenic plants. EMBO Journal *10,* 1723-1732.

Büschges, R., Hollricher, K., Panstruga, R., Simons, G., Wolter, M., Frijters, A., et al. (1997). The barley Mlo gene: A novel control element of plant pathogen resistance. Cell *88,* 695-705.

Caltagirone, A., Weiss, G., and Pantopoulos, K. (2001). Modulation of cellular iron metabolism by hydrogen peroxide. Effects of H_2O_2 on the expression and function of iron-responsive element-containing mRNAs in B6 fibroblasts. Journal of Biological Chemistry *276,* 19738-19745.

Canadian Grain Commission (2006). 4. Wheat. In: Official grain grading guide. CGC Industry Services, Winnipeg.

Carol, R.J., Takeda, S., Linstead, P., Durrant, M.C., Kakesova, H., Derbyshire, P., Drea, S., Zarsky, V., and Dolan, L. (2005). A RhoGDP dissociation inhibitor spatially regulates growth in root hair cells. Nature *438,* 1013-1016.

Cataldo, D.A., McFadden, K.M., Garland, T.R. and Wildung, R.E. (1988). Organic constituents and complexation of nickel(II), iron(III), cadmium(II), and plutonium(IV) in soybean xylem exudates. Plant Physiology *86,* 734-739.

Chen, S., and Dickman, M. B. (2004). Bcl-2 family members localize to tobacco chloroplasts and inhibit programmed cell death induced by chloroplast-targeted herbicides. Journal of Experimental Botany *55,* 2617-2623.

Choi, E, Kim, E., Oh, H., Kim, S., Lee, H., and Cho, E. et al. (2004). Iron chelator triggers inflammatory signals in human intestinal epithelial cells: Involvement of p38 and extracellular signal-regulated kinase signaling pathways. Journal of Immunology *172,* 7069-7077.

Christensen, A.B., Thordal-Christensen, H., Zimmermann, G., Gjetting, T., Lyngkjær, M.F., Dudler, R., and Schweizer, P. (2004). The germinlike protein GLP4 exhibits superoxide dismutase activity and is an important component of quantitative resistance in wheat and barley. Molecular Plant-Microbe Interactions *17,* 109-117.

Clarke, A., Desikan, R., Hurst, R.D., Hancock, J.T., and Neill, S.J. (2000). NO way back: Nitric oxide and programmed cell death in *Arabidopsis thaliana* suspension cultures. Plant Journal *24,* 667-677.

Clay, K., and Kover, P. X. (1996). The red queen hypothesis and plant/pathogen interactions. Annual Review of Phytopathology *34,* 29-50.

Clay, M.D., Jenney Jr., F.E., Hagedoorn, P.L., George, G.N., Adams, M.W.W., and Johnson, M.K. (2002). Spectroscopic studies of *Pyrococcus furiosus* superoxide reductase: Implications for active-site structures and the catalytic mechanism. Journal of the American Chemical Society *124,* 788-805.

Cobbett, C., and Goldsbrough, P. (2002). Phytochelatins and Metallothioneins: Roles in heavy metal detoxification and homeostasis. Annual Review of Plant Biology *53,* 159-182.

Cohen, A., Nelson, H. and Nelson, N. (2000). The family of SMF metal ion transporters in yeast cells. Journal of Biological Chemistry *275,* 33388-33394.

Collins, N.C., Thordal-Christensen, H., Lipka, V., Bau, S., Kombrink, E., Qiu, J. et al. (2003). SNARE-protein-mediated disease resistance at the plant cell wall. Nature *425,* 973-977.

Conklin, P.L., Williams, E.H., and Last, R.L. (1996). Environmental stress sensitivity of an ascorbic acid-deficient *Arabidopsis* mutant. Proceedings of the National Academy of Sciences of the United States of America *93,* 9970-9974.

Correll, J.C., Klittich, C.J.R. and Leslie, J.F. (1987). Nitrate nonutilizing mutants of *Fusarium oxysporum* and their use in vegetative compatibility tests. Phytopathology *77,* 1640-1646.

Creissen, G., Firmin, J., Fryer, M., Kular, B., Leyland, N., and Reynolds, H. et al. (1999). Elevated glutathione biosynthetic capacity in the chloroplasts of transgenic tobacco plants paradoxically causes increased oxidative stress. Plant Cell *11,* 1277-1291.

Curie, C., and Briat, J.-F. (2003). Iron Transport and Signaling in Plants. Annual Review of Plant Biology *54,* 183-206.

Dat, J., Vandenabeele, S., Vranová, E., Van Montagu, M., Inzé, D., and Van Breusegem, F. (2000). Dual action of the active oxygen species during plant stress responses. Cellular and Molecular Life Sciences *57,* 779-795.

Davis, K.R., and Hahlbrock, K. (1987). Induction of defence responses in cultured parsley cells by plant cell wall fragments. Plant Physiology *85,* 1286-1290.

De Bary, A. (1863). Recherches sur le développement de quelques champignons parasites. Ann. Sci. Nat. (Bot.) *20,* 5-148.

de Hoogt, R., Luyten, W.H., Contreras, R. and De Backer, M.D. (2000). PCR- and ligation-mediated synthesis of split-marker cassettes with long flanking homology regions for gene disruption in *Candida albicans*. Biotechniques *28,* 1112-1116.

Deák, M., Horváth, G.V., Davletova, S., Tör̈ök, K., Sass, L., Vass, I., Barna, B., Király, Z., and Dudits, D. (1999). Plants ectopically expressing the iron-binding protein, ferritin, are tolerant to oxidative damage and pathogens. Nature Biotechnology *17,* 192-196.

Dellagi, A., Rigault, M., Segond, D., Roux, C., Kraepiel, Y., Cellier, F., Briat, J., Gaymard, F., and Expert, D. (2005). Siderophore-mediated upregulation of *Arabidopsis* ferritin expression in response to *Erwinia chrysanthemi* infection. Plant Journal *43,* 262-272.

Dexter, J.E., Clear, R.M. and Preston, K.R. (1996). Fusarium Head Blight: effect on the milling and baking of some Canadian wheats. Cereal Chemistry *73,* 695-701.

Dix, D.R., Bridgham J.T., Broderius, M.A., Byersdorfer, C.A. and Eide, D.J. (1994). The *FET4* gene encodes the low affinity Fe(II) transport protein of *Saccharomyces cerevisiae*. Journal of Biological Chemistry *269,* 26092-26099.

Dodds, P. N., Lawrence, G. J., Catanzariti, A., Teh, T., Wang, C.A., and Ayliffe, M. A. et al. (2006). Direct protein interaction underlies gene-for-gene specificity and coevolution of the flax resistance genes and flax rust avirulence genes. Proceedings of the National Academy of Sciences of the United States of America *103,* 8888-8893.

Doke, N. (1983). Involvement of superoxide anion generation in the hypersensitive response of potato-tuber tissues to infection with an incompatible race of *Phytophthora infestans* and to the hyphal wall components. Physiological Plant Pathology *23,* 345-357.

Eichhorn, H., Lessing, F., Winterberg, B., Schirawski, J., Kamper, J., Muller, P. and Kahmann, R. (2006). A Ferroxidation/Permeation Iron Uptake System Is Required for Virulence in *Ustilago maydis*. Plant Cell *18,* 3332-3345.

Eisendle, M., Oberegger, H., Zadra, I. and Haas, H. (2003). The siderophore system is essential for viability of *Aspergillus nidulans*: functional analysis of two genes encoding l-ornithine N^5-monooxygenase (*sidA*) and a non-ribosomal peptide synthetase (*sidC*). Molecular Microbiology *49,* 359-375.

El Hassouni, M., Chambost, J.P., Expert, D., Van Gijsegem, F., and Barras, F. (1999). The minimal gene set member *msrA*, encoding peptide methionine sulfoxide reductase, is a virulence determinant of the plant pathogen *Erwinia chrysanthemi*. Proceedings of the National Academy of Sciences of the United States of America *96,* 887-892.

Ellis, J. (2006). Insights into nonhost disease resistance: Can they assist disease control in agriculture? Plant Cell *18,* 523-528.

Ellis, J., Dodds, P., and Pryor, T. (2000). Structure, function and evolution of plant disease resistance genes. Current Opinion in Plant Biology *3,* 278-284.

Expert, D. (1999). Withholding and exchanging iron: Interactions between *Erwinia* spp. and their plant hosts. Annual Review of Phytopathology *37,* 307-334.

Farr, D.F., Bills, G.F., Chamuris, G.P., and Rossman, A.Y. (1989). Fungi on plants and plant products in the United States. American Phytopathological Society Press, St. Paul.

Feng, J., Liu, G., Selvaraj, G., Hughes, G.R. and Wei, Y. (2005). A secreted lipase encoded by *LIP1* is necessary for efficient use of saturated triglyceride lipids in *Fusarium graminearum*. Microbiology *151,* 3911-3921.

Flor, H.H. (1955). Host-parasite interaction in flax rust - its genetics and other implications. Phytopathology *45,* 680-685.

Fobert, P.R., and Després, C. (2005). Redox control of systemic acquired resistance. Current Opinion in Plant Biology *8,* 378-382.

Forrester, M.T., and Stamler, J.S. (2007). A classification scheme for redox-based modifications of proteins. American Journal of Respiratory Cell and Molecular Biology *36,* 136-137.

Fotopoulos, V., Gilbert, M.J., Pittman, J.K., Marvier, A.C., Buchanan, A.J., Sauer, N., Hall, J.L., and Williams, L.E. (2003). The monosaccharide transporter gene, *AtSTP4*, and the cell-wall invertase, *Atβfruct1*, are induced in *Arabidopsis* during

infection with the fungal biotroph *Erysiphe cichoracearum*. Plant Physiology *132,* 821-829.

Frahry, G., and Schopfer, P. (2001). NADH-stimulated, cyanide-resistant superoxide production in maize coleoptiles analyzed with a tetrazolium-based assay. Planta *212,* 175-183.

Franza, T., Mahé, B. and Expert, D. (2005). *Erwinia chrysanthemi* requires a second iron transport route dependent of the siderophore achromobactin for extracellular growth and plant infection. Molecular Microbiology *55,* 261-275.

Freytag, S., Arabatzis, N., Hahlbrock, K., and Schmelzer, E. (1994). Reversible cytoplasmic rearrangements precede wall apposition, hypersensitive cell death and defense-related gene activation in potato/*Phytophthora infestans* interactions. Planta *194,* 123-135.

Fry, S.C. (1986). Cross-linking of matrix polymers in the growing cell walls of angiosperms. Annual Review of Plant Physiology *37,* 165-186.

Fryer, M.J., Oxborough, K., Mullineaux, P.M., and Baker, N.R. (2002). Imaging of photo-oxidative stress responses in leaves. Journal of Experimental Botany *53,* 1249-1254.

Fujiwara, M., Umemura, K., Kawasaki, T., and Shimamoto, K. (2006). Proteomics of Rac GTPase Signaling Reveals Its Predominant Role in Elicitor-Induced Defense Response of Cultured Rice Cells. Plant Physiology *140,* 734-745.

Furrer, J.L., Sanders, D.N., Hook-Barnard, I.G. and McIntosh, M.A. (2002) Export of the siderophore enterobactin in *Escherichia coli*: involvement of a 43 kDa membrane exporter. Molecular Microbiology *44,* 1225-1234.

Garnett, T.P. and Graham, R.D. (2005). Distribution and remobilization of iron and copper in wheat. Annals of Botany *95,* 817-826.

Georgatsou, E. and Alexandraki, D. (1994). Two distinctly regulated genes are required for ferric reduction, the first step of iron uptake in *Saccharomyces cerevisiae*. Molecular Cell Biology *14,* 3065-3073.

Gilchrist, D. G. (1998). Programmed cell death in plant disease: The purpose and promise of cellular suicide. Annual Review of Phytopathology *36,* 393-414.

Govrin, E.M. and Levine A. (2000). The hypersensitive response facilitates plant infection by the necrotrophic pathogen *Botrytis cinerea*. Current Biology *10,* 751-757.

Green, J. R., Carver, T. L. W., and Gurr, S. J. (2002). The formation and function of infection and feeding structures. In: The Powdery Mildews: A Comprehensive Treatise. R. R. Belanger, W. R. Bushnell, A. J. Dik, and T. L. W. Carver, eds. American Phytopathological Society Press, St. Paul 66-82.

Greenberg, J. T., and Yao, N. (2004). The role of regulation of programmed cell death in plant-pathogen interactions. Cellular Microbiology *6,* 201-211.

Greenshields, D.L., Liu, G., and Wei, Y. (2007). Roles of iron in plant defence and fungal virulence. Plant Signaling and Behavior *2, In press*.

Greenshields, D.L., Liu, G., Selvaraj, G. and Wei, Y. (2005). Differential regulation of wheat quinone reductases in response to powdery mildew infection. Planta *222,* 867-875.

Greenshields, D.L., Liu, G., Selvaraj, G., and Wei, Y. (2004a). New insights into ancient resistance: The molecular side of cell wall appositions. Phytoprotection *85,* 49-52

Greenshields, D.L., Wang, F., Selvaraj, G., and Wei, Y. (2004b). Activity and gene expression of acid invertases in einkorn wheat (*Triticum monococcum*) infected with powdery mildew. Canadian Journal of Plant Pathology *26,* 506-513.

Gross, P., Julius, C., Schmelzer, E., and Hahlbrock, K. (1993). Translocation of cytoplasm and nucleus to fungal penetration sites is associated with depolymerization of microtubules and defence gene activation in infected, cultured parsley cells. EMBO Journal *12,* 1735-1744.

Haas, H. (2003). Molecular genetics of fungal siderophore biosynthesis and uptake: the role of siderophores in iron uptake and storage. Applied Microbiology and Biotechnology *62,* 316-330.

Haas, H., Schoeser, M., Lesuisse, E., Ernst, J.F., Parson, W., Abt, B., Winkelmann, G. and Oberegger, H. (2003). Characterization of the *Aspergillus nidulans* transporters for the siderophores enterobactin and triacetylfusarinine C. Biochemical Journal *371,* 505-513.

Hall, J.L., and Williams, L.E. (2003). Transition metal transporters in plants. Journal of Experimental Botany *54,* 2601-2613.

Halliwell, B., and Gutteridge, J. M. C. (1999). Free radicals, other reactive species, and disease. In: Free Radicals in Biology and Medicine, 3rd edn, Oxford University Press, Oxford, 617–783.

Hamel, F., Breton, C., and Houde, M. (1998). Isolation and characterization of wheat aluminum-regulated genes: Possible involvement of aluminum as a pathogenesis response elicitor. Planta *205,* 531-538.

Harborne, J.B. (1979). Variation in and functional significance of phenolic conjugation in plants. Recent Advances in Phytochemistry, Vol.12: Biochemistry of Plant Phenolics *12,* 457-474.

Heath, M. C. (1999). The enigmatic hypersensitive response: Induction, execution, and role. Physiological and Molecular Plant Pathology *55,* 1-3.

Heath, M.C. (1991). The role of gene-for-gene interactions in the determination of host species specificity. Phytopathology *81,* 127-130.

Hegedus, D.D., and Rimmer, S.R. (2005). Sclerotinia sclerotiorum: When "to be or not to be" a pathogen? FEMS Microbiology Letters *251,* 177-184.

Hentze, M.W., Muckenthaler, M.U., and Andrews, N.C. (2004). Balancing acts: Molecular control of mammalian iron metabolism. Cell *117,* 285-297.

Hideg, E., Kalai, T., Hideg, K., and Vass, I. (2000). Do oxidative stress conditions impairing photosynthesis in the light manifest as photoinhibition? Philisophical Proceedings of the Royal Society of London, Biological Sciences *355,*1511-1516.

Hissen, A.H.T., Wan, A.N.C., Warwas, M.L., Pinto, L.J., and Moore, M.M. (2005). The *Aspergillus fumigatus* siderophore biosynthetic gene sidA, encoding L-ornithine N5-oxygenase, is required for virulence. Infection and Immunity *73,* 5493-5503.

Hope, B.T., and Vincent, S.R. (1989). Histochemical characterization of neuronal NADPH-diaphorase. Journal of Histochemistry and Cytochemistry *37,* 653-661.

Hückelhoven, R., and Kogel, K.-H. (1998). Tissue-specific superoxide generation at interaction sites in resistant and susceptible near-isogenic barley lines attacked by the powdery mildew fungus (*Erysiphe graminis* f. sp. *hordei*). Molecular Plant-Microbe Interactions *11,* 292-300.

Hückelhoven, R., and Kogel, K.-H. (2003). Reactive oxygen intermediates in plant-microbe interactions: Who is who in powdery mildew resistance? Planta *216,* 891-902.

Hückelhoven, R., Fodor, J., Preis, C., and Kogel, K.-H. (1999). Hypersensitive cell death and papilla formation in barley attacked by the powdery mildew fungus are associated with hydrogen peroxide but not with salicylic acid accumulation. Plant Physiology *119,* 1251-1260.

Jacobs, A.K., Lipka, V., Burton, R.A., Panstruga, R., Strizhov, N., Schulze-Lefert, P., and Fincher, G.B. (2003). An *Arabidopsis* Callose Synthase, GSL5, Is Required for Wound and Papillary Callose Formation. Plant Cell *15,* 2503-2513.

Jansen, C., von Wettstein, D., Schäfer, W., Kogel, K.H., Felk, A. and Maier, F.J. (2005). Infection patterns in barley and wheat spikes inoculated with wild type and trichodiene synthase gene disrupted *Fusarium graminearum*. Proceedings of the National Academy of Sciences of the United States of America *102,* 16892-16897.

Jensen Jr., K.A., Ryan, Z.C., Wymelenberg, A.V., Cullen, D., and Hammel, K.E. (2002). An NADH: Quinone oxidoreductase active during biodegradation by the brown-rot basidiomycete *Gloeophyllum trabeum*. Applied and Environmental Microbiology *68,* 2699-2703.

Kaku, H., Nishizawa, Y., Ishii-Minami, N., Akimoto-Tomiyama, C., Dohmae, N., and Takio, K. et al. (2006). Plant cells recognize chitin fragments for defense signaling through a plasma membrane receptor. Proceedings of the National Academy of Sciences of the United States of America *103,* 11086-11091.

Kapiotis, S., Hermann, M., Exner, M., Sturm, B.N., Scheiber-Mojdehkar, B., Goldenberg, H., Kopp, S., Chiba, P., and Gmeiner, B.M.K. (2005). Aluminum ions stimulate the oxidizability of low density lipoprotein by Fe^{2+}: Implication in hemodialysis mediated atherogenic LDL modification. Free Radical Research *39,* 1225-1231.

Keyer, K., and Imlay, J.A. (1996). Superoxide accelerates DNA damage by elevating free-iron levels. Proceedings of the National Academy of Sciences of the United States of America *93,* 13635-13640.

Kim, K., and Suk, H. (1999). Biochemical Properties of NAD(P)H-Quinone Oxidoreductase from *Saccharomyces cerevisiae*. Journal of Biochemistry and Molecular Biology *32,* 127-132.

Knight, H., and Knight, M.R. (2001). Abiotic stress signalling pathways: specificity and cross-talk. Trends in Plant Science *6,* 262-267.

Kobae, Y., Sekino, T., Yoshioka, H., Nakagawa, T., Martinoia, E., and Maeshima, M. (2006). Loss of AtPDR8, a plasma membrane ABC transporter of *Arabidopsis thaliana*, causes hypersensitive cell death upon pathogen infection. Plant and Cell Physiology *47,* 309-318.

Kobayashi, I., and Hakuno, H. (2003). Actin-related defense mechanism to reject penetration attempt by a non-pathogen is maintained in tobacco BY-2 cells. Planta *217,* 340-345.

Kobayashi, I., Kobayashi, Y., Yamaoka, N., and Kunoh, H. (1992). Recognition of a pathogen and a nonpathogen by barley coleoptile cells. III. Responses of microtubules and actin filaments in barley coleoptile cells to penetration attempts. Can. J. Bot. *70,* 1815-1823.

Kobayashi, Y., Kobayashi, I., Funaki, Y., Fujimoto, S., Takemoto, T., and Kunoh, H. (1997). Dynamic reorganization of microfilaments and microtubules is necessary for the expression of non-host resistance in barley coleoptile cells. Plant Journal *11,* 525-537.

Koh, S., André, A., Edwards, H., Ehrhardt, D., and Somerville, S. (2005). *Arabidopsis thaliana* subcellular responses to compatible *Erysiphe cichoracearum* infections. Plant Journal *44,* 516-529.

Kovtun, Y., Chiu, W., Tena, G., and Sheen, J. (2000). Functional analysis of oxidative stress-activated mitogen-activated protein kinase cascade in plants. Proceedings of the National Academy of Sciences of the United States of America *97,* 2940-2945.

Kruger, W.M., Carver, T.L.W., and Zeyen, R.J. (2002). Effects of inhibiting phenolic biosynthesis on penetration resistance of barley isolines containing seven powdery mildew resistance genes or alleles. Physiological and Molecular Plant Pathology *61,* 41-51.

Kuge, S., Arita, M., Murayama, A., Maeta, K., Izawa, S., Inoue, Y., and Nomoto, A. (2001). Regulation of the yeast Yap1p nuclear export signal is mediated by redox signal-induced reversible disulfide bond formation. Molecular and Cellular Biology *21,* 6139-6150.

Lam, E., Kato, N., and Lawton, M. (2001). Programmed cell death, mitochondria and the plant hypersensitive response. Nature *411,* 848-853.

Laskowski, M.J., Dreher, K.A., Gehring, M.A., Abel, S., Gensler, A.L., and Sussex, I.M. (2002). *FQR1*, a novel primary auxin-response gene, encodes a flavin mononucleotide-binding quinone reductase. Plant Physiology *128,* 578-590.

Lee, J., Godon, C., Lagniel, G., Spector, D., Garin, J., Labarre, J., and Toledano, M.B. (1999). Yap1 and Skn7 control two specialized oxidative stress response regulons in yeast. Journal of Biological Chemistry *274,* 16040-16046.

Lemmens, M., Scholz, U., Berthiller, F., Dall'Asta, C., Koutnik, A., Schuhmacher, R., Adam, G., Buerstmayr, H., Mesterházy, A., Krska, R., and Ruckenbauer, P. (2005). The ability to detoxify the mycotoxin deoxynivalenol colocalizes with a major quantitative trait locus for fusarium head blight resistance in wheat. Molecular Plant-Microbe Interactions *18,* 1318-1324.

Levine, A., Tenhaken, R., Dixon, R., and Lamb, C. (1994). H_2O_2 from the oxidative burst orchestrates the plant hypersensitive disease resistance response. Cell *79,* 583-593.

Lin, S.J. and Culotta, C.V. (1995). The *ATX1* gene of *Saccharomyces cerevisiae* encodes a small metal homeostasis factor that protects cells against reactive oxygen toxicity. Proceedings of the National Academy of Sciences of the United States of America *92,* 3784-3788.

Lin, S.J., Pufahl, R.A., Dancis, A., O'Halloran, T.V. and Culotta, V.C. (1997). A role for the *Saccharomyces cerevisiae ATX1* gene in copper trafficking and iron transport. Journal of Biological Chemistry *272,* 9215-9220.

Ling, H., Koch, G., Bäumlein, H., and Ganal, M.W. (1999). Map-based cloning of *CHLORONERVA*, a gene involved in iron uptake of higher plants encoding nicotianamine synthase. Proceedings of the National Academy of Sciences of the United States of America *96,* 7098-7103.

Lipka, V., Dittgen, J., Bednarek, P., Bhat, R., Wiermer, M., and Stein, M. et al. (2005). Pre- and postinvasion defenses both contribute to nonhost resistance in *Arabidopsis*. Science *310,* 1180-1183.

Liu, G., Sheng, X., Greenshields, D.L., Ogieglo, A., Kaminskyj, S., Selvaraj, G., and Wei, Y. (2005). Profiling of wheat class III peroxidase genes derived from powdery mildew-attacked epidermis reveals distinct sequence-associated expression patterns. Molecular Plant-Microbe Interactions *18,* 730-741.

Liu, G.S., Greenshields, D.L., Sammynaiken, R., Hirji, R.N., Selvaraj, G. and Wei, Y. (2007). Targeted alterations in iron homeostasis underlie plant defense responses. Journal of Cell Science *120,* 596-605.

Lyngkjaer, M.F., Newton, A.C., Atzema, J.L., and Baker, S.J. (2000). The barley mlo-gene: An important powdery mildew resistance source. Agronomie *20,* 745-756.

Mano, J., Babiychuk, E., Belles-Boix, E., Hiratake, J., Kimura, A., Inzé, D., Kushnir, S., and Asada, K. (2000). A novel NADPH:diamide oxidoreductase activity in *Arabidopsis thaliana* p1 ζ-crystallin. European Journal of Biochemistry *267,* 3661-3671.

Mathur, J., and Chua, N. (2000). Microtubule stabilization leads to growth reorientation in *Arabidopsis* trichomes. Plant Cell *12,* 465-477.

Matvienko, M., Wojtowicz, A., Wrobel, R., Jamison, D., Goldwasser, Y., and Yoder, J.I. (2001). Quinone oxidoreductase message levels are differentially regulated in parasitic and non-parasitic plants exposed to allelopathic quinones. Plant Journal *25,* 375-387.

Maxwell, D.P., Wang, Y., and McIntosh, L. (1999). The alternative oxidase lowers mitochondrial reactive oxygen production in plant cells. Proceedings of the National Academy of Sciences of the United States of America *96,* 8271-8276.

McLusky, S.R., Bennett, M.H., Beale, M.H., Lewis, M.J., Gaskin, P., and Mansfield, J.W. (1999). Cell wall alterations and localized accumulation of feruloyl-3′-methoxytyramine in onion epidermis at sites of attempted penetration by *Botrytis allii* are associated with actin polarisation, peroxidase activity and suppression of flavonoid biosynthesis. Plant Journal *17,* 523-534.

Mei, B.G., Budde, A.D., and Leong, S.A. (1993). *sid1*, a gene initiating siderophore biosynthesis in *Ustilago maydis*: molecular characterization, regulation by iron, and role in phytopathogenicity. Proceedings of the National Academy of Sciences of the United States of America *90,* 903-907.

Mendgen, K., and Hahn, M. (2002). Plant infection and the establishment of fungal biotrophy. Trends in Plant Science *7,* 352-356.

Mendgen, K., and Nass, P. (1988). The activity of powdery-mildew haustoria after feeding the host cells with different sugars, as measured with a potentiometric cyanine dye. Planta *174,* 283-288.

Mittler, R. (2002). Oxidative stress, antioxidants and stress tolerance. Trends in Plant Science *7,* 405-410.

Mittler, R., and Lam, E. (1997). Characterization of nuclease activities and DNA fragmentation induced upon hypersensitive response cell death and mechanical stress. Plant Molecular Biology *34,* 209-221.

Mittler, R., Simon, L., and Lam, E. (1997). Pathogen-induced programmed cell death in tobacco. Journal of Cell Science *110,* 1333-1344.

Mittler, R., Vanderauwera, S., Gollery, M., and Van Breusegem, F. (2004). Reactive oxygen gene network of plants. Trends in Plant Science *9,* 490-498.

Molina-Holgado, F., Hider, R.C., Gaeta, A., Williams, R., and Francis, P. (2007). Metals ions and neurodegeneration. Biometals *20,* 639-654.

Morel, J., and Dangl, J. L. (1997). The hypersensitive response and the induction of cell death in plants. Cell Death and Differentiation *4,* 671-683.

Mori, S. (1999). Iron acquisition by plants. Current Opinion in Plant Biology *2,* 250-253.

Muckenthaler, M., Richter, A., Gunkel, N., Riedel, D., Polycarpou-Schwarz, M., Hentze, S., Falkenhahn, M., Stremmel, W., Ansorge, W., and Hentze, M.W. (2003). Relationships and distinctions in iron-regulatory networks responding to interrelated signals. Blood *101,* 3690-3698.

Murata, Y., Ma, J.F., Yamaji, N., Ueno, D., Nomoto, K., and Iwashita, T. (2006). A specific transporter for iron(III)-phytosiderophore in barley roots. Plant Journal *46,* 563-572.

Murphy, T.H., So, A.P., and Vincent, S.R. (1998). Histochemical detection of quinone reductase activity *in situ* using LY 83583 reduction and oxidation. Journal of Neurochemistry *70,* 2156-2164.

Negishi, T., Nakanishi, H., Yazaki, J., Kishimoto, N., Fujii, F., Shimbo, K., Yamamoto, K., Sakata, K., Sasaki, T., Kikuchi, S., Mori, S., and Nishizawa, N.K. (2002). cDNA microarray analysis of gene expression during Fe-deficiency stress in barley suggests that polar transport of vesicles is implicated in phytosiderophore secretion in Fe-deficient barley roots. Plant Journal *30,* 83-94.

Nielsen, K.A., Nicholson, R.L., Carver, T.L.W., Kunoh, H., and Oliver, R.P. (2000). First touch: An immediate response to surface recognition in conidia of *Blumeria graminis*. Physiological and Molecular Plant Pathology *56,* 63-70.

Nishimura, M.T., Stein, M., Hou, B., Vogel, J.P., Edwards, H., and Somerville, S.C. (2003). Loss of a callose synthase results in salicylic acid-dependent disease resistance. Science *301,* 969-972.

Noctor, G. (2006). Metabolic signalling in defence and stress: The central roles of soluble redox couples. Plant, Cell and Environment *29,* 409-425.

Noctor, G., Gomez, L., Vanacker, H., and Foyer, C.H. (2002). Interactions between biosynthesis, compartmentation and transport in the control of glutathione homeostasis and signalling. Journal of Experimental Botany *53,* 1283-1304.

Nürnberger, T., and Lipka, V. (2005). Non-host resistance in plants: New insights into an old phenomenon. Molecular Plant Pathology *6,* 335-345.

O'Brien, P.J. (1991). Molecular mechanisms of quinone cytotoxicity. Chemico-Biological Interactions *80,* 1-41.

Oide, S., Moeder, W., Krasnoff, S., Gibson, D., Haas, H., Yoshioka, K., and Turgeon, B.G. (2006). *NPS6*, encoding a nonribosomal peptide synthetase involved in siderophore-mediated iron metabolism, is a conserved virulence determinant of plant pathogenic ascomycetes. Plant Cell *18,* 2836-2853.

Oliver, R.P., and Ipcho, S.V.S. (2004). *Arabidopsis* pathology breathes new life into the necrotrophs-vs.-biotrophs classification of fungal pathogens. Molecular Plant Pathology *5,* 347-352.

Park, Y.S., Choi, I.D., Kang, C.M., Ham, M.S., Kim, J.H., Kim, T.H., Yun, S.H., Lee, Y.W., Chang, H.I., Sung, H.C. and Yun, C.W. (2006a). Functional identification of high-affinity iron permeases from *Fusarium graminearum*. Fungal Genetics and Biology *43,* 273-282.

Park, Y.S., Kim, T.H., Chang, H.I., Sung, H.C. and Yun, C.W. (2006b). Cellular iron utilization is regulated by putative siderophore transporter FgSit1 not by free iron transporter in *Fusarium graminearum*. Biochemical and Biophysical Research Communications *345,* 1634-1642.

Passardi, F., Penel, C., and Dunand, C. (2004). Performing the paradoxical: How plant peroxidases modify the cell wall. Trends in Plant Science *9,* 534-540.

Patel, M., and Day, B.J. (1999). Metalloporphyrin class of therapeutic catalytic antioxidants. Trends in Pharmacological Sciences *20,* 359-364.

Payne, S.M. (1994). Detection, isolation, and characterization of siderophores. Methods Enzymology *235,* 329-344.

Pekker, I., Tel-Or, E., and Mittler, R. (2002). Reactive oxygen intermediates and glutathione regulate the expression of cytosolic ascorbate peroxidase during iron-mediated oxidative stress in bean. Plant Molecular Biology *49,* 429-438.

Pestka, J.J., and Smolinski, A.T. (2005). Deoxynivalenol: Toxicology and potential effects on humans. Journal of Toxicology and Environmental Health - Part B: Critical Reviews *8,* 39-69.

Petit, J., Van Wuytswinkel, O., Briat, J.-F., and Lobréaux, S. (2001). Characterization of an Iron-dependent Regulatory Sequence Involved in the Transcriptional Control of *AtFer1* and *ZmFer1* Plant Ferritin Genes by Iron. Journal of Biological Chemistry *276,* 5584-5590.

Petrat, F., De Groot, H., and Rauen, U. (2001). Subcellular distribution of chelatable iron: A laser scanning microscopic study in isolated hepatocytes and liver endothelial cells. Biochemical Journal *356,* 61-69.

Pham, C.G., Bubici, C., Zazzeroni, F., Papa, S., Jones, J., and Alvarez, K. et al. (2004). Ferritin heavy chain upregulation by NF-κB inhibits TNFα-induced apoptosis by suppressing reactive oxygen species. Cell *119,* 529-542.

Philpott, C.C. (2006). Iron uptake in fungi: A system for every source. Biochimica Et Biophysica Acta-Molecular Cell Research *1763,* 636-645.

Philpott, C.C., Protchenko, O., Kim, Y.W., Boretsky, Y. and Shakoury-Elizeh, M. (2002). The response to iron deprivation in *Saccharomyces cerevisiae*: expression of siderophore-based systems of iron uptake. Biochemical Society Transactions *30,* 698-702.

Pich, A., Manteuffel, R., Hillmer, S., Scholz, G., and Schmidt, W. (2001). Fe homeostasis in plant cells: Does nicotianamine play multiple roles in the regulation of cytoplasmic Fe concentration? Planta *213,* 967-976.

Pierre, J.L., and Fontecave, M. (1999). Iron and activated oxygen species in biology: The basic chemistry. BioMetals *12,* 195-199.

Proctor, R.H., Hohn, T.M. and McCormick, S.P. (1997). Restoration of wild-type virulence to *Tri5* disruption mutants of *Gibberella zeae* via gene reversion and mutant complementation. Microbiology *143,* 2583-2591.

Punt P.J., Oliver, R.P., Dingemanse, M.A., Pouwels, P.H. and van den Hondel, C.A.M.J.J. (1987). Transformation of *Aspergillus* based on the hygromycin B resistance marker from *Escherichia coli*. Gene *56,* 117-124.

Quayyum, H.A., Gijzen, M., and Traquair, J.A. (2003). Purification of a necrosis-inducing, host-specific protein toxin from spore germination fluid of *Alternaria panax*. Phytopathology *93,* 323-328.

Rae, T.D., Schmidt, P.J., Pufahl, R.A., Culotta, V.C., and V. O'Halloran, T. (1999). Undetectable intracellular free copper: The requirement of a copper chaperone for superoxide dismutase. Science *284,* 805-808.

Rao, P.V., Krishna, C.M., and Zigler Jr., J.S. (1992). Identification and characterization of the enzymatic activity of ζ-crystallin from guinea pig lens. A novel NADPH:quinone oxidoreductase. Journal of Biological Chemistry *267,* 96-102.

Rauth, A.M., Goldberg, Z., and Misra, V. (1997). DT-diaphorase: possible roles in cancer chemotherapy and carcinogenesis. Oncology Research *9,* 339-349.

Rentel, M.C., Lecourieux, D., Ouaked, F., Usher, S.L., Petersen, L., Okamoto, H., Knight, H., Peck, S.C., Grierson, C.S., Hirt, H., and Knight, M.R. (2004). OXI1

kinase is necessary for oxidative burst-mediated signalling in *Arabidopsis*. Nature *427,* 858-861.

Rikkerink, E.H.A., Solon, S.L., Crowhurst, R.N. and Templeton, M.D. (1994). Integration of vectors by homologous recombination in the plant pathogen *Glomerella cingulata*. Current Genetics *25,* 202-208.

Sambrook, J. and Russell, D.W. (2001) Molecular Cloning: A Laboratory Manual 3rd edn. Cold Spring Harbor Laboratory Press, Cold Spring Harbor.

Schaible, U.E., and Kaufmann, S.H.E. (2004). Iron and microbial infection. Nature Reviews Microbiology *2,* 946-953.

Schiestl, R.H. and Gietz, R.D. (1989) High efficiency transformation of intact yeast cells using single stranded nucleic acids as a carrier. Current Genetics *16,* 339-346.

Schmidt, W. (2003). Iron solutions: acquisition strategies and signaling pathways in plants. Trends in Plant Science *8,* 188-193.

Schrettl, M., Bignell, E., Kragl, C., Joechl, C., Rogers, T., Arst Jr., H.N., Haynes, K., and Haas, H. (2004). Siderophore biosynthesis but not reductive iron assimilation is essential for *Aspergillus fumigatus* virulence. Journal of Experimental Medicine *200,* 1213-1219.

Schroeder, H.W. and Christensen, J.J. (1963). Factors affecting resistance of wheat to scab caused by *Gibberella zeae*. Phytopathology *53,* 831-838.

Schulze-Lefert, P. (2004). Knocking on the heaven's wall: Pathogenesis of and resistance to biotrophic fungi at the cell wall. Current Opinion in Plant Biology *7,* 377-383.

Schützendübel, A., and Polle, A. (2002). Plant responses to abiotic stresses: Heavy metal-induced oxidative stress and protection by mycorrhization. Journal of Experimental Botany *53,* 1351-1365.

Schwyn, B. and Neilands, J. B. (1987). Universal chemical assay for the detection and determination of siderophores. Analytical Biochemistry *160,* 47–56.

Scott-Craig, J.S., Kerby, K.B., Stein, B.D., and Somerville, S.C. (1995). Expression of an extracellular peroxidase that is induced in barley (*Hordeum vulgare*) by the powdery mildew pathogen (*Erysiphe graminis* f.sp. *hordei*). Physiological and Molecular Plant Pathology *47,* 407-418.

Shigeoka, S., Ishikawa, T., Tamoi, M., Miyagawa, Y., Takeda, T., Yabuta, Y., and Yoshimura, K. (2002). Regulation and function of ascorbate peroxidase isoenzymes. Journal of Experimental Botany *53,* 1305-1319.

Škalamera, D., and Heath, M.C. (1998). Changes in the cytoskeleton accompanying infection-induced nuclear movements and the hypersensitive response in plant cells invaded by rust fungi. Plant Journal *16,* 191-200.

Smart, M.G. (1991). The plant cell wall as a barrier to fungal invasion. In: The fungal spore and disease initiation in plants and animals. Cole, G.T., and Hoch, H.C. (eds.) Plenum Press, New York 47-66.

Smith, M.A., Harris, P.L.R., Sayre, L.M., and Perry, G. (1997). Iron accumulation in Alzheimer disease is a source of redox-generated free radicals. Proceedings of the National Academy of Sciences of the United States of America *94,* 9866-9868.

Sparla, F., Tedeschi, G., and Trost, P. (1996). NAD(P)H:(quinone-acceptor) oxidoreductase of tobacco leaves is a flavin mononucleotide-containing flavoenzyme. Plant Physiology *112,* 249-258.

Sparla, F., Tedeschi, G., Pupillo, P., and Trost, P. (1999). Cloning and heterologous expression of NAD(P)H:quinone reductase of *Arabidopsis thaliana*, a functional homologue of animal DT-diaphorase. FEBS Letters *463,* 382-386.

Stakman E.C. (1915). Relation between *Puccinia graminis* and plants highly resistant to its attack. Journal of Agricultural Research *4,* 193–200.

Stearman, R., Yuan, D.S., Yamaguchi-Iwai, Y., Klausner, R.D. and Dancis, A. (1996). A permease-oxidase complex involved in high-affinity iron uptake in yeast. Science *271,* 1552-1557.

Stein, M., Dittgen, J., Sánchez-Rodríguez, C., Hou, B.-., Molina, A., Schulze-Lefert, P., Lipka, V., and Somerville, S. (2006). *Arabidopsis* PEN3/PDR8, an ATP binding cassette transporter, contributes to nonhost resistance to inappropriate pathogens that enter by direct penetration. Plant Cell *18,* 731-746.

Stephan, U.W., Schmidke, I. and Pich, A. (1994). Phloem translocation of Fe, Cu, Mn, and Zn in *Ricinus* seedlings in relation to the concentrations of nicotianamine, an endogenous chelator of divalent metal ions, in different seedling parts. Plant and Soil *165,* 181-188.

Strange, R.N., and Scott, P.R. (2005). Plant disease: A threat to global food security. Annual Review of Phytopathology *43,* 83-116.

Sutton, P.N., Henry, M.J., and Hall, J.L. (1999). Glucose, and not sucrose, is transported from wheat to wheat powdery mildew. Planta *208,* 426-430.

Takemoto, D., Jones, D.A., and Hardham, A.R. (2003). GFP-tagging of cell components reveals the dynamics of subcellular re-organization in response to infection of *Arabidopsis* by oomycete pathogens. Plant Journal *33,* 775-792.

Talalay, P., and Dinkova-Kostova, A.T. (2004). Role of Nicotinamide Quinone Oxidoreductase 1 (NQO1) in Protection against Toxicity of Electrophiles and Reactive Oxygen Intermediates. Methods in Enzymology *382,* 355-364.

Tangen, K.L., Jung, W.H., Sham, A.P., Lian, T. and Kronstad, J.W. (2007). The iron- and cAMP-regulated gene *SIT1* influences ferrioxamine B utilization, melanization and cell wall structure in *Cryptococcus neoformans*. Microbiology *153,* 29-41.

Thaler, J.S. (1999). Jasmonate-inducible plant defences cause increased parasitism of herbivores. Nature *399,* 686-688.

Teng, F.Y.H., Wong, Y., and Tang, B.L. (2001). The syntaxins. Genome Biology *2*, reviews3012.1-3012.7.

Thomas, F., Serratrice, G., Béguin, C., Saint Aman, E., Pierre, J.L., Fontecave, M., and Laulhère, J.P. (1999). Calcein as a fluorescent probe for ferric iron. Application to iron nutrition in plant cells. Journal of Biological Chemistry *274,* 13375-13383.

Thomas, S.W., Rasmussen, S.W., Glaring, M.A., Rouster, J.A., Christiansen, S.K., and Oliver, R.P. (2001). Gene identification in the obligate fungal pathogen *Blumeria graminis* by expressed sequence tag analysis. Fungal Genetics and Biology *33,* 195-211.

Thordal-Christensen, H. (2003). Fresh insights into processes of nonhost resistance. Current Opinion in Plant Biology *6,* 351-357.

Thordal-Christensen, H., and Smedegaard-Petersen, V. (1988). Comparison of resistance-inducing abilities of virulent and avirulent races of *Erysiphe graminis* f.sp. *hordei* and a race of *Erysiphe graminis* f.sp. *tritici* in barley. Plant Pathology *37,* 20-27.

Thordal-Christensen, H., Zhang, Z., Wei, Y., and Collinge, D.B. (1997). Subcellular localization of H_2O_2 in plants. H_2O_2 accumulation in papillae and hypersensitive response during the barley-powdery mildew interaction. Plant Journal *11,* 1187-1194.

Tiedemann, A.V. (1997). Evidence for a primary role of active oxygen species in induction of host cell death during infection of bean leaves with *Botrytis cinerea*. Physiological and Molecular Plant Pathology *50,* 151-166.

Tobiasen, C., Aahman, J., Ravnholt, K.S., Bjerrum, M.J., Grell, M.N. and Giese, H. (2007). Nonribosomal peptide synthetase (NPS) genes in *Fusarium graminearum*, *F. culmorum* and *F. pseudograminearium* and identification of NPS2 as the producer of ferricrocin. Current Genetics *51,* 43-58.

Torres, M.A., Dangl, J.L., and Jones, J.D.G. (2002). *Arabidopsis* gp91phox homologues Atrbohd and Atrbohf are required for accumulation of reactive oxygen intermediates in the plant defense response. Proceedings of the National Academy of Sciences of the United States of America *99,* 517-522.

Torres, M.A., Jones, J.D.G., and Dangl, J.L. (2005). Pathogen-induced, NADPH oxidase-derived reactive oxygen intermediates suppress spread of cell death in Arabidopsis thaliana. Nat. Genet. *37,* 1130-1134.

Torti, F.M., and Torti, S.V. (2002). Regulation of ferritin genes and protein. Blood *99,* 3505-3516.

Trost, P., Bonora, P., Scagliarini, S., and Pupillo, P. (1995). Purification and properties of NAD(P)H: (quinone-acceptor) oxidoreductase of sugarbeet cells. European Journal of Biochemistry *234,* 452-458.

Trujillo, M., Altschmied, L., Schweizer, P., Kogel, K.H., and Hückelhoven, R. (2006). Respiratory Burst Oxidase Homologue A of barley contributes to penetration by the powdery mildew fungus *Blumeria graminis* f. sp *hordei*. Journal of Experimental Botany *57,* 3781-3791.

Trujillo, M., Kogel, K.H., and Hückelhoven, R. (2004). Superoxide and hydrogen peroxide play different roles in the nonhost interaction of barley and wheat with inappropriate formae speciales of *Blumeria graminis*. Molecular Plant-Microbe Interactions *17,* 304-312.

Uldschmid, A., Engel, M., Dombi, R. and Marbach, K. (2002). Identification and functional expression of *tahA*, a filamentous fungal gene involved in copper trafficking to the secretory pathway in *Trametes versicolor*. Microbiology *148,* 4049-4058.

Valko, M., Morris, H., and Cronin, M.T. (2005). Metals, toxicity and oxidative stress. Current Medical Chemistry *12,* 1161-1208.

Valko, M., Morris, H., and Cronin, M.T.D. (2005). Metals, toxicity and oxidative stress. Current Medicinal Chemistry *12,* 1161-1208.

van Kan, J.A.L. (2006). Licensed to kill: the lifestyle of a necrotrophic plant pathogen. Trends in Plant Science *11,* 247-253.

Van Loon, L.C. (1997). Induced resistance in plants and the role of pathogenesis-related proteins. European Journal of Plant Pathology *103,* 753-765.

Wallace, G., and Fry, S.C. (1999). Action of diverse peroxidases and laccases on six cell wall-related phenolic compounds. Phytochemistry *52,* 769-773.

Walter, P.B., Knutson, M.D., Paler-Martinez, A., Lee, S., Xu, Y., Viteri, F.E., and Ames, B.N. (2002). Iron deficiency and iron excess damage mitochondria and mitochondrial DNA in rats. Proceedings of the National Academy of Sciences of the United States of America *99,* 2264-2269.

Wang, D., Weaver, N.D., Kesarwani, M., and Dong, X. (2005). Induction of protein secretory pathway is required for systemic acquired resistance. Science *308,* 1036-1040.

Wang, Y., Santa-Cruz, K., Decarli, C., and Johnson, J.A. (2000). NAD(P)H:quinone oxidoreductase activity is increased in hippocampal pyramidal neurons of patients with Alzheimer's disease. Neurobiology of Aging *21,* 525-531.

Watts, R.N., Hawkins, C., Ponka, P., and Richardson, D.R. (2006). Nitrogen monoxide (NO)-mediated iron release from cells is linked to NO-induced glutathione efflux via multidrug resistance-associated protein 1. Proceedings of the National Academy of Sciences of the United States of America *103,* 7670-7675.

Wei, Y., Zhang, Z., Andersen, C.H., Schmelzer, E., Gregersen, P.L., Collinge, D.B., Smedegaard-Petersen, V., and Thordal-Christensen, H. (1998). An epidermis/papilla-specific oxalate oxidase-like protein in the defence response of

barley attacked by the powdery mildew fungus. Plant Molecular Biology *36,* 101-112.

Wilkins, T.A., and Smart, L.B. (1996). Isolation of RNA from plant tissue. In: A Laboratory Guide to RNA: Isolation, Analysis, and Synthesis. Kreig, P.A. (ed), Wiley, New York 21-41.

Willekens, H., Chamnongpol, S., Davey, M., Schraudner, M., Langebartels, C., Van Montagu, M., Inze, D., Van Camp, W. (1997). Catalase is a sink for H_2O_2 and is indispensable for stress defence in C3 plants. EMBO Journal *16,* 4806-4816.

Wilson, T.J.G., Thomsen, K.K., Petersen, B.O., Duus, J.Ø, and Oliver, R.P. (2003). Detection of 3-hydroxykynurenine in a plant pathogenic fungus. Biochemical Journal *371,* 783-788.

Wolpert, T.J., Dunkle, L.D., and Ciuffetti, L.M. (2002). Host-selective toxins and avirulence determinants: What's in a name? Annual Review of Phytopathology *40,* 251-285.

Wong, H.L., Sakamoto, T., Kawasaki, T., Umemura, K., and Shimamoto, K. (2004). Down-regulation of metallothionein, a reactive oxygen scavenger, by the small GTPase OsRac1 in rice. Plant Physiology *135,* 1447-1456.

Wood, M.J., Storz, G., and Tjandra, N. (2004). Structural basis for redox regulation of Yap1 transcription factor localization. Nature *430,* 917-921.

Wrobel, R.L., Matvienko, M., and Yoder, J.I. (2002). Heterologous expression and biochemical characterization of an NAD(P)H:quinone oxidoreductase from the hemiparasitic plant *Triphysaria versicolor*. Plant Physiology and Biochemistry *40,* 265-272.

Wynn, W.K. (1976). Appressorium formation over stomates by the bean rust fungus: response to the surface contact stimulus. Phytopathology *66,* 136-146.

Xu, J.R., Peng, Y.L., Dickman, M.B. and Sharon, A. (2006). The dawn of fungal pathogen genomics. Annual Review of Phytopathology *44,* 337-366.

Yamada, O., Na Nan, S., Akao, T., Tominaga, M., Watanabe, H., Satoh, T., Enei, H. and Akita, O. (2003). *dffA* gene from *Aspergillus oryzae* encodes L-ornithine N^5-oxygenase and is indispensable for deferriferrichrysin biosynthesis. Journal of Bioscience and Engineering *95,* 82-88.

Yang, W., Ni, L., and Somerville, R.L. (1993). A stationary-phase protein of *Escherichia coli* that affects the mode of association between the trp repressor protein and operator-bearing DNA. Proceedings of the National Academy of Sciences of the United States of America *90,* 5796-5800.

Yoshioka, H., Numata, N., Nakajima, K., Katou, S., Kawakita, K., Rowland, O., Jones, J.D.G., and Doke, N. (2003). *Nicotiana benthamiana* gp91phox homologs Nbrboha and Nbrbohb participate in H_2O_2 accumulation and resistance to *Phytophthora infestans*. Plant Cell *15,* 706-718.

Yuan, W.M., Gentil, G.D., Budde, A.D. and Leong, S.A. (2001) Characterization of the *Ustilago maydis sid2* gene, encoding a multidomain peptide synthetase in the ferrichrome biosynthetic gene cluster. Journal of Bacteriology *183,* 4040-4051.

Yun, B., Atkinson, H.A., Gaborit, C., Greenland, A., Read, N.D., Pallas, J.A., and Loake, G.J. (2003). Loss of actin cytoskeletal function and EDS1 activity, in combination, severely compromises non-host resistance in *Arabidopsis* against wheat powdery mildew. Plant Journal *34,* 768-777.

Zamboni, P., Izzo, M., Tognazzo, S., Carandina, S., De Palma, M., Catozzi, L., Caggiati, A., Scapoli, G., and Gemmati, D. (2006). The overlapping of local iron overload and HFE mutation in venous leg ulcer pathogenesis. Free Radical Biology and Medicine *40,* 1869-1873.

Zhang, S., Du, H., and Klessig, D.F. (1998). Activation of the tobacco SIP kinase by both a cell wall-derived carbohydrate elicitor and purified proteinaceous elicitins from *Phytophthora* spp. Plant Cell *10,* 435-449.